

https://dspace.org/

Gravitational torques of the dust penetrated stellar backbone of extragalactic spiral disks

Groess, Robert

2008-06-24T12:11:43Z
http://hdl.handle.net/10539/4979

Downloaded from a DSpace repository. https://dspace.org/

GRAVITATIONAL TORQUES OF THE DUST PENETRATED STELLAR BACKBONE OF EXTRAGALACTIC SPIRAL DISKS

ROBERT GROESS

A thesis submitted to the Faculty of Science, University of the Witwatersrand, Johannesburg, South Africa, in fulfillment of the requirements for the degree of Doctor of Philosophy.

JOHANNESBURG, SEPTEMBER 2007

DECLARATION

I declare that this thesis is my own, unaided work, whereby although the material delineated within was obtained through the cumulative efforts of various collaborations, the compilation of this thesis is uniquely my own. It has not been submitted for any degree or examination at any other university or research institution.

_____ _____

ROBERT GROESS (CANDIDATE) **DATE**

CONTENTS

ABSTRACT…… vii
ACKNOWLEDGEMENTS…… viii
LIST OF FIGURES……xi
LIST OF TABLES……... xx
ABBREVIATIONS…….. xxii
PREFACE…… xxiv
CHAPTER ONE – INTRODUCTION……. 1
1.1 Classification of Hubble's Nebulae……. 1
1.1.1 The Rationale behind Classification…….. 1
1.1.2 Classification for Description…… 2
1.1.3 The Hubble Tuning Fork Strikes a New Note…….. 5
1.1.4 The Elegant Simplicity of the Hubble Scheme…… 8
1.1.5 Classification beyond the Legacy of the Hubble Scheme…. 9
1.2 Identification of Interstellar Dust…… 13
1.2.1 The Prevalence of Dark Bands…….. 13
1.2.2 Properties of Interstellar Dust Grains…….. 15
1.2.3 Composition of Interstellar Dust Grains……... 16
1.2.4 Warm Cosmic Dust……19
1.3 Penetrating the Mask of Cosmic Dust……. 22
1.3.1 Galaxy Classification in the 21st Century…….. 22
1.3.2 Introduction to Near-infrared Morphology……22
1.4 Scope of this thesis…….. 25

CHAPTER TWO – THE TRIANGULUM GALAXY AS A ROSETTA STONE FOR BUILDING GALACTIC DISKS……. 27
2.1 Introduction…… 28
2.1.1 Early Descriptions of Messier 33…… 28
2.1.2 Optical Morphology of Messier 33…….. 28

2.2 Image Processing Techniques for Near-infrared Disk Galaxies……. 30
2.2.1 A Deep 2MASS Subsample of M33…… 30
2.2.2 Removal of Foreground (Milky Way) Stellar Sources……..31
2.3 Gravitational Torques of Disk Galaxies…….. 33
2.3.1 The Gravitational Torque Method…… 33
2.3.2 Gravitational Potential and Force Ratio Maps……...37
2.3.3 The Gravitational Torque Parameter Q_g…… 38
2.3.4 Error Analysis of the GTM……39
2.3.5 Gravitational Torques in the Stellar Backbone of M33…… 40
2.4 A Fourier Approach to Calculating Spiral Arm Pitch Angles……41
2.4.1 A Dust Penetrated Spiral Arm Classification…… 41
2.4.2 Description of the Fourier Coefficients A(p,m)…… 42
2.4.3 Fourier Detection of a Faint Stellar Arc
in the Outer Disk of M33…….. 45
2.5 The Case for Giant Arcs of Carbon Stars……... 47
2.5.1 Colour-Colour Photometry of the Outer Disk of M33…….. 47
2.5.2 Keck Spectroscopic Verification of Carbon Stars…… 47
2.5.3 Spitzer IRAC Observations……56
2.6 Insights into Building of Galactic Disks……58
2.6.1 Origin of Carbon Star-Bearing Arcs……..58
2.6.2 Inferring Carbon Star Populations
in the Outer Disks of High-Z Galaxies…….. 59

CHAPTER THREE – SPITZER MORPHOLOGY OF THE GREAT NEBULA IN ANDROMEDA – LORD OF THE RINGS…… 61

3.1 Introduction……. 61
3.2.1 Early Descriptions of Messier 31…….. 61
3.2.2 Optical Morphology of Messier 31……62
3.2 Spitzer Observations of M31 with IRAC……64
3.2.1 Introduction……64
3.2.2 Spitzer's Infrared Array Camera……64

3.2.3 Wide Field IRAC Mosaic of M31…… 64
3.3 Dust-penetrated 8.0μm IRAC Morphology ……. 65
3.3.1 PAHs in Emission…… 65
3.3.2 A non-stellar 8.0μm Dust Map of M31…… 66
3.3.3 Two Off-Centre Rings of Dust…….. 68
3.4 Collisional Interpretation…… 71
3.4.1 Introduction……71
3.4.2 The Prevalence of Ringed Galaxies at High-z……...74
3.4.3 Comparison with the Cartwheel Galaxy……75
3.4.4 N-body Simulations by Bournaud & Combes…….. 76
3.4.5 Dynamics of the induced velocity field……79

CHAPTER FOUR – SEPARATION OF BAR AND SPIRAL ARM TORQUES IN NEARBY DISK GALAXIES…….. 82

4.1 Introduction……. 82
4.1.1 The Hubble-Jeans Tuning Fork Revisited……82
4.1.2 Quantitative Bar Strength Classification…….. 83
4.2 Bar and Spiral Arm Torque Classification using the Modified GTM… 84
4.2.1 Introduction…….. 84
4.2.2 A Fourier Technique to Separate Bars and Spiral Arms…. 85
4.2.3 Synthetic Bar/Spiral Arm Generation through Inverse Fourier Transforms…….. 88
4.3 A Combined Sample of 40 Nearby Barred Galaxies…….. 90
4.3.1 Details of the Spitzer IRAC Sample…… 90
4.3.2 Details of the AAT IRIS2 Sample……91
4.3.3 Calculated Bar and Spiral Arm Torques……92
4.4 Relationship between Bar and Spiral Arm Torques…… 100
4.4.1 Do Stronger Bars Drive Stronger Spirals? ……100
4.4.2 Prominent Bars with Weak Spiral Arms……105
4.4.3 Grand Design Structure with Relatively Weak Bars……. 107
4.4.4 Bars as Transient Morphological Features –

Further Evidence for Accretion? …….. 109

CHAPTER FIVE – BAR MORPHOLOGY AS SEEN IN DUST EMISSION AT 8.0μm ……. 113

5.1 Introduction……. 113

5.1.1 Dust Morphology Characteristics of Barred Spirals…… 113

5.2 Surprising insights from quantitative dust emission analyses……..….. 115

5.2.1 Three Distinct Bar Form Families…… 115

5.3 Type Θ1 Stellar Bars – as seen through the eyes of Spitzer…….. 118

5.3.1 The Coupling of 3.6μm and 8.0μm images…….…… 118

5.4 Type Θ2 Stellar Bars – S-shaped Dust Shock-Fronts……. 121

5.4.1 The Decoupling of 3.6μm and 8.0μm bar morphologies… 121

5.4.2 Characteristics of Bars and the Hydrodynamics of Shock Loci…… 124

5.5 Type Θ3 Stellar Bars – Bars devoid of Dust……..…… 127

5.5.1 Strongly Decoupled 3.6μm and 8.0μm bar morphologies… 127

5.6 Conclusion……..…… 130

CHAPTER SIX - CONCLUSION……. 131

6.1 Classification for the starry vault of the “nebulae”……. 131

6.2 Lessons from the Local Group of Galaxies……..….. 133

6.2.1 M33 – A Rosetta Stone for the building of galactic disks… 133

6.2.2 Glowing Rings of Fire – Galaxy Morphology induced only millions of years ago…….. 134

6.3 Dust penetrated IRAC Morphology…….…….. 134

6.3.1 Separating bars from their parent disks of stars…..…… 134

6.3.2 Dust Grains in Emission – The Morphology of Spiral Galaxies at 8.0μm…….. 135

6.4 The exploration of space……...……. 136

REFERENCES…….…….. 138

ABSTRACT

"The nature of the nebulae and their place in the scheme of the universe have been favorite subjects of controversy since the very dawn of telescopic observations. In these later days, when the non-galactic nebulae have been clearly differentiated from the diffuse and the planetary, the discussion has concentrated around the spectacular forms of the spirals… island universes, scattered through the remote depths of space."

– Edwin P. Hubble

It was only a mere 45 years ago, that some of the foremost astronomers such as Allan Sandage and Donald Lynden Bell believed that spiral galaxies were monolithic islands which were dynamically closed. This thesis has awaited the dawning of a new era wherein the disks of spiral galaxies can be "dust penetrated". Prevalent ideas in the literature are overturned. Unprecedented images from IRAC onboard the Spitzer Space Telescope reveal the dynamic nature of nearby disk galaxies, including the two dominant spirals in our Local Group beyond the Milky Way. We show that M33 is a spiral galaxy whose disk grows outwards with time and which serves as a local Rosetta stone of a dynamically open system. We next show that the present-day morphology of M31 was induced only 210 million years ago. IRAC images betray its tumultuous recent past with the presence of two spectacular off-centre rings of dust, glowing at 8.0μm. A collision scenario seems most likely, with one of its larger satellite galaxies, M32. In our local universe, the bar phenomenon is ubiquitous. We separate bars from their parent disks in a sample of about 40 spiral galaxies, revealing that stronger spirals are not necessarily driven by stronger bars. Bars are not the universal excitation mechanism by which spiral structure is induced. Finally, surprising insights are gleaned from the IRAC 8.0μm window pertaining to the dust morphology of barred spirals. Three distinct form families of stellar bars are presented. May this thesis serve as "one small step for man" in our quest to expand our knowledge in the new epoch of quantitative galaxy classification in the dust-penetrated regime.

ACKNOWLEDGEMENTS

As with any venture of the magnitude of a thesis, this one has been critically dependant on the support and guidance from a great number of people. Moreover, it has equally been dependent upon the student's eternal *Fata Morgana*, funding. Crucial funding, without which this thesis would never have seen the light of day, has come from Professor David L. Block and Professor George F.R. Ellis. It is with gratitude and pride that I present this thesis as a result of this unfaltering support.

I have met many people, and made a great number of friends in my career as a doctoral student. What follows is a mere token of appreciation to those who have been instrumental in all the techniques I have mastered and experiences I have enjoyed over the past few years. It is by no means complete, but for the sake of immediate relevance, I would like to mention a few names.

It has been a great pleasure and a singular honour to have met Professor Giovanni G. Fazio, principal investigator for the Infrared Array Camera onboard NASA's Spitzer Space Telescope. Giovanni's generosity, both scientifically, and also as a host in Cambridge, Massachusetts, is simply first class. Much of the work presented in this thesis would not have been possible were it not for Giovanni.

Professor Kenneth C. Freeman has likewise been a great inspiration to me.

I owe a great deal of gratitude to Dr. Ivânio Puerari, for teaching me much of the Fourier analysis described in this thesis, for helping me out with countless lines of code and for giving up some of his precious time to teach me some tricks of the trade when it comes to IRAF and the nuances that go along with it. Ivânio, many thanks for your great friendship too and for all the gifts you have brought me from Mexico.

I also thank Professor Ron Buta for teaching me much of the bar/spiral separation techniques used throughout this thesis and for sharing one of his more prized possessions, an ancient lycopod bark impression, which, at 310 million years, is older than even the Andromeda collision.

Dr. Tom Jarrett (IPAC/Caltech), thank you too for your hospitality and assistance when we stayed in Pasadena and for the great collaboration on the M33 2MASS data. It is thanks to Tom that a whole suite of papers have been written (and continue to be written) on M33.

Mike Fitzpatrick, from the IRAF centre at NOAO, while being the only person in this list of acknowledgements that I have not met in person, I thank you too for critical help with my initial acquaintance with IRAF. I am truly amazed at Mike's proficiency in debugging a problem after receiving only a few scraps of diagnostic code from me. Thanks to Mike, I have been able to install various versions of IRAF and supporting code on the computer network in the Cosmic Dust Laboratory at the University of the Witwatersrand.

The IRAC team at the Harvard-Smithsonian Center for Astrophysics, alphabetically, I thank Drs. Matt Ashby, Michael Pahre and Steve Wilner for their generous collaboration on the IRAC data presented in this thesis, and in particular for the seminal research performed on M31, which has been published in NATURE. It was also a great honour to meet you all at the CfA in December 2004, and your hospitality was likewise very welcoming.

Kartik Sheth and Karín Menéndez-Delmestre (Caltech), thanks for spending your precious time with me in Pasadena and for your hospitality when we came to visit.

On home (South African) soil, I have to thank Brian Maistry for his active support and for cheering me on with, what at times, has seemed like a never-ending task to complete this thesis. Thank you for all the continuous encouragement you have given me over my young career.

Professor David Sherwell, Head of School, thank you for keeping an eye on me and ensuring great progress is made on my thesis, as well as for the useful nuggets of advice which you have shared with me, all of which have helped make the progress of a work like this thesis seem like a much more manageable task. It has also been a great pleasure to get to know Professors Ebrahim Momoniat, David Mason, David Taylor, Shirley Ableman and Mrs. Rosemary Gray.

What would the school of Computational & Applied Mathematics be without the departmental secretaries? I'd like to collectively thank you all for the help you have given me over the years, from the binding of some draft copies of my thesis, to picking up the trail of confetti I once accidentally left strewn in the corridors behind me. Alphabetically, Florence Goetze, Zahn Gowar, Wendy Moss, Sam Naidoo, Alena Nagy and last but not least Thembisile (Emily) Nkabinde.

Some of the real stars in my life are my friends who have stuck with me through thick and thin. In no particular order, Antonia Cardwell, Florian Breuer, Richard Lai, Encarni Romero Colmenero and Trevor Gould. You have NO IDEA what your support has meant to me, and how much a part of my life you are. Thank you for everything!!

My family too, have put up with me over these past few years when it seemed like I was married to my computer, without time for anything else. I thank my parents, Chris and Gerhard for giving me the opportunity to touch the stars, and the same goes for my brother and sister, Kenan and Heidi.

Professor David L. Block, the person who taught me the true meaning of supernova, it has positively been an exciting adventure to be a part of your world. From the highest echelons of galaxy morphology to the intense work of hosting conferences and through a multitude of other activities in this universe, the words thank you somehow pale into insignificance. And if that were not enough, forevermore these words will be a part of me; always look up – never, never, never give up!

LIST OF FIGURES

Figure 1.1: The Wolf descriptive classification scheme (1908), where like-objects were classified according to their observed morphology in 17 bins, denoted (g) through (w)....2

Figure 1.2: Hubble's Tuning Fork diagram, much as it is presented in 'The Realm of the Nebulae' (1936), with the S0 problem being resolved (see §1.1.5). This provided a novel graphical representation of the continuity of "Nebular types"……....5

Figure 1.3: The characteristic 'Y'-shaped Tuning Fork diagram as first presented by Jeans (1929) to convey the continuity of the Hubble classification scheme. The separation of ordinary and barred spirals is very clear and branch off on the two separate prongs/tynes of the tuning fork much the same as in the Hubble tuning fork…….7

Figure 1.4: The de Vaucouleurs (1959) classification volume, based upon the Hubble scheme and fully accommodating the intermediate cases of SA, SAB and SB galaxies with (r) and (s) sub-types. The transition cases between barred and un-barred galaxies are also accommodated naturally in this classification volume……...11

Figure 1.5: Schematic of a dust grain found in diffuse clouds (top) and a precometary dust grain (bottom), with silicate cores. The refractory inner mantels of the two types of grains comprise organic molecules, and in the case of precometary grains, are covered with outer mantels of volatile ices, such as CH4, NH3 and water ice……...17

Figure 1.6: Infrared spectra scaled by starlight intensity ($\lambda I_\lambda/(\chi_{MMP}N_H)$ as a function of wavelength (λ) for the standard grain model of Li & Draine (2001) for various grain illumination fields. The shape of the spectra remain essentially unchanged in the region $\lambda < 15\mu m$ for star light intensities differing over 5 orders of magnitude. The same ionization fraction as the local diffuse ISM has been assumed. Wavelength coverage of the 4 IRAC bands and the MIPS bands on Spitzer are included.…….20

Figure 1.7: The dust penetrated z ~ 0 tuning fork template by Block et al. (2001). Galaxies are binned according to quantitative criteria. The pitch angle families α, β and γ are determined from Fourier spectra (see §2.4) while the bar strength is derived from the gravitational potential (see §2.3). Examples of early type "b" galaxies NGC3992, NGC2543, NGC7083, NGC5371 and NGC1365 are distributed within all three families……...24

Figure 2.1: The Triangulum Spiral Galaxy, Messier 33, as photographed by Keeler (1908), with north up and east to the left. NGC604, seen as a dark knot to the upper left of the galaxy, is one of the brightest HII regions known. The Triangulum galaxy extends over one degree along its major axis and its distance modulus of 24.64m corresponds to a linear distance of 840 kpc (Freedman, Wilson & Madore, 1991). This implies a linear diameter of ~ 17 kpc, approximately one-half that of the Milky Way. M33 has an inclination of 53.9º ($\log R_{25} = 0.23$)……..29

Figure 2.2: A combined 2MASS JHK_s mosaic of M33, extending approximately 6 times deeper than the nominal 2MASS survey, revealing the underlying older Population I disk morphology with hitherto unprecedented spatial resolution at these passbands……...31

Figure 2.3: Histogram of $J - K_s$ Point Source Catalogue colours for stars in the M33 field – labeled as the target. Flanking fields 2 degrees east and 2 degrees west of the target represent the control number density of foreground Milky Way stars, the average of which were removed from the deep M33 mosaic. All counts refer to a 0.864 deg^2 area down to 15th magnitude at K_s……....33

Figure 2.4: Force ratio map of M33. The butterfly pattern is a distinct signature for the presence of a (mini)bar in the central region of this galaxy. Extreme dark and light areas denote the maxima/minima of the force ratios in each of four quadrants…….38

Figure 2.5: A deep deprojected JHK_s 2MASS image of M33, where the GTM (with further bar/spiral separation – see §4.2.2) reveals a class '2' bar. The gravitational bar torque maxima (white squares) have been superimposed on the inner oval/bar……...41

Figure 2.6: A 2.1μm image of NGC309 (left) and an optical image of NGC718 (right) taken with the 5m Hale reflector. Both exhibit the same number of arms with very similar pitch angles (18° and 24°, respectively), even though they are classified as Sc and Sa in the Hubble scheme, respectively (Block & Puerari 1999)…….42

Figure 2.7: Normalized amplitude versus pitch angle of Fourier modes m=1 through m=10. The dominant peak at m=2, where $P_{max} \neq 0$, reveals the presence of two large open outer arcs hitherto undetected. The smaller peak is a signature of the inner 'grand design' spiral arms…….46

Figure 2.8: This J–H, $H–K_s$ colour-colour diagram reveals the presence of extremely red stars in the outer arcs. The sample presented has been cleaned of low detection sources, with S/N < 10. The evolved giant and main-sequence dwarf tracks (solid and dashed lines, respectively) are from Bessell and Brett (1988). In this figure, foreground Milky Way stars appear with blue colours of $H–K_s < 0.2$, $J–H < 0.8$ and $J–K_s < 1.0$ magnitude. Most M33 sources in the outer arcs are redder with $H–K_s > 0.4$, $J–H > 0.9$ and $J–K_s > 1.3$ magnitude. Colour uncertainties of the red sources are less than 10%.....……...53

Figure 2.9: A Keck II Spectrum of a carbon star approximately 5 scalelengths away from the centre of M33. The dominant CN absorption features are clearly evident and are a definitive signature of TP-AGB carbon stars. Carbon stars contain a host of molecular spectral features such as the CN bands and the C2 Swan bands. The conclusive presence of CN bands near 7000Å, 8000Å and 9000Å are indicated above……....54

Figure 2.10: Keck I spectra of targets listed in Table 2.2……..55

Figure 3.1: The Great Nebula in Andromeda (the Andromeda Spiral Galaxy), is situated at a distance of approximately 780 kpc, is inclined at 77.5 degrees to the line of sight (Rubin and Ford 1971, Nieten et al. 2005) and has a position angle (PA) of 37.7 degrees east of north (Nieten et al. 2005)……...63

Figure 3.2: A non-stellar Spitzer IRAC image of the central region of the Andromeda Spiral at 8.0μm, shows the distribution of very small grains as well as macromolecules, all seen in emission……66

Figure 3.3: Spitzer IRAC imaging of the Andromeda galaxy at 8.0μm reveals the presence of two off-centre rings of dust. Both rings are interpreted to be density waves induced by an almost head-on collision. The famous outer 10kpc ring has an offset of ~10% from the centre of the galaxy, while the first time discovery of an inner 1.5kpc by 1.0kpc ring is off-centre by about 40%. A scaled subtraction of the 3.6μm map was used to reveal the underlying dust morphology by removing light from stellar photospheres. The remaining luminosity therefore traces the emission of warm dust grains and macromolecules in the interstellar medium. The most likely impactor candidate is the elliptical dwarf companion galaxy M32, seen to the lower right in the white square. M32 appears faint in this image because its dust content is relatively low and much of the prominent starlight at 3.6μm has been subtracted away……....70

Figure 3.4: Fourier spectra generated from a deprojected 8.0μm image of the central region of Messier 31. The Fourier spectra confirms that the dominant Fourier mode is m=2, indicative of the two inner Baade dust arms, whose pitch angle is computed from the m=2 spectral panel to be 57 degrees……...72

Figure 3.5: The central region of the Andromeda Spiral Galaxy secured at non-stellar 8.0μm with the Spitzer Space Telescope. Full observing details in Block et al. NATURE (2006). This is a close up of the 1.5 by 1 kpc inner ring of M31. The ring is off-centre by approximately 40%, from the centre of the nuclear bulge position and the two inner dust arms identified by Baade (Baade & Payne-Gaposchkin, 1963) commence at the bright

regions along the apparent major axis of the ring as seen here. The image shown here was subjected to Fourier spectral analysis and a 0.28 scaled subtraction of the 3.6μm image carefully revealed where the Baade arms of dust themselves actually begin. A distinct morphological component – a central mini-spiral of dust identified by Rubin and Ford (1971), Johnson and Hanna (1972) and Ciardullo et al. (1998) whose aspect ratio is significantly different and more face-on than the highly inclined disk of M31 itself, lies within the ring……....73

Figure 3.6: A Hubble Space Telescope (HST) blue-band image of the Cartwheel galaxy (ESO 350-40) (Borne et al. 1994) has revealed massive star formation taking place in the outer ring of the Cartwheel. Evident are blazing OB associations, as well as the dusty structure of the elongated and off-centered inner ring. As in M31, the Hα, radio-continuum and HI 21cm emissions trace the outer ring (Higdon 1996). The HST image of the Cartwheel is projected with the same inclination as Andromeda in Figure 3.6 and the similarity of the double-ringed eccentricity is highly compelling in that this B band image of the Cartwheel gives the closest analogue to the double-ringed 8.0μm IRAC morphology of M31……..75

Figure 3.7: Numerical simulation by Bournaud & Combes (Block et al., 2006) of a head-on encounter between M31 and M32 forming two ring-like density-waves, both of which are offset from the galaxy centre. The mass we invoke for the companion (a ratio 1/13th in stellar mass with M31, or 1/10th including dark matter) is compatible with the present mass of M32. The collision is not exactly head-on, but the companion path is inclined with respect to the perpendicular of the M31 plane by 35 degrees. The companion crosses the M31 disk at a velocity of 265km/s, with an impact parameter of 4 kpc, 210 Myr ago. It would now be located at a distance of 35kpc and at a galactic latitude of about 45 degrees, which is fully compatible with the present position of M32……...77

Figure 4.1: The NGC7479 relative Fourier intensity amplitude for m=2 is plotted as a function of radius (solid line). The extrapolated synthetic bar profile is represented by the dashed line. The bar profile is reflected about a radius of 37 arcsec, and it is assumed not to end abruptly but that it decays to zero similarly to the way in which the profile slope reached a maximum. The "double-hump" near the bar profile "centre" is an artifact of this method, but the alternative of modeling the original profile slope to ~100 arcsec did not result in a satisfactory bar decomposition in the case of NGC7479. All galaxies that have been bar/spiral separated in this thesis have been selected using this prescription...87

Figure 4.2: This K_s band image of NGC4593, secured with the IRIS2 instrument on the 3.9m AAT, reveals the power of the bar spiral decomposition technique. All four quadrants have the same orientation, with the bar rotated to horizontal. Top left is the deprojected AAT image. The image at top right was generated by displaying only the terms (m=0, 1, 2,…10). This "Fourier-smoothed" version of the full image demonstrates that the first 10 m terms are sufficient to retain essentially all the large scale morphological detail. The image at lower left was generated using only the terms m = 2, 4, 6, 8, 10. This effectively selects the bar-only contribution to the light intensity distribution of the galaxy. The lower right image shows the axisymmetric disk plus spiral arms, generated by subtracting the "bar-only" contribution from the m=0..10 smoothed image. The positions of the torque maxima are indicated by the four squares on each of the images containing the bar……....89

Figure 4.3: The effect of determining gravitational torques from images generated using only the terms m = 0, 1, …, 10 as compared with "unprocessed" images, for 17 Spitzer IRAC and 23 IRIS2 AAT galaxies combined. The greatest source for scatter is attributed to mildly prominent star forming regions which are smoothed out in the m = 0, 1, …, 10 Inverse Fourier transform……..93

Figure 4.4: Assuming scaleheights of 225pc and 325pc for each galaxy in the combined sample of 40, reveals a negligible change in the classification of bar and spiral arm torque class. Bar torques (seen in the panel on the left), have a minimum value of $Q_b \sim 0.14$, compared with spiral arm torques, which are down to $Q_s \sim 0.04$……94

Figure 4.5: Similar to Figure 4.4 above, but with assumed scaleheights of 225pc and 425pc. A change of a single bar strength class is the most severe deviation, and only when torque values are high, $Q_b > 0.5$. Spiral arm torques are far less affected due to their radial distance from the bulge, where the exponential form of the scaleheight function has tapered off, thereby representing a thinner disk…….……...94

Figure 4.6: Relative gravitational torques for separated bars and spiral arms for the full sample of 40 galaxies reveal that stronger spirals are not necessarily driven by stronger bars. Bars are not the universal excitation mechanism by which spiral structure is induced, with bar strengths revealing a broad range of values for given spiral arm torques. Error bars represent the relative errors as determined from the GTM……....100

Figure 4.7: Figure 4.6 without error bars allows specific cases of galaxies which represent the outlying regions of $Q_s - Q_b$ space, to be discussed in detail…….101

Figure 4.8: NGC986…….103
Figure 4.9: UGC10862…….104
Figure 4.10: NGC7479…….104
Figure 4.11: NGC3368…….105
Figure 4.12: NGC5101…….106
Figure 4.13: NGC7155…….107
Figure 4.14: NGC1566…….107
Figure 4.15: NGC4536…….108
Figure 4.16: NGC4321…….109

Figure 4.17: Histogram of gravitational bar torques for a sample of 163 near-infrared disk galaxies investigated by Block et al. (2002). The solid line indicates actual observations. The dashed line is derived from galaxy simulations which double their disk mass due to gas accretion in a Hubble time. The dotted line represents simulations without accretion. The non-observation of galaxies with zero bar torques, as the non-accreting models suggest, argues strongly in favor of the external gas accretion scenario and is fully compatible with the observed distribution of spiral torques in Figure 4.6 and Figure 4.7……111

Figure 5.1: Barred spiral galaxies, NGC986 (top left), NGC5383 (top right), NGC1365 (lower left) and NGC1300 (lower right) each show very prominent dust lanes (seen as white filaments in the images above). These dust lanes are the signature of shock loci at the leading edges of bars. The presence of flocculent dust spurs emanating from the dust lanes at the shock positions reveal a well ordered but intricate velocity field along the shock loci. The fainter dust wisps are along the trailing edge of the bars, and are nearly perpendicular to the resulting prominent dust lanes……114

Figure 5.2: Three distinct "form families" of barred spiral galaxies: Type Θ1 reveal 8.0μm dust morphologies induced by stars, type Θ2 have 8.0μm dust morphologies induced by gas only, and type Θ3 are bars (and possibly even spiral arms) completely devoid of gas and dust. All three families show prominent bars in stars at 3.6μm…….117

Figure 5.3: Type Θ1 Barred Spirals – Dust which delineates the bar morphology induced by stars. These bars contain both stars and dust, with the dust distribution being a very good tracer of the underlying stellar morphology. A scaleheight of 325pc was assumed for all galaxies in determining Q_g……....119

Figure 5.4: Type Θ2 Barred Spirals – Dust filaments are observed to connect the spiral arms with the nuclear region of these galaxies which have a very definite stellar bar at 3.6μm. The dust morphologies are induced by the gas only and there is no evidence of a bar at 8.0μm……122

Figure 5.5: A model of the gas response in the presence of a bar (Athanassoula, 2000, Figure 1). At left, gas density is presented in grey-scale with dark areas representing regions of lower densities. The right panel depicts gas flow lines and the velocity vectors. The bar is at rest in this frame of reference…….125

Figure 5.6: Type Θ3 Barred Spirals – Stellar bars devoid of gas and dust bars. These prototypically barred galaxies have very pronounced bars at 3.6μm, with no associated gas or dust at 8.0μm……..…128

LIST OF TABLES

Table 2.1: Relative gravitational torque classes……39

Table 2.2: Magnitude and colours of 7 candidate Carbon stars in the outer disk of M33……....52

Table 4.1: Position angle, inclination and distances to 17 galaxies of the Fazio GTO sample of Spitzer IRAC galaxies. The Spitzer data used in this chapter are exclusively 3.6μm (Channel 1) images. All distances assume the Hubble parameter as used in Tully & Fisher as 75km/s/Mpc……91

Table 4.2: Position angle, inclination and distances to 23 galaxies of the Knapen 3.9m AAT sample of IRIS2 K_s band galaxies. Distances determined from the RC3 use the Tully & Fisher value for the Hubble parameter as 75km/s/Mpc……...92

Tables 4.2.1 – 4.2.3: Gravitational torques as computed on the combine sample of 17 IRAC Spitzer and 23 IRIS2 AAT galaxies. Q_g represents the relative gravitational torque of correctly deprojected images of each galaxy, with no further processing. Q_t is the torque value for synthetic recreation of the entire galaxy using only the lower Fourier terms, m = 0, 1, …, 10. Q_b is the separated bar torque (m = 2, 4, 6, 8) and Q_s is the spiral arm only component……..96

Table 4.2.1: Scaleheight ~ 225pc……..97
Table 4.2.2: Scaleheight ~ 325pc……..98
Table 4.2.3: Scaleheight ~ 425pc……..99

Table 4.3: Examples of galaxies in the three difference regions of $Q_s - Q_b$ space. These scenarios for the distribution of bar and spiral arms torques are discussed in detail below……102

Table 5.1: Type Θ1 Barred spiral galaxies……..120
Table 5.2: Type Θ2 Barred spiral galaxies……..124
Table 5.3: Type Θ3 Barred spiral galaxies……..129

LIST OF ABBREVIATIONS

2MASS	–	Two Millimeter All Sky Survey
AAT	–	Anglo Australian Telescope
AGB	–	Asymptotic Giant Branch
AOR	–	Astronomical Observation Request (Spitzer)
CFHT	–	Canada-France-Hawaii-Telescope
ESI	–	Echellette Spectrograph and Imager on Keck II
FWHM	–	Full Width at Half Maximum
GOODS	–	Great Observatories Origins Deep Survey
GTM	–	Gravitational Torque Method (Buta & Block, 2002)
HDF	–	Hubble Deep Field (HST)
HST	–	Hubble Space Telescope
IR	–	Infrared
IRAC	–	Infrared Array Camera (onboard Spitzer)
IRAF	–	Image Reduction and Analysis Facility
IRAS	–	Infrared Astronomical Satellite
IRIS2	–	Infrared Imager and Spectrograph (on AAT)
IRS	–	Infrared Spectrograph (onboard *Spitzer*)
JWST	–	James Web Space Telescope
LMC	–	Large Magellanic Cloud
LRIS	–	Low Resolution Imaging Spectrometer on Keck I
MIPS	–	Multiband Imaging Photometer for Spitzer (onboard *Spitzer*)
NGC	–	New General Catalogue (Dreyer, 1888)
NGST	–	Next Generation Space Telescope (now JWST)
NICMOS	–	Near Infrared Camera and Multi Object Spectrometer (HST)
NIR	–	Near-infrared
PAH	–	Polycyclic Aromatic Hydrocarbon
QFG	–	Quillen, Frogel & Gonzalez (1994)

RC2	–	'*Second Reference Catalogue of Bright Galaxies*'
RC3	–	'*Third Reference Catalogue of Bright Galaxies*'
RSA	–	'*A Revised Shapley Ames Catalogue*'
SIRTIF	–	Space Infrared Telescope Facility (now *Spitzer*)
SMC	–	Small Magellanic Cloud
SST	–	Spitzer Space Telescope (also, *Spitzer*)
TP-AGB	–	Thermally Pulsating Asymptotic Giant Branch (Stars)
UDF	–	Ultra Deep Field (HST)
WIRC	–	Wide field Infrared Camera (Hale Reflector)

– PREFACE –

"Two roads diverged in a wood, and I –
I took the one less traveled by.
And that has made all the difference",
– Robert Frost

There is a land down south – a country vibrant with change. Here paradigm shifts have become the norm. Change is everywhere. Change is constant. Projecting these sentiments onto the global village, a past-president from this land says of the astronomical endeavour, "One of the striking features of modern times is the emergence of men and women who have chosen the entire world as the theater of their operations. We are the beneficiaries of this inspiring phenomenon." – Nelson R. Mandela, South Africa.

It has been my great fortune and privilege to have been intimately involved with being at the epicenter not once, not twice, but three times, of major international conferences, held on the subject of Galaxy Morphology on South African soil. '*New Extragalactic Perspectives in the New South Africa*' (1996) set the tone. It was in a time of significant change in South Africa, with new-found political stability that was endorsed the world over. As an undergraduate, it was a distinct honour to be involved with assisting with miscellaneous tasks that, I trust, helped the conference run that little more smoothly. It also gave me the unique opportunity to meet such people as the late J. Mayo Greenberg, Cosmic Dust pioneer and Laboratory Astrophysicist extraordinaire, on a one-on-one basis, when doubling as his chauffeur. This was also the time when the first Hubble Deep Field photons were captured barely a month before. The JWST (before it was even known as the NGST!) was still in the early conceptual phases, and I recall John Mather inviting input for a telescope meant for the "young people" in the audience. Tremendously positive reports were received for this conference and, I've been told, set a new benchmark regarding the calibre of galaxy morphology conferences.

This precedent set the stage for two more highly successful conferences, '*Toward a New Millennium in Galaxy Morphology*' (1999), in which I was involved just prior to my MSc, and, one that I have been most intimately involved with during my doctoral studies, '*Penetrating Bars through Masks of Cosmic Dust*' (2004).

Before the 2004 conference, David Block and I had been discussing the dramatic impact which infrared morphology has recently had on galaxy classification schemes. It was with this stimulating exchange that inspired me to exclaim, "*The Hubble Tuning Fork strikes a New Note*". We both took an instant liking to it – and it became the subtitle of the 2004 conference. I wore many hats to that conference as conference secretariat, co-editor of the 900 page conference volume, logo designer, technical assistant (with the A/V equipment in the conference venue) and even sated my photographic interests in being conference photographer. This conference was planned to coincide with the occasion of David Block's 50th birthday and, the rare spectacle of a Transit of Venus.

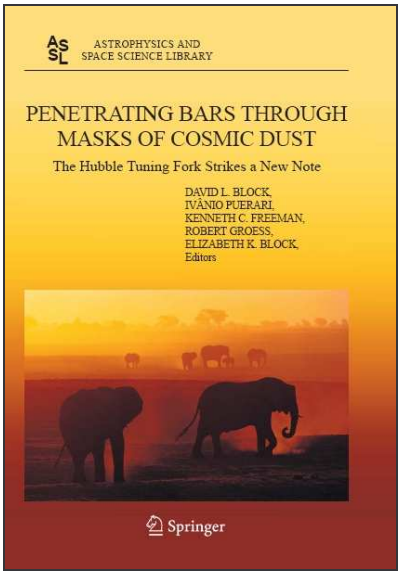

African elephants parade through veils of dust on the front cover of 'Penetrating Bars through Masks of Cosmic Dust: The Hubble Tuning fork Strikes a New Note', 2004, ASSL Vol. 319, Springer, New York, ISBN: 1-4020-2861X

"By 1930, the global village was already a real (if comparatively quaint) construction."

– Alan Stern & Jacqueline Mitton.

I feel a personal connection to much of the historical introduction to this thesis. I have been immensely fortunate to have accompanied David Block to the Lowell Observatory archives, in Flagstaff – *They don't make towns like this any more* – Arizona. Vesto M. Slipher, Director of the Lowell observatory from 1926-1954, was a meticulous correspondent and was geographically situated in an ideal position to be at the nexus of astronomical communiqués in the early 20th century. The closest we have come to time travelling is by reading what others before us have written. And in a very real sense, they speak to us as clearly as they had done generations ago. Thus Slipher, Hubble, Lundmark, and others spoke to us, letter after letter – indulging us with first hand accounts of the early heyday of galaxy morphology.

It is sad to think such opportunities may well be a thing of the past. With the advent of email, who will, centuries from now, be treated to such thrilling tales as our contemporary state of affairs? Astronomy historians have their work cut out for them, ensuring the skeins and threads of today's astronomical web, will project objectively into distant reaches of space and time.

The spirit in which this thesis has been written is to capture, succinctly, as much of the essence of near-infrared morphology as what I have been involved with over my career as a doctoral student. As with the production of a large scale motion picture, there are many people behind the scene. The final product is merely the tip of the ice-berg of a production that has endured many out-takes and deleted scenes, all with the express aim of providing a truly entertaining masterpiece. As regards my direct involvement in the research presented in Chapter 2 and Chapter 3: The gravitational torque analysis performed on M33 is completely my own, and I have performed partial image processing of the 2MASS image which illustrates the first time detection of large arcs of Carbon stars. I also performed the final proof reading of the Block et al. (2007) paper. The research presented on M31 in Chapter 3 is a large collaborative effort of which each

member of the team performed specialised tasks. My direct involvement includes the cleaning of selected foreground stars of the IRAC mosaic supplied by Barmby et al. (2006), Fourier spectral analysis of the inner region of M31, as well as the Baade arms, at 3.6μm and 8.0μm. The final revised version of the Letter to Nature was edited by D.L. Block, S.P. Willner, M.L.N. Ashby and myself. These results were publically released at simultaneous press conferences held at the University of the Witwatersrand, the Harvard-Smithsonian Center for Astrophysics, USA and the Observatoire de Paris, France at 18:00UTC 18 October 2006. All other analysis presented in this thesis is uniquely my own. The amount of work I have been involved with, and new friends that I have made, far exceeds the scope of any thesis – and so this document you are reading is necessarily the richly distilled 'final' product. I have endeavored to capture as much of the essence of the research I have been involved with these past few years and as such I trust the diversity presented provides an inkling into the rich tapestry that is contemporary near-infrared galaxy morphology.

…there would be nothing more poetic,
no outcome more graceful,
no unification more complete,
than for us to confirm our theories of the ultra-small
– our theories about the ultramicroscopic makeup of space, time, and matter
– by turning our most powerful telescopes skyward and gazing silently at the stars.

– Brian Greene, The Fabric of the Cosmos

– CHAPTER 1 –

INTRODUCTION

"Often the possibility or impossibility of reducing a mass of facts to order depends upon the right apprehension of some single observation or experiment."

– Anonymous (1863)

1.1 Classification of Hubble's Nebulae

1.1.1 The Rationale behind Classification

The Hubble classification scheme is the hallmark of 20th century extragalactic astronomy. That it became such, requires an historic interlude dating back to the early 1920's. In the era when the true extent of the observable cosmos was just beginning to be fully appreciated, the young subject of the morphological classification of spiral galaxies was taking shape. As with any scientific endeavour, with the power of almost a century worth of hindsight, we are in a position to ask what a truly explanative classification system should set to accomplish, and to reflect back on the multitude of classification systems that marked the birth of what is today the elaborate subject of galaxy morphology.

Alan Sandage (2005) writes, "The power of any mature classification system is in its systematic arrangements of like objects into connective patterns that themselves suggest explanations external to the classification itself." This is the key criterion formalizing any useful classification scheme. Sandage continues by saying that there is "the danger in devising a classification from scratch … that if the classifier has preconceived notions of what those explanations might be, then the classification becomes circular if it is later used to provide the explanations." A tautology with the benefit of hindsight, it is precisely this caveat that distinguishes a basic classification scheme, from an exceptional one. Before reviewing the intrinsic power of the Hubble scheme, it is beneficial to explore some of the prior alternatives suggested, and to distinguish the elements that have made the Hubble scheme stand the test of time.

1.1.2 Classification for Description

William Herschel provides one of the earliest attempts at cataloging a significant fraction of nearby galaxies. Augmented later by his son John, the Herschels' catalogue comprises 5079 nonstellar objects which formed the basis of Dreyer's (1888) expanded listing of "nebulae". It is upon this list that the modern NGC (New General Catalogue) of galaxies is based upon. The Herschels did not attempt to classify nebulae into any sort of morphological categories, except to note descriptive features without drawing analogies of any kind. A more systematic scheme was pioneered by Wolf (1908) who devised a purely descriptive classification where he proposed 17 morphological bins and gave them letters (g) through (w). There was no sense of 'connection' to a nebula (galaxy) in one bin, compared to a nebula in any other, but it provided a simplistic form of 'shelving' nebulae into like-appearing objects. Cumbersome it may have been, but very comprehensive it was. Even by today's standards, most optical nearby galaxies could easily be arranged in the Wolf scheme – with the notable exception of dwarf galaxies.

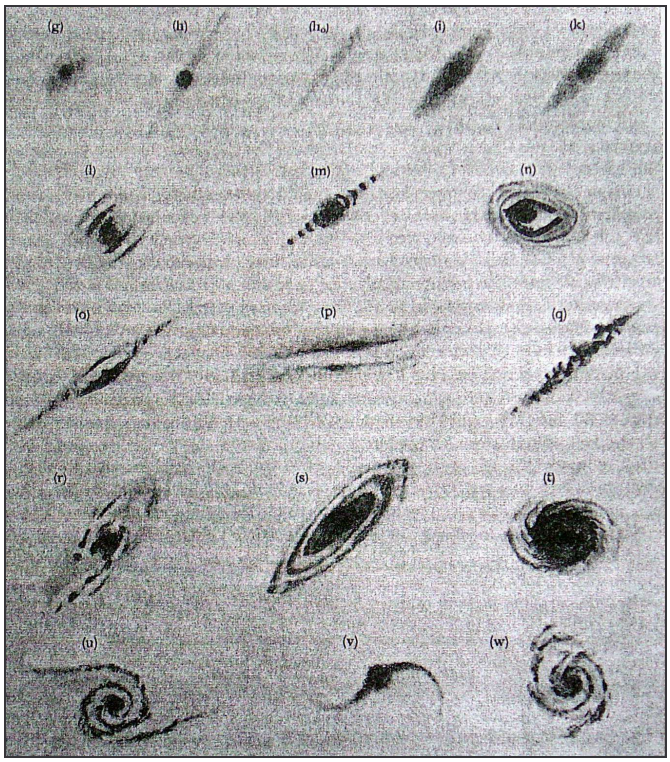

Figure 1.1: *The Wolf descriptive classification scheme (1908), where like-objects were classified according to their observed morphology in 17 bins, denoted (g) through (w).*

Hubble himself, having determined the positions and classified the forms of nongalactic nebulae (galaxies outside of the Milky Way) for his PhD thesis (1917), noted that the Wolf classification would be adequate for these early classifications until "a more suitable classification shall be devised." Heber D. Curtis (1918a) published descriptions of 762 nebulae and clusters, of which 513 were 'spiral nebulae', after maintaining that "the growing interest in nebular studies renders it advisable that descriptions of these be published."

So what then separates a cumbersome "description" from an elegant one? What is the missing element that could well meet the demand for having a classification scheme that is not encumbered by "preconceived notions" and to be greater than the sum of its parts? In a word: continuity.

One of the first developments that provided much of the solidity that the Hubble scheme rests upon today, was pioneered by Reynolds (1920), who made the connection between the morphology of spiral forms by suggesting that a morphological continuity exists between them. By measuring the intensity profiles of spiral galaxy bulges, Reynolds derived an empirical equation that shows surface brightness decreasing from the centre of the galaxy, outward. This Reynolds wrote as:

$$I(r)(1+x)^2 = const. \tag{1-1}$$

Reynolds subsequently derived seven divisions for a classification scheme which showed certain characteristics changing continuously with form type, using the notation I – VII. The descriptions he provided are:

I. "Spirals consisting entirely of amorphous nebulosity."
II. "Spirals showing incipient condensations in the outer whorls only."
III. "In this class the condensations in the outer regions have advanced considerably towards the nucleus. This is the stage reached by NGC3031 … where the outer

half is of the condensed type, including what appear to be actual star disks, while the nuclear region is of the amorphous type and has a light distribution similar to the Andromeda Nebula."

IV. "Includes the great majority of spirals. The nebular condensations appear in all regions except the nucleus itself, but a hazy background is still more or less conspicuous."

V. "An advanced stage of Class IV: the whole nebula is of the condensed type, the nucleus often having a definite boundary like a planetary nebula. The hazy background has practically disappeared in all the regions."

VI. In this class, Reynolds describes nebulae of the intermediate type, with outer rings and "condensations" in the inner arms.

VII. "Spirals of the course granular type which have no definite nucleus at all, such as NGC253…"

Classes I – VII are very analogous with Hubble types Sa through late Sc to the extent that Sandage (2005) remarks, "The correspondence is one-to-one (Section 4.4)". While Reynolds did not claim to present his scheme as a replacement to any forerunners, it certainly was, and yet even he himself failed to recognize the true significance of what he was advocating.

In order to fully appreciate this, we turn our attention to Hubble's landmark paper of 1926 – his only technical paper on the classification of spiral galaxies. It was developed using exclusively photographic (optical) images and provides a classification scheme to a wide dynamic range of morphologies observed in the "spiral nebulae". The Hubble scheme differentiates continuously between varying degrees of elliptical and spiral galaxies with the spiral galaxies being further divided into barred and unbarred variants; (SBa, SBb, SBc) and (Sa, Sb, Sc), respectively. These divisions having already been recognized by Curtis (1918a), who mentions, "It is my belief that all the many thousands of nebulae not definitely to be classed as diffuse or planetaries, are true spiral and that the very minute spirals appear as textureless disks or ovals solely because of their small (apparent) size." He also continues to distinguish between barred versus un-barred types.

While having published such findings in the literature, it is not Curtis whom we credit for the modern sequence of galaxies today. In what is seemingly a crucial feature to its success, the Hubble scheme was graphically presented in the form of the now famous 'Hubble Tuning Fork':

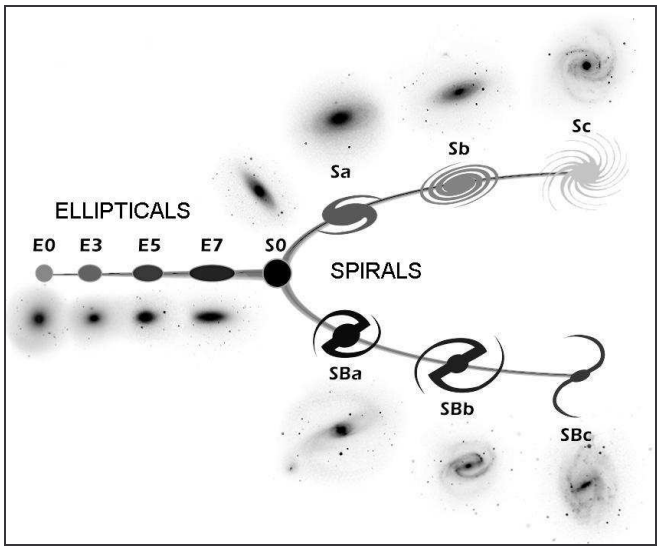

Figure 1.2: *Hubble's Tuning Fork diagram, much as it is presented in 'The Realm of the Nebulae' (1936), with the S0 problem being resolved (see §1.1.5). This provided a novel graphical representation of the continuity of "Nebular types".*

1.1.3 The Hubble Tuning Fork Strikes a New Note

While the origin of the Hubble classification scheme has its roots in the work done by Reynolds (1920) (see also Sandage, 2005), where Reynolds very distinctly uses the concept of continuity when distinguishing between classification classes, the true origin of the Tuning Fork diagram is less clear. The earliest notions of the separation of *spiral* galaxies into two separate skeins or sequences came from Jeans' Smith Prize essay, "*Problems of Cosmology and Stellar Dynamics*" (1919).

Jeans had been intensely interested in the spectroscopic confirmation that galaxies rotate. Already in 1914, Vesto M. Slipher had observed NGC4594 in 1914, and exclaimed, "The inclination of the lines … is unmistakable and leads one directly to the conclusion that the nebula is rotating about an axis." He continues, "The discovery of the rotation of this

nebula has opened a new field for investigation and that further observations will disclose other nebulae to be in rapid rotation may be confidently expected." This later led to Jeans speculating that the flattened structure of the nebulae was due to evolution of gaseous or possibly even liquid bodies, all dependent upon their rotation rate. These ideas were indeed acknowledged by Hubble in his 1926 paper, where he states, "Although deliberate effort was made to find a descriptive classification which should be entirely independent of theoretical considerations, the results are almost identical with the path of development derived by Jeans." He continues with regard to Jeans' '*Problems of Cosmology and Stellar Dynamics*' (1919), "The agreement is very suggestive in view of the wide field covered by the data, and Jeans' theory might have been used both to interpret the observations and guide research. It should be borne in mind however, that the basis of the classification is descriptive and entirely independent of any theory."

With hindsight however, it seems that Hubble contending that Jeans' ideas had no influence on him at all, may not have been entirely accurate. Especially in conceptualizing the division between the ellipticals and spirals, as well as presenting the spirals in a series of contiguous classification bins in which their bulges decreased in size and the spiral arm structure became more pronounced and resolved. Indeed in Jeans' book '*Astronomy and Cosmogony*' (1929), he gave a very novel *graphical representation* underscoring the continuum that connects the various morphological types that Hubble proposed. This graphical representation of Hubble's *scheme* is morphologically identical to the now famous Tuning Fork, with the exception that Jeans' depiction represents a 'Y'-shaped diagram (Figure 53 in Jeans' book; Figure 1.3 this thesis). Hubble presented in his semi-popular book '*The Realm of the Nebulae*' (Hubble 1936), the Tuning Fork diagram much as it is known today (with the exception of the S0 problem, which was resolved post 1954 – see §1.1.5). However, in Hubble's landmark paper of 1926, no graphic description is evident at all.

While it remains contentious as to whether Hubble plagiarized the Jeans diagram, it is clear that the Hubble scheme was laid out in full in 1926 and that it was Jeans' idea to represent the scheme diagrammatically in the form of a "Tuning Fork". Whatever the

course of events were that transpired in the 17 years between Jeans' essay and Hubble's book (1936), it appears that both Jeans and Hubble complimented each other even though Jeans is not cited at all, and especially not for having published a diagram which greatly aids the notion of continuity of the Hubble scheme. In reviewing the forensic evidence building up to 1936, it would thus seem more appropriate to call the diagram the *Hubble-Jeans Tuning Fork*, when representing the *Hubble Classification Scheme*. It is also historically interesting to note, that the only occurrence of *Hubble's* Tuning Fork diagram was not in the technical journals but rather in the book entitled "*The Realm of the Nebulae*" – which was sufficient to ensure its lasting fame.

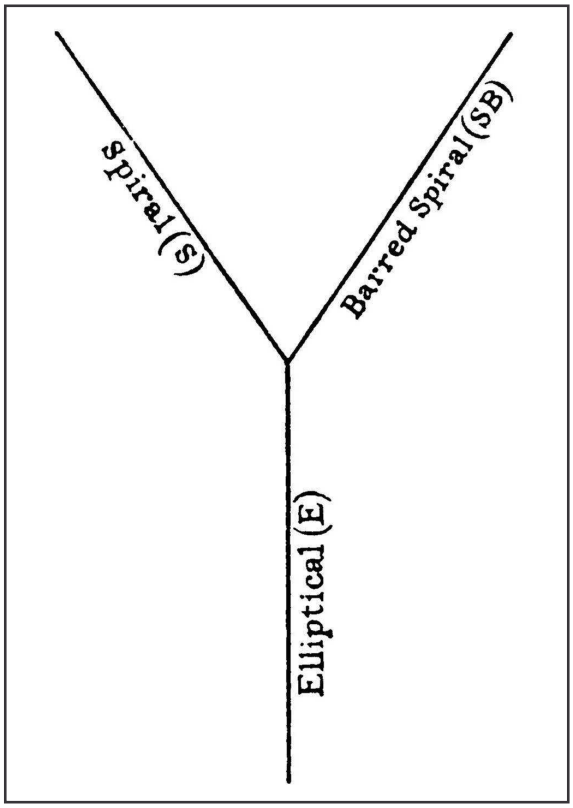

Figure 1.3: *The characteristic 'Y'-shaped Tuning Fork diagram as first presented by Jeans (1929) to convey the continuity of the Hubble classification scheme. The separation of ordinary and barred spirals is very clear and branch off on the two separate prongs/tynes of the tuning fork much the same as in the Hubble tuning fork.*

1.1.4 The Elegant Simplicity of the Hubble Scheme

The Tuning Fork diagram notwithstanding, Reynolds furthermore took great exception to the classification scheme proposed by Hubble. One of the major objections that Reynolds championed was the lack of detail in the Hubble scheme regarding the specific attributes of spiral arms, by labelling it as being too simple. He argued that the scheme paid insufficient attention to the multitude of variations observed in spirals that were simply placed into a small number of large bins and that a classification scheme ought to account for much of the detail that galaxies exhibit – detail which is conspicuously absent in the Hubble formulation. In Reynolds' own words (Reynolds, 1927), "The classification of spirals seems to me to be altogether too simple for the great range of types." He goes on by saying "The problem I have always found in attempting a general classification of spiral nebulae is that one meets case after case where a special class is required for the individual object. Spectral classification of stars is a simple and straightforward matter compared with this." The attributes that Reynolds insisted that a classification scheme should accommodate are the extent to which spiral arms wind around the bulge (anything from half a revolution to almost two revolutions), as well as the strength or "*massiveness*" of the spiral arm pattern.

This comes in stark contrast to Reynolds' own seven-binned classification scheme in which he proposed classification in a manner which is very analogous to the Hubble scheme. It is not clear what reasons Reynolds had *in the face of his own classification proposal*, as to why he downplayed the Hubble sequence. Were it not for his fierce repudiation of the "simplicity" of Hubble's scheme, he would today have been considered one of the pioneers of modern galaxy classification.

As far as optical morphology is concerned, the Hubble scheme is elegant in its simplicity. It is the reason for its widespread use today, and does not attempt to branch specifically to classify separately such parameters as luminosity and arm/interarm density – intensity parameters which do not form part of a continuum of morphological evolution. These Hubble took to be "residuals" which are, in his words, small in comparison with "the path of the sequence". (Sequence here referring to what is today called the "Hubble

sequence".) That extensions to the original Hubble classification are continuously suggested, ironically serves to underscore the power of the Hubble system. It is precisely because the Hubble scheme deals with these variants intrinsically, that it provides much power to the classification of spiral galaxies and is the core reason as to why the Hubble scheme has garnered widespread acceptance.

One of the truly fascinating questions that remains open is why Hubble never cited Jeans nor Reynolds in any of his papers and correspondence relating to the classification of galaxies. Was it because he was unaware of the Reynolds' scheme (1920) or Jeans' tuning fork-like diagram (1929)? As regards Jeans, the only account of acknowledgment Hubble (1936) gives is, "The terms "early" and "late" are used to denote relative position in the empirical sequence without regard to their temporal implications. The explanations emphasize the purely empirical nature of the sequence of classification. The consideration is important because the sequence closely resembles the line of development indicated by the current theory of nebular evolution as developed by Sir James Jeans." Similarly, Sandage (2005, page 595) presents a suggestive account that Hubble did indeed know about the Reynolds scheme – the chronology of events however is not that trivial to disentangle.

1.1.5 Classification Beyond the Legacy of the Hubble Scheme

At about the same time as Hubble's scheme was proposed, Lundmark (1926) also defined a classification scheme of the nebulae. The two separate classifications which Hubble called Elliptical and Spiral, were also proposed by Lundmark. However, in his terminology, Lundmark called them anagalactic and galactic nebulae, denoted, A and G, respectively. The anagalactic division was further subdivided into elliptical, elongated, globular, lenticular and ovate morphologies. These were already recognized earlier by Reynolds (1920), and even before that by Knox-Shaw (1915). Furthermore, Lundmark introduced the "Magellanic nebulae" which he denoted Am, and provided for 6 degrees of "compression" towards the centre. Spiral nebulae were likewise ordered in terms of "compression towards the center".

Hubble forwardly accused Lundmark of plagiarism in his 1926 paper, even though it is clear that this was not Lundmark's intent, as Lundmark (1927) noted that his system is not at all dependent on the basis of the Hubble scheme. Lundmark's classification was hinged on the light-concentration of galactic images, whereas Hubble's system is more heavily based upon the specific morphology of galaxies, such as the size of the bulge, the resolution of the spiral arms and the tightness of their winding patterns.

One noteworthy remark is the revision of the Hubble scheme, between 1936 and the publication of the Hubble Atlas (by Sandage, 1961). The continuity between S0 and SBa galaxies was unsatisfactory as depicted in the original 1936 Hubble diagram. After Hubble's death in 1953, Sandage and Humason found an unpublished reapportionment as proposed by Hubble, which provides a fix to the discontinuity. The Sa galaxies in the 1936 scheme were re-classified into the new S0 and Sa classes. The original SBa galaxies were regrouped into the new SB0 class, and the SBb galaxies reassessed for the new SBa or SBb subdivisions. The Hubble Atlas as prepared by Sandage (1961) serves to honour Hubble by adopting the 'new' Hubble bins to this end. It is also the reason that the galaxy classifications used in the Hubble atlas make use of the *classical* Hubble types, as opposed to the more detailed variations by some schemes which followed.

Reynolds' desire to increase the fidelity of descriptiveness has been entertained by numerous augmentations and embellishments to the representation of spiral disk galaxies by the Hubble scheme. Many such classification enhancements have been made and further addition of subdivisions and detail are attributed to de Vaucouleurs, Morgan, Sandage and van den Bergh.

De Vaucouleurs (1956) introduced the concept of a classification volume, a necessary development in preparation for the Hubble Atlas – the work on which had started in 1954. The de Vaucouleurs scheme recognizes the observed morphology of spiral arms, where arm multiplicity as well as branching are given their own symbols. The arm detail of (r) denoting "arms that begin tangent to an internal ring" as well as (s) representing "spiral arm subtypes", was first represented on the surface of a rectangular box (Figure 5,

page 26 of the Hubble Atlas). De Vaucouleurs generalized this into a continuous classification volume, where the interior represents (rs) and (sr) subtypes, and the major Sa, Sab, Sb, Sbc, Sc, Scd, Sd, Sdm, Sm and Im classes were continuously connected along the long axis of an ellipsoid-shaped volume – representing a natural extension to the two dimensional Tuning Fork diagram.

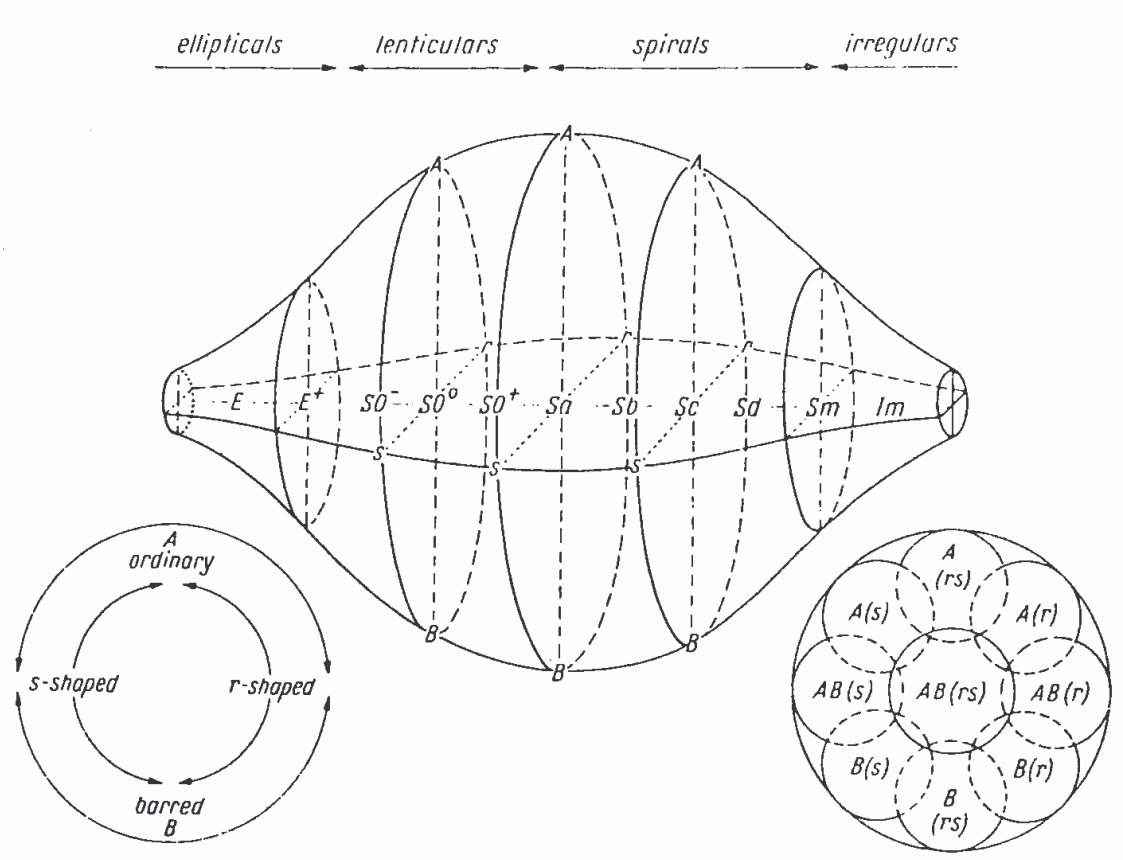

Figure 1.4: *The de Vaucouleurs (1959) classification volume, based upon the Hubble scheme and fully accommodating the intermediate cases of SA, SAB and SB galaxies with (r) and (s) sub-types. The transition cases between barred and un-barred galaxies are also accommodated naturally in this classification volume.*

Galaxies with external rings were designated capital 'R', such as RSBab(r) for example, which represents an external ring surrounding a galactic disk with a bar and is of type 'ab' with a set of (r)-type arms tangent to the bar. This notation de Vaucouleurs used extensively in his Stromlo Survey catalogue (1956).

One more significant advancement was made on the Hubble scheme, pioneered by van den Bergh (1960a,b), by introducing a "luminosity class" where he describes the "beauty" or "regularity" of spiral disks. This essentially relates to the degree of symmetry exhibited by a particular galaxy.

It is significant to note that all of these embellishments to the Hubble scheme are purely descriptive and make no attempt at relating to the underlying physics which govern the morphology of the galaxies that are being classified. The advent of bars or lack thereof, along with the relative sizes of bulges and the effect of these structures on the dynamics of galaxies, has not been explicitly considered. *This* is the true power of all classification schemes based upon the Hubble premise – that they *do* conform morphologically to rotation rates, star formation rates, and inner Lindblad resonances, without the circularity of having been introduced as a tenet of the classification scheme from the outset.

While some, such as King (1992), have argued that the passage of time since Hubble has sounded the death knell for a scheme as simplistic as Hubble's, it would appear that the scheme has survived even this ultimate test of acceptance. In what essentially endorses the coming-of-age of the family of Hubble-based classification schemes, Kormendy & Kennicutt (2004) remark, "At the level of detail that we nowadays try to understand, the time has passed when we can make effective progress by defining [optical] morphological bins with no guidance from a theory. Years ago, people commonly reacted badly to a classification as complicated as (R)SB(r)b. The reason, we believe, was that the phenomenology alone didn't sell itself. People did not see why this level of detail was important." These authors go on to emphasize that "every letter in the above classification has a clearcut meaning in terms of formation physics. This is the goal of physical morphology." It would seem that the Hubble Tuning fork has indeed struck a new note.

1.2 Identification of Interstellar Dust

1.2.1 The Prevalence of Dark Bands

It was Herschel who in 1884 exclaimed that there was undoubtedly a hole in the sky (Greenberg & Shen, 1999) when looking at the copious distribution of dark nebulae as was observed especially in the region towards the Milky Way galactic centre. Early astrophotography pioneer, E.E. Barnard reported a ubiquity of patchy dark cloud distributions, with remarkable structure, such as dark lanes and holes or gaps. Agnes Clerke (1903) was moved to pen the words, "The fact is a general one, that in all the forest of the universe there are glades and clearings. How they come to be thus diversified we cannot pretend to say; but we can see that the peculiarity is structural – that it is an outcome of the fundamental laws governing the distribution of cosmic matter. Hence the futility in trying to explain its origin, as a consequence, for instance, of the stoppage of light by the interposition of obscure bodies, or aggregations of bodies, invisibly thronging space."

In Publications of the Lick Observatory, Curtis (1918b) stated, "It has long been a matter of common knowledge that certain spiral nebulae seen edgewise show a dark lane running down the length of the spiral, an appearance generally explained as due to a band of absorbing or occulting matter." He goes on to say, "the occurrence of such dark bands in the spiral nebulae is a relatively common phenomenon."

Even before this, Slipher (1917) already noted, "It is well known that spiral nebulae presenting their edge to us are commonly crossed by a dark band." Furthermore, "It doubtless has its origin in dark or deficiently illuminated matter on our edge of the nebula." As enigmatic as the "occulting" material was, Slipher correctly proposed a way of determining the near-side of a galaxy by simply looking at its "dark band" morphology. He says that "if we view such a nebula from a point outside its plane the dark band would shift to the side and render the nebula unsymmetrical – the deficient edge [dark band] being of course the one nearer us."

The existence of these dark lanes also took centre stage in the famous Shapley-Curtis debate (Shapely & Curtis, 1921) on whether the dark lanes were indicative of obscuring matter. Curtis was very much in favour of the obscuring matter argument, while Shapely was more cautious in declaring that he had no evidence for such a contention when observing globular clusters. Shapley's argument was later deemed irrelevant because the globular clusters he observed were outside of the galactic plane, whereas the dark lanes and patches seemed very much confined to this "plane of avoidance".

While having been discussed at length at the turn of the 20th century, the idea of interstellar obscuring matter was not a new one. Already in 1847, Struve (Greenberg & Shen, 1999) had noticed that the number of stars observed per unit volume seemed to diminish in all directions outward from the Sun. There were two explanations. Firstly, the Sun was at the centre of a true "stellar condensation". Secondly, there was some sort of selection bias at work – something was progressively limiting the number of interstellar sources that were detected. This second explanation thus provided an argument that the observed dearth of stars at larger distances was only an apparent effect, and did not bear a true reflection on the actual stellar count in the solar neighbourhood and beyond. Even in 1904, Kapteyn had found a roughly spherical distribution of stars around the Sun. He then assumed the distribution was far more homogenous than what it had appeared and calculated an extinction parameter to quantify the observed effect. It is a tribute to him that his value of A = 1.6 mag per kpc is comparable to modern values, where Burton & Gordon (1976), for example, find an average A(V) ~ 2 mag per kpc in the galactic plane.

Later, Schalén (1929) reexamined stellar densities as a function of distance and noted that different values for the extinction coefficient were required for difference regions and in particular the extinction was higher in regions close to the large dark patches. But it was not until the work of Trumpler (1930) that evidence for interstellar reddening was conclusive. Trumpler compared the distances and luminosities of open clusters – his distance measurements were based upon the assumption that all cluster diameters were the same. By measuring their luminosities and knowing the spectral distribution of the cluster members, he calculated the colour excess as a function of distance. This led to a

reddening curve – and was prevalent even in regions where no obvious dark clouds were observed.

Whitford (1948) measured stellar colours versus spectral types and covered a wavelength range from about 350nm to the near-infrared regime. The observed spectroscopic response alluded to the possibility of explaining this phenomenon by means of small particle scattering theory.

1.2.2 Properties of Interstellar Dust Grains

Today we understand that the dark bands are veils of cosmic dust, and in order to fully appreciate their impact on galaxy morphology, it is very instructive to understand some of the physical properties of the mask. While the Infrared Astronomical Satellite (IRAS) revealed a new window on the near-infrared universe in 1983, predictions by Greenberg (1970) that there exist vast quantities of cold cosmic dust in galaxies, with typical temperatures of only 13 – 14 K, could not be verified with IRAS. These dust grains were far too cold to be radiating at near-infrared wavelengths. Cold cosmic dust was estimated to comprise at least 90% of the total dust mass of a galaxy – none of which was *directly* detectable in the near-infrared.

Galaxy morphology is inexorably intertwined with the presence of interstellar dust grains. Tracing of this interstellar dust has not been straightforward. The optical depths inferred from dust grain extinction can be quite misleading, since not all scattered starlight by dust implies a loss in surface brightness of a galaxy. Extinction by dust grains is due to absorption as well as scattering. The presence of a relatively high dust mass fraction does not necessarily imply a large decrease in the surface brightness profile, because scattering may fill in some of the intensity lost due to absorption. Surface scattering off the dust may attribute to an *increase* in the otherwise expected loss of apparent luminosity, as is the case with the reflection nebula discernable in NGC2841 as an amorphous linear strip transverse to the nearside minor axis, documented in Block et al. (1999). The nebula exhibits an identical spectrum to that of the Bulge light, and has been attributed to this

bulge light reflecting off a dense dust lane. The spectrum composition is typical of late type stars found primarily in the nuclear (bulge) region.

The naïve supposition that reddening in galaxies was a robust method of deducing the presence of cold cosmic dust was challenged by Witt et al. (1992), who showed that scattering in the radiative transfer process introduces a "bluing" effect. With sufficient amounts of dust, this bluing can result in almost neutral broad-band photometric colours.

Holmberg (1958) calculates that internal optical dust extinction effects are at a minimum for galaxies that are face-on in appearance (i.e.: perpendicular to the galactic plane), and increase in severity with higher inclination. There have been some challenges to this assertion, most notably from Disney et al. (1989) as regards dust distribution models discussed by Valentijn (1990) (essentially arguing that the extinction due to dust based upon optical thickness, is highly model dependent). However, most studies favour Holmberg's results.

That the wavelength of observation affects the observed morphology of spiral galaxies has been presented by Block & Wainscoat (1991) as well as Block & Puerari (1999) who describe these variations as a "duality of spiral structure" when optical observations are compared with those taken in the near-infrared. Buta & Block (2001) further describe, "A rich duality of spiral structure has been found from studies of optical and near-infrared images; a spiral galaxy may present two completely different morphologies when examined optically and in the near infrared." This duality was alluded to already by Burstein & Rubin (1985), who found that there was no correlation between their rotation form families and Hubble type. Galaxies of all Hubble types Sa, Sb and Sc could belong to the same rotation form family, with the implication that the underlying stellar mass distributions in an early as well as a late type spiral galaxy, may be similar.

1.2.3 Composition of Interstellar Dust Grains

In 1949, van de Hulst published results of compounds that could be synthesized out of atoms that were known to exist in the interstellar medium, such as H, He, C, N and O.

Van de Hulst assumed these atoms could combine on a surface to form frozen saturated molecules. This later became known as the "dirty ice" model. The dirty ice model was a logical follow up to the then existing models of how interstellar ices such as Methane (CH4), Ammonia (NH3) and water ice were formed. The theory had to wait however, until the advent of near-infrared imaging in order to be verified, by revealing silicate particles in emission at ~10μm in the upper atmospheres of cool stars. Conclusive evidence of the existence of these silicate particles thereby provided credibility to the idea that they are the cores upon which mantels of molecules could form.

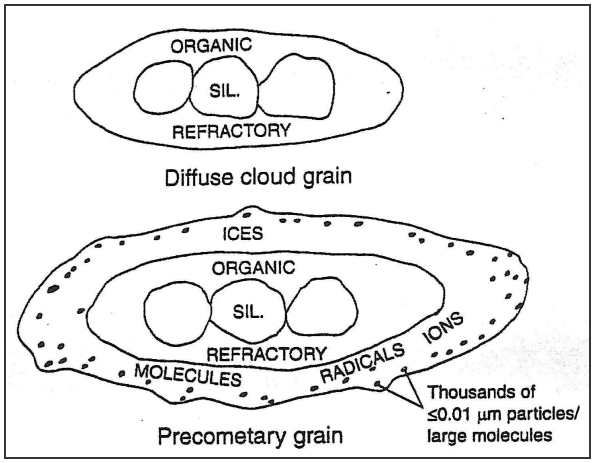

Figure 1.5: *Schematic of a dust grain found in diffuse clouds (top) and a precometary dust grain (bottom), with silicate cores. The refractory inner mantels of the two types of grains comprise organic molecules, and in the case of precometary grains, are covered with outer mantels of volatile ices, such as CH4, NH3 and water ice.*

The interstellar grains of dust in spiral galaxies comprise a dynamic range of sizes and physical properties. Typically dust grains are so small they resemble the constituency of smoke, being anything from true macro-molecules up to 10μm in size (Greenberg & Li, 1996). (See also the near-infrared albedo studies of Block (1996) and references therein.) It is these particles which are responsible for dust extinction and reddening in galaxies. Interstellar light traversing through a galaxy encounters these tiny dust grains and those whose wavelengths are shorter than the physical size of the dust grains, are preferentially absorbed. The longer, redder wavelengths are far less affected and when the radiation

wavelength approaches the near-infrared regime the attenuation due to scattering is less than 10% that of the optical passband at V (Rieke & Lebofski, 1985).

Over the past half century our understanding of interstellar cosmic dust has been revolutionized with the advent of three major breakthroughs in this regard. Our window on the ultraviolet and infrared regions of the spectrum has conclusively shown the range of dust particle sizes to be very wide. The infrared window furthermore provides a robust diagnostic on the constituents of these dust particles by revealing their chemistry spectroscopically. Thirdly, cosmic dust astrophysics can be performed in ground based laboratories, as was epitomized by the work of Greenberg.

These revolutions were by no means straightforward. The first attempt by Danielson et al. (1965) to find the 3.1μm spectroscopic feature of water ice was unsuccessful. This at first seemed a devastating blow to the dirty ice model. Greenberg (1972) took up the challenge to conduct ultraviolet photoprocessing of low temperature mixtures incorporating molecules which simulated the dirty ice grains, in order to understand the null result of the Danielson et al. observation. This research led directly to the prediction of complex organic molecules as mantels on silicate cores (see Figure 1.5).

It is precisely because of advances in infrared detector technology that the chemical properties of cosmic dust are able to be determined. The chemical constituents of these dust grains comprise silicates, ices and carbonaceous material. Moreover, it is believed that one of the most ubiquitous types of macromolecules proposed for tiny interstellar grains are polycyclic aromatic hydrocarbons (PAH). The variation in the relative proportions of these different constituents is one of the most important characteristics of interstellar cosmic dust. The spectral properties of cosmic dust in infrared emission provides a way of determining the size distribution of the dust particles as well as the typical intensity of the starlight to which the dust is exposed to. This provides a way for the total dust mass to be calculated (Draine & Li, 2007).

With the advent of the Spitzer Space Telescope, infrared emission spectra are now available with unprecedented sensitivity, and have been observed from a wide range of galaxy sizes and morphologies (Werner et al. 2004). It is in the 8.0μm passband that we detect the feeble glow of ultrasmall dust grains. What Keeler, Curtis, Hubble and others saw as enigmatic dark bands, are now strikingly visible in emission. It is principally the morphology of these transiently heated particles of dust which is addressed in this thesis.

This forensic approach to deducing the composition of interstellar cosmic dust requires an assumed dust model with the physical properties of the dust comprehensively specified. The models span three broad categories: (1) the silicate-graphite and silicate-graphite-PAH models, (2) the silicate core, carbonaceous mantle model and (3) the low-density silicate-carbonaceous particles model. Predicted parameters such as extinction, polarization and scattering are subsequently compared with observations. (For extensive references, see Draine & Li, 2007).

1.2.4 Warm cosmic dust

The general environment of dust particles is in a radiation field with copious ultraviolet radiation, but with a low energy density. Absorption of energy leads to heating of the dust grains. These dust grains absorb energy by absorbing photons and undergo temperature spiking. This energy is then re-radiated at infrared wavelengths. Grains with sizes of less than 250 Ångstroms harbour a typical thermal energy content comparable to that of a single starlight photon.

Each time a photon is absorbed by these macromolecules, the PAH temperature rises to a peak value. Greenberg & Li (1996) showed that a 40 Ångstrom-diameter dust particle absorbing a 6eV photon will rise to a peak temperature of about 68 K, before declining to about 21 K. Draine & Li (2007) show that smaller grains undergo far more extreme departures from equilibrium temperature, which is the temperature for which the rate of radiative cooling would equal the time-averaged rate of energy absorption. PAH's with diameters typically a = 3.55Å may reach T > 2000K, whereas larger grains (e.g., a = 300 Å) have temperature distribution functions that are very sharply peaked, corresponding to

only small deviations from an equilibrium temperature. It is primarily the emission from the warm (peak ~ 60 K) tiny dust grains whose emission is detected at 8.0 μm. The larger cold dust grains (20 K) emit their radiation at much longer wavelengths – the Kirchoff-Planck function for a grain temperature of 20 K peaks at about 180 μm. Figure 1.6 shows that for an increase in the rate of interstellar heating, the equilibrium temperature approximation becomes valid for smaller grains. The grain-radius below which single photon heating is important, and above which the grain temperature can be approximated as being constant, is the size for which the time between photon absorption and radiative cooling becomes equal. This condition is met when the size of the dust particle is such that its thermal energy is equal to the most energetic photons heating the dust grains (Li & Draine 2001).

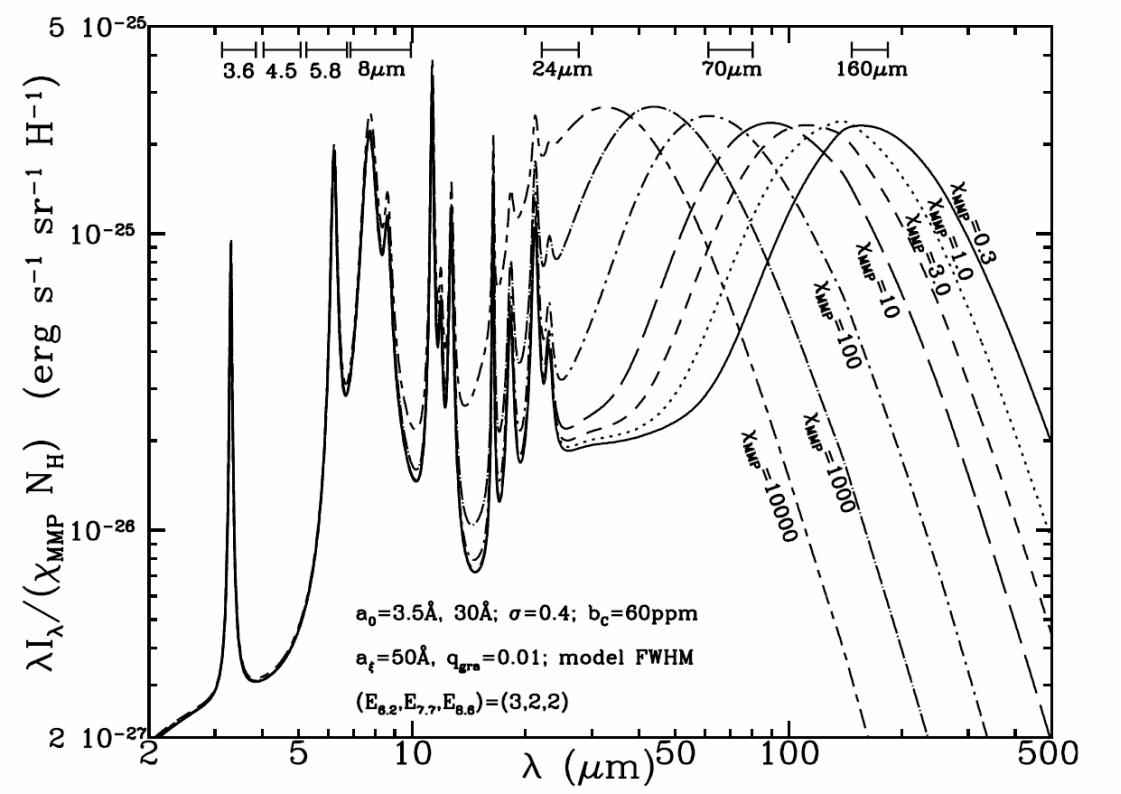

Figure 1.6: *Infrared spectra scaled by starlight intensity ($\lambda I_\lambda/(\chi_{MMP}N_H)$ as a function of wavelength (λ) for the standard grain model of Li & Draine (2001) for various grain illumination fields. The shape of the spectra remain essentially unchanged in the region λ < 15μm for star light intensities differing over 5 orders of magnitude. The same ionization fraction as the local diffuse ISM has been assumed. Wavelength coverage of the 4 IRAC bands and the MIPS bands on Spitzer are included.*

Ultraviolet photoprocessing of interstellar grains results in the chemical evolution of the dust mantels to ever increasingly complex organic molecules. Greenberg & Li (1996) estimate the ubiquity of such complex organic dust to comprise at least 20% of all the galactic dust mass. This chemical evolution takes place alternately in dense and low density clouds. Dense clouds contract gravitationally and become proto-stars. When thermonuclear reactions are induced, the resulting stellar-wind pressure drives the remaining *outlying* dust grains into the low density regions. Greenberg calculates the average time a typical dust grain is harboured in a dense cloud is of the order of 50 Myrs, with about an equal duration in low-density regions. With these timespans, the chemical evolution of dust mantels by ultraviolet photoprocessing is inevitable. A typical dust grain is consumed in stellar formation about once every 25 cycles. The small fraction of dust which barely escapes being a part of the protostar becomes protoplanetary disk material and is the constituent from which planets are made. Pristine remnants of such material are found in the form of comets. As such, comets in our solar system are the most primitive relics of original interstellar dust that was aggregated to form our solar system.

The evolution of dust particles is affected in various ways by stellar processes, and while photoprocessing is a method for increasing the chemical complexity of the mantels on silicate grains, they are also destroyed by evaporation in the proximity of hot star forming regions. These processes result in the production of carbonaceous particles typically 0.1μm in diameter, with a ubiquity which accounts for at least 1% of all the matter in the interstellar medium.

The origin of cosmic dust continues to be a very active field of research. High-z galaxies could only have created these complex molecules after the first generation of stars and the first supernovae. Due to the high redshift of these galaxies, it is the mid to far infrared domain (350 – 850 μm) which is expected to tell us the most about the origin of these dust particles.

1.3 Penetrating the Mask of Cosmic Dust

1.3.1 Galaxy classification in the 21st Century

For as mature and comprehensive as they are, all of the classification schemes discussed in §1.1 are firmly rooted in the photographic era. It is on this note that this thesis addresses the next generation of galaxy classification schemes and demonstrates the far more intricate interplay between the traditional "Hubble-based" classification and near-infrared morphology enshrouded beneath scores of galactic dust veils.

Sandage (2004) remarks, "The call now for making new classifications by introducing "physical morphology" into the classification … seems to me to be correct as long as one can avoid the slippery slope of a hermeneutical circularity." Is it this "hermeneutical circularity" that was discussed earlier in §1.1.1, which serves to short-circuit the power of any (un)worthy classification scheme. Any new classification that encompasses "physical morphology" must be free from intrinsic preconceptions, especially if that is what they are sought to explain. Sandage (2004) continues by saying, "In the initial absence of knowledge of an underlying physical explanation for the origin of the objects, how does the classifier begin when there is no a prior [sic] knowledge of an "explanation"" and continues "once a classification system is so mature and "good" so as to suggest an underlying physics, it must be consistent in its final form with whatever the final physics turns out to be." Hubble (1936) himself asserted, "The features must be significant … they must indicate physical properties of the nebulae themselves and not chance effects of orientation … and also they must be conspicuous enough to be seen in large numbers of nebulae."

1.3.2 Introduction to Near-infrared Morphology

Near-infrared imaging allows the dust mask to effectively be penetrated and therefore expose the stellar backbone comprising older Population I stars. Extinction due to dust at K band is only ~10% that in V (Martin & Whittet, 1990). The ubiquity of these older stars also presents a far smoother morphology than the younger population. Already evident in some of the pioneering work performed by Zwicky (1955, 1957), he notes that

underlying red stars appear far more organized than the blue population suggests for NGC5194. This is corroborated by Schweizer (1976) noting that the surface mass density of the older Population I component exhibits greater order as regards spiral structure. The mixing of main sequence stars with the giant population is very thorough, and so K band emission should be a faithful tracer of the underlying mass density (Depoy et al. 1996). Red supergiant stars, as well as young stars in general contribute less than 20% to the luminosity at K (Rix & Rieke 1993, Rix & Zaritsky 1995). This implies the galactic backbone ubiquitously harbours, almost without exception, an intermediate to old (1 ~ 10 Gyr) stellar population embedded in the disk. Zwicky's detection of grand design "red" arms in M51=NGC5194, highlighted that the established disk population need not identify regions where young Population I tracers are evident. Hot, blue stars, as well as OB associations and ionized hydrogen regions which comprise the younger Population I candidates, are most prominent in the U, B and V bands. At these wavelengths, dusty masks may completely obscure a significant fraction of the underlying older Population I component, and represent only 5% of the dynamical mass of a galaxy. As a result, the morphology of galactic disks is highly dependent on the dust content, since the optically-obscured older Population I backbone often displays a significantly, almost radically, different morphology. Furthermore, a fundamental limit exists on predicting what the infrared morphology of a galaxy would be, by looking exclusively at an optical image, and vice versa.

The dust-penetrated classification scheme proposed by Block & Puerari (1999) serves to address the challenge of providing a robust quantitative approach to the classification of galaxies observed in the near-infrared. Key parameters in the Block & Puerari scheme are spiral arm pitch (opening) angles and the dominant Fourier *m*-mode. Dust penetrated arms classes are grouped into three bins. These are labelled α, β and γ, and represent average spiral arm opening angles of ~10º, ~25º and ~40º, respectively. Block & Puerari (1999) have published a vertical three-pronged classification fork, in which each prong represents the arm classes, while the sequence moving down the fork, represents *stronger* torques (i.e.: galaxies with larger gravitational torques; discussed in §2.3 and §4.2).

A wide range of optical morphologies are accommodated by each of these classification bins, and it appears there is no correlation between optical Hubble type and dust-penetrated spiral arm classification. A number of examples, such as NGC718 versus NGC309 (Block & Wainscoat, 1991) exist, which are optically unmistakably distinct, however would fit well in the same classification category when observed in the near-infrared.

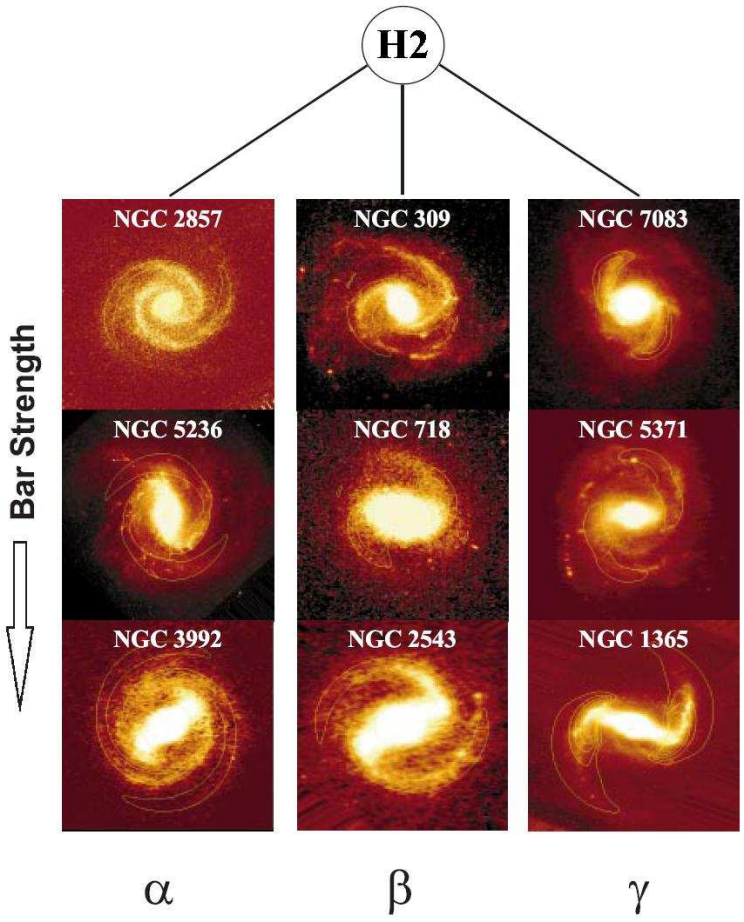

Figure 1.7: *The dust penetrated z ~ 0 tuning fork template by Block et al. (2001). Galaxies are binned according to quantitative criteria. The pitch angle families α, β and γ are determined from Fourier spectra (see §2.4) while the bar strength is derived from the gravitational potential (see §2.3). Examples of early type "b" galaxies NGC3992, NGC2543, NGC7083, NGC5371 and NGC1365 are distributed within all three families.*

The power of this classification method is twofold. Firstly, it is a *quantitative* classification scheme, where image processing performed by a computer provides an *objective* measure used to categorize the galaxy. Secondly, through the power of near-infrared window, there is a direct physical correlation with the classification bins (Seigar & James, 1998). The classification highlights the rate of shear in stellar disks. i.e.: The tightly wrapped spirals which would be classified as belonging to the α class, generally have falling rotation curves. The tightly wound arms are due to enhanced differential rotation with a larger shear. Dark matter is less prevalent in the outer reaches of such galaxies. Galaxies in class β and γ have correspondingly less shear, their arms are less tightly wound and their rotation curves are generally much flatter – which ultimately suggests a greater prevalence of dark matter.

While the dust penetrated classification fork (Figure 1.7) as proposed by these authors appears vaguely similar in construction to the Hubble-Jeans tuning fork, there is no correlation between the two, and Hubble type is totally independent of the near-infrared morphology.

Ron J. Allen (1996) summarizes this succinctly by stating, "We're now looking at a transition to a possible change in the way we look at galaxies. Sometimes … we see disks that have a spiral structure that we couldn't possibly have dreamt existed from looking at the optical picture … we've got the possibility here of applying the morphology to a physical framework, perhaps in a way that none of us could have dreamt of before we had the capability of sweeping the dust away [from galaxies] in a figurative sense."

1.4 Scope of this thesis

Exploration of the window on the near-infrared universe is very recent, compared with the photographic era, with true large format near-infrared detector arrays only becoming available from the early 1990s. There remains an important niche to classify the nearby near-infrared universe in terms of quantitative techniques, some of which are explored in this thesis. Furthermore, examples are provided that conclusively show that dust emission morphology may have little or no bearing on near-infrared and/or optical counterparts.

The importance of the near-infrared window in understanding spiral galaxies has resulted in numerous surveys/studies, such as, *inter alia*, Thronson et al. (1989); Wainscoat et al. (1990); Block & Wainscoat (1991); Peletier et al. (1994); Terndrup et al. (1994); Block & Puerari (1999); Buta & Block (2001); et al. The scope of this thesis involves lifting the younger Population I dust mask from the underlying older stellar backbone to reveal new views on the Triangulum Spiral galaxy, Messier 33 (Chapter 2) and the Great Nebula in Andromeda, Messier 31 (Chapter 3). This thesis also explores the morphology of dust grains in emission (at 8.0μm) and presents a relative gravitational torque analysis of 40 nearby spiral galaxies (Chapter 4). First time comparisons between dust-penetrated morphology and dust-in-emission maps from the Spitzer Space Telescope are presented in Chapter 5.

Numerical analyses in this thesis draw strongly from fast Fourier analysis techniques, which prove to be both elegant and concise for the gravitational torque calculations as well as dust-penetrated morphology quantification. This power is further exploited by providing a bar-spiral separation technique for some 40 nearly face-on barred galaxies, providing some results for answering the question, 'do stronger bars drive stronger spirals?' and gives further evidence for bar evolution scenarios being indicative of gas accretion in the outer disks of spiral galaxies.

This investigation is envisioned to pave the way for future higher-redshift surveys, particularly suited to rest-frame near-infrared morphology classification. This is in response to the diverse range of morphologies observed with deep surveys, such as the Hubble Deep Field and Ultra Deep Field. Many (most) of the galaxies observed fall outside traditional classification bins and may be very well suited to a near infrared scheme instead.

– CHAPTER 2 –

THE TRIANGULUM GALAXY AS A ROSETTA STONE FOR BUILDING GALACTIC DISKS

"How often have I said to you that
when you have eliminated the impossible,
whatever remains, however improbable,
must be the truth"
– Sir Arthur Conan Doyle

Based on:

Bar and Spiral Torques in the Triangulum Galaxy M33

Robert Groess, David L. Block and Ivânio Puerari

In 'Penetrating Bars through masks of cosmic dust', Springer New York (2004)

AND

Very Luminous Carbon Stars in the Outer Disk of the Triangulum Spiral Galaxy

David L. Block, Kenneth C. Freeman, Thomas H. Jarrett, Ivânio Puerari, Guy Worthey, Françoise Combes, **Robert Groess**

Astronomy and Astrophysics, 425, L37-L40, July 2004

AND

Keck spectroscopy and Spitzer Space Telescope analysis of the outer disk of the Triangulum Spiral Galaxy M33

David L. Block, Ivânio Puerari, Alan Stockton, Gabriela Canalizo, Kenneth C. Freeman, Thomas H. Jarrett, Françoise Combes, **Robert Groess**, Guy Worthey, Robert D. Gehrz, Charles E. Woodward, Elisha F. Polomski and Giovanni G. Fazio

Astronomy & Astrophysics, 471, 467, May 2007

2.1 Introduction

2.1.1 Early Descriptions of Messier 33

The Local Group of galaxies comprises approximately thirty members, three of which are large, spiral disks. These are the "Great Nebula in Andromeda" (Messier 31=NGC224), the Triangulum spiral (Messier 33=NGC598) and the Milky Way. Presumably discovered by Giovanni Hodierna in 1654, and later catalogued by Messier on 25 August 1764, the Triangulum Galaxy provides a crucial Rosetta stone in the bridge between the local universe and the high-z milieu, due to its close proximity (high angular resolution), relatively low inclination and semi-stellar bulge. In his description of nebulae and clusters photographed with the Crossley reflector at the Lick Observatory, Heber D. Curtis (1918a) described the Triangulum Galaxy as "a close rival to the Nebula of Andromeda" as "the most beautiful spiral known".

M33 provides an unique opportunity for studying the morphology of a disk galaxy almost devoid of a bulge. Morphologically, M33 has a flocculent (fleece-like) appearance at optical wavelengths (Sandage & Humphreys, 1980). This was already noted by Lord Rosse in his early drawings and moved him to exclaim "the whole nebula in [sic] flocculi". M33 is rich in star clusters, emission regions and supernovae remnants (see Hodge, Skelton & Ashizawa (2002) for a complete atlas of these), and harbours one of the largest HII regions known, classified as NGC 604 seen north-east of the galaxy in Figure 2.1. The stellar content of M33 has been discussed in detail by Humphreys & Sandage (1980) where these authors addressed the optical morphology such as the spiral pattern, the dust distribution, as well as the brightest resolved red and blue stars.

2.1.2 Optical Morphology of Messier 33

Optically, the disk of Messier 33 is considered to be the prototype for Sc(s)II-III galaxies, and has historically been the Local Group template by which other galaxies of this type of luminosity class are compared.

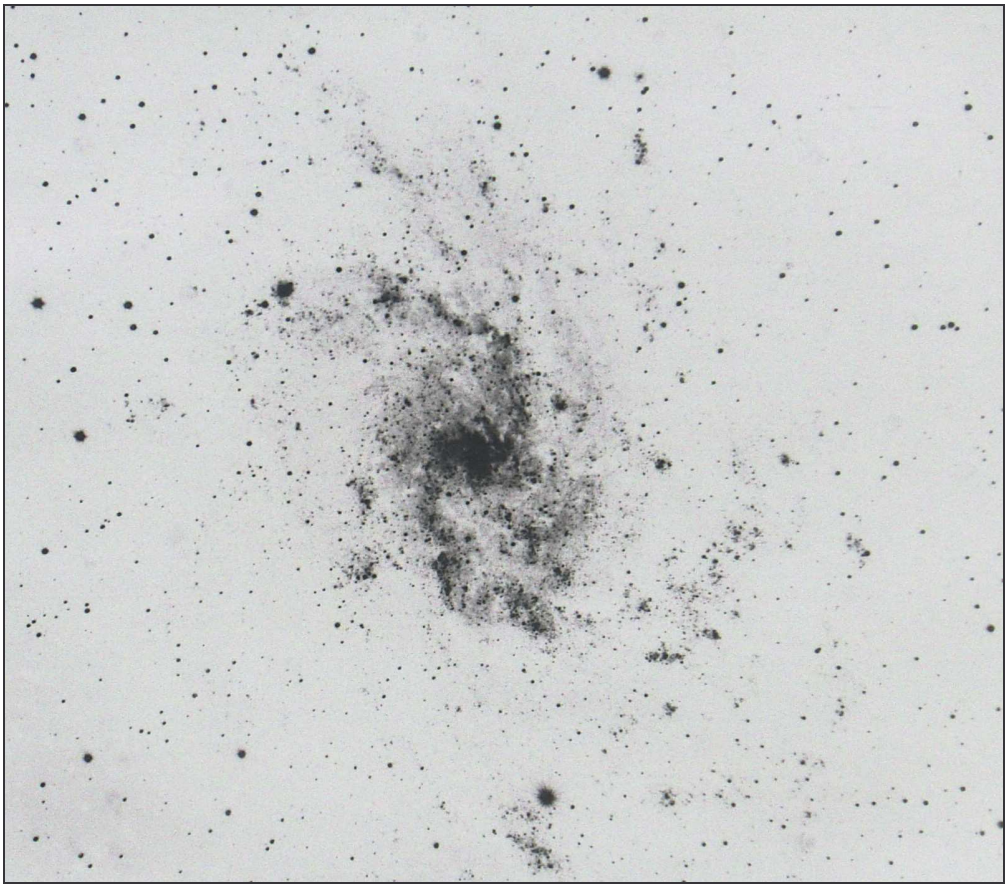

Figure 2.1: *The Triangulum Spiral Galaxy, Messier 33, as photographed by Keeler (1908), with north up and east to the left. NGC604, seen as a dark knot to the upper left of the galaxy, is one of the brightest HII regions known. The Triangulum galaxy extends over one degree along its major axis and its distance modulus of 24.64^m corresponds to a linear distance of 840 kpc (Freedman, Wilson & Madore, 1991). This implies a linear diameter of ~ 17 kpc, approximately one-half that of the Milky Way. M33 has an inclination of 53.9^o (logR_{25} = 0.23).*

While two prominent inner spiral arms are one of its most striking features, Sandage & Humphreys (1980) find that ten spiral arms are evident in deep optical images of M33. These authors write "The two main inner arms have a different projected geometry than the outer eight arms. This was interpreted as a warp of the spiral-arm plane, as in the tilted angular ring model of Rogstad, Wright and Lockhart (1976)." UBV photometry by de Vaucouleurs (1959) concludes that the inner spiral arms are trailing. Further developments regarding spiral arm classification have been developed by Elmegreen (1981) and Elmegreen & Elmegreen (1982, 1987) who have explored the symmetry and

continuity in the arms of spiral galaxies in depth, by devising a qualitative classification scheme based entirely on the optical morphology of spiral arms. The original Elmegreen & Elmegreen scheme consists of 12 distinct arm classes in a range from 1 through 12. Arm classes close to 1 represent "filamentary" or "flocculent" (fleece like) structured arms, namely spirals that have short, multiple, broken-up arms, while those at the opposite end of the scale are classified as being more "grand design" recognized by two long, well defined symmetric arms dominating the optical disk. Galaxies with long, continuous, "grand design" arms reveal a stronger bimodal symmetry than the more optically flocculent variants. An entire range of intermediate cases exist. As such, Elmegreen & Elmegreen (1987) place the Triangulum Galaxy in their class 5 bin, which represents "two symmetric, short arms in the inner regions" with "irregular outer arms".

2.2 Image Processing Techniques for Near-infrared Disk Galaxies

2.2.1 A Deep 2MASS Subsample of M33

A wide-field mosaic of M33 was created from a subsample of 2MASS observations in which the integration time was increased by a factor of six, thereby extending approximately 1 magnitude deeper than the nominal 2MASS survey (e.g.: Jarrett et al., 2003). Wide-field imaging of this galaxy is complicated by the extremely large angular diameter which it subtends as well as its relatively low galactic latitude. This poses a challenge as regards the ubiquity of foreground (Milky Way) stars, with the centre of M33 being placed at galactic coordinates of b=-31.33°, l=133.61°. Images at K_s band (2.17μm) reveal a typical density of foreground stars of about 1000 degree^{-2} down to 14th magnitude.

Three deep 2MASS mosaics of the M33 region were constructed (Block et al. 2004a), each covering an area of approximately 1 deg^2. The three mosaics correspond to the J (1.25 μm), H (1.65 μm), and K_s (2.17 μm) bands with a typical 1σ background noise of 21.9, 20.8 and 20.5 mag arcsec^{-2} for J, H and K_s respectively.

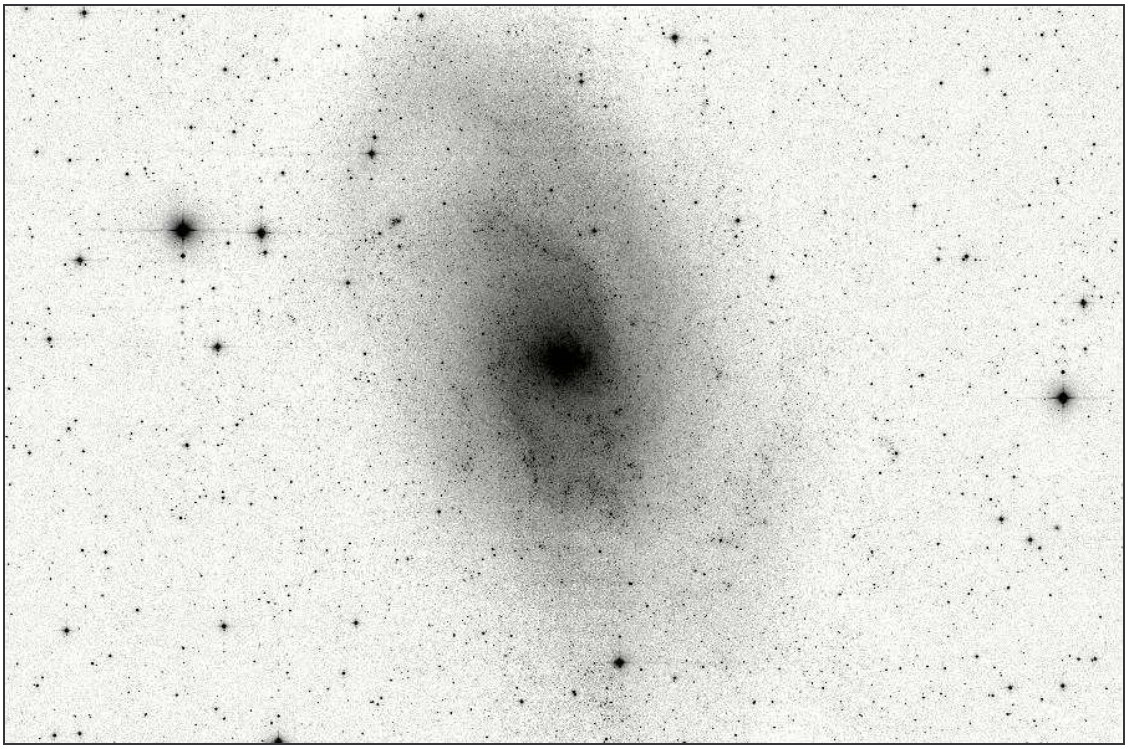

Figure 2.2: *A combined 2MASS JHK_s mosaic of M33, extending approximately 6 times deeper than the nominal 2MASS survey, revealing the underlying older Population I disk morphology with hitherto unprecedented spatial resolution at these passbands.*

One of the formidable challenges of ground-based near-infrared imaging is background subtraction, particularly for the H band, because of the highly variable atmospheric OH emission. This results in a typical aggregate sky brightness of 13 mag arcsec^{-2}. Consequently, each of the three mosaics include small-scale background systematics that are impossible to fully remove. These are not critical to the Fourier and gravitational torque analyses to be performed on these images. In order to enhance extremely faint surface features in the region observed, a "master" JHK_s mosaic was constructed by combining the three individual J, H and K_s mosaics (see Figure 2.2). The resulting combined mosaic reveals small, compact features as faint as 22.5 mag arcsec^{-2} (Block et al. 2004a).

2.2.2 Removal of Foreground (Milky Way) Stellar Sources

The deep M33 mosaic spans an area of approximately one square degree, which reveals ~7000 point sources, most of which are associated with the evolved stellar population in

the M33 disk. By contrast, the foreground Milky Way field stars are dominated by late-type G/K dwarfs. These two populations separate statistically in integrated magnitude due to the enhanced distance of M33 and in colour with the cool giant population belonging to M33 being redder by peaking at $J - K_s$ colours of 0.8 to 1.3 mag. The magnitude limits of point sources (stars) in the deep 2MASS image are K_s ~ 15.5 magnitude. These stars were stochastically isolated using the shape of the $J - K_s$ histogram by comparing the populations observed in flanking control fields to the east and west of M33, at the same galactic latitude. The first flanking star field was centered 2 degrees to the east of M33, with a total area of 0.864 deg^2. A total of ~2700 stars were found in this region. A corresponding flanking field was centered 2 degrees to the west of M33 and detected ~2600 stars. Differential star counts (magnitude versus number per magnitude per square degree) for each field were conducted with extrapolations of the east and west flanking field star counts to fainter magnitudes, so as to match the deep M33 region star counts. Both flanking fields were found to have roughly the same color distribution, and the average between the two fields was used to generate the $J - K_s$ colour histogram of the "foreground" Milky Way population.

Of the original ~7000 sources, ~2300 were removed as being likely to belong to the Milky Way down to 15th magnitude. This statistical distribution represents the foreground population of stars through which M33 itself is revealed and while not all stars in this grouping necessarily represent Milky Way members, the ensemble as a statistical whole provides an objective method for foreground star removal. Subtraction within the inner 0.01 deg^2 of the nucleus of M33 was avoided, where the population is completely dominated by M33 stars, and moreover the number-density confusion noise renders the stochastic photometry and colour number-density as very uncertain.

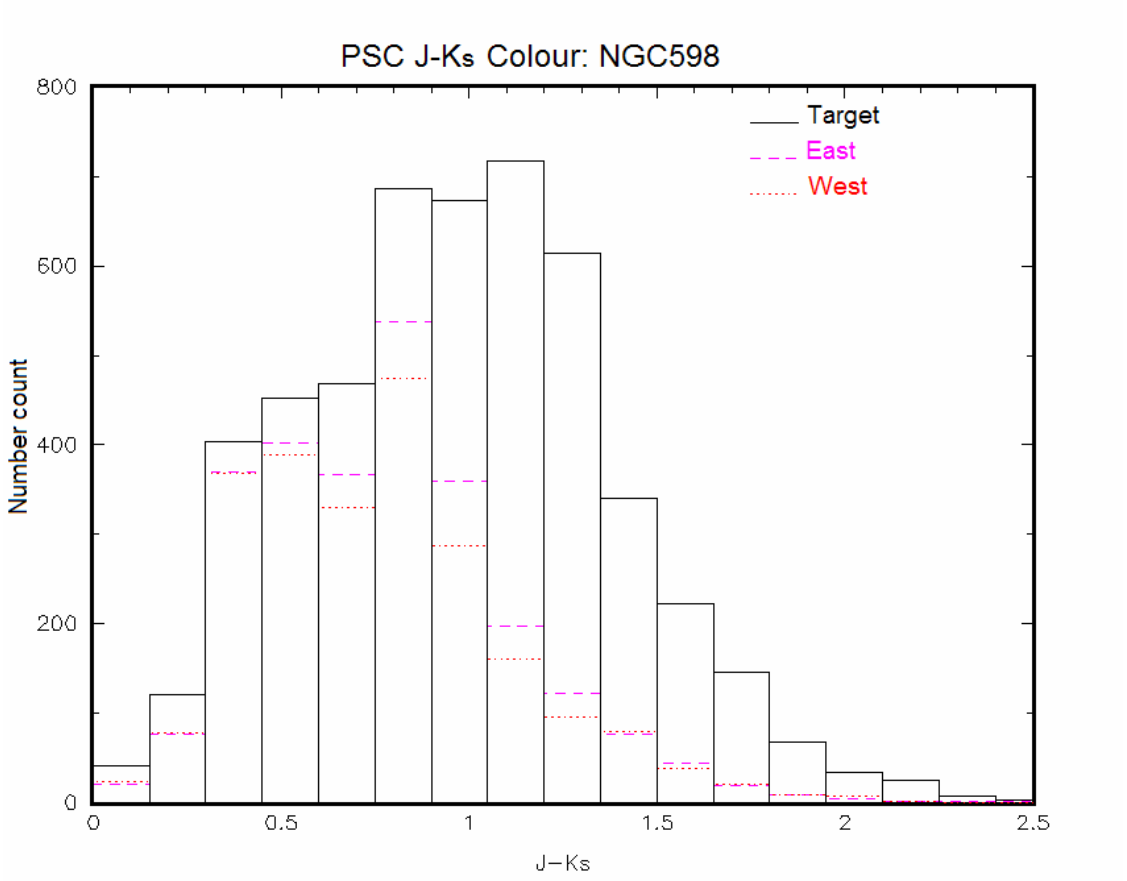

Figure 2.3: *Histogram of J – K_s Point Source Catalogue colours for stars in the M33 field – labeled as the target. Flanking fields 2 degrees east and 2 degrees west of the target represent the control number density of foreground Milky Way stars, the average of which were removed from the deep M33 mosaic. All counts refer to a 0.864 deg^2 area down to 15th magnitude at K_s.*

The 2MASS Point Source Catalog (available from the Infrared Science Archive) was used to construct the stellar J – K_s colours. Since the Point Source Catalog is not as deep as these image mosaics, photometry was conducted and colours extracted from the fainter sources in the M33 region, thereby supplementing the Catalog.

2.3 Gravitational Torques of Disk Galaxies

2.3.1 The Gravitational Torque Method

Before determining a gravitational bar torque for M33, the general methodology is introduced here. The near-infrared window affords a particularly powerful handle on the morphological classification of spiral disk galaxies. Bars in particular, are directly

responsible for the dynamics and morphology of galaxy evolution and affect a wide range of galaxy evolution mechanisms such as inducing gas inflows that promote bar destruction and rejuvenation, or drive spiral density waves that generate gas resonance-rings. These non-axisymmetric features are thus an integral part of galactic disk dynamics driven by gravitational torques prevalent in the backbone of these spiral disks.

Critical to the analysis is a constant mass-to-light ratio assumption. Confidence in this assumption is based on the work by Freeman (1992) and Mathewson et al. (1992) as regards near-infrared images of a wide range of Hubble types and therefore provide a way to study gravitational torques by means of Poisson's equation. Sanders & Tubbs (1980) and Combes & Sanders (1981) proposed that the ratio of the tangential force with respect to the mean axisymmetric background radial force could be used to provide a quantitative measure to gauge relative gravitational torque strength. It is on this basis that Buta & Block (2001) pioneered the Gravitational Torque Method (hereafter, GTM) used in this thesis. Gravitational torque analysis is based on deprojected images of galaxies; spirals with high inclinations cannot be subjected to a gravitational torque analysis.

Removal of foreground Milky Way stars can usually be facilitated by means of using the IRAF routine IMEDIT, with the exception of a few wide field galaxies, such as Messier 33. (See the discussion on foreground star removal in §2.2.2)

The gravitational torque method relies on some basic assumptions. These are as follows:

(a) Spiral galaxies can be deprojected to circular disks.
(b) Near-infrared spiral disk surface brightness follows a constant mass-to-light ratio.
(c) The vertical density profile is exponential where the vertical scaleheight is denoted h_z.

As regards assumption (a), disk galaxies are assumed to have circular outer isophotes, so that they can effectively be deprojected to face-on, provided that their inclination angle is not too extreme ($\leq 65°$). Pertinent parameters thus required are the position angle (hereafter PA) and inclination of a particular galaxy. Inclination is measured as the angle

by which the galactic plane has been tilted along its line-of-nodes, with respect to the observer's line-of-sight. PA is the angle between the line-of-nodes through the disk, swept out eastwards from north.

Inclination can be determined from photometric axial ratios (b/a) where kinematic data from spectroscopic studies readily facilitates a more accurate determination of the position angle, by providing the orientation of the line of nodes. Improved kinematic studies and a wider range of imaging passbands also provide a more accurate handle on the orientation of galaxies particularly suited to the GTM. Although it is a first order idealization to believe that disks are actually circular when deprojected, the uncertainties introduced by such an assumption have been explored by Block et al. (2002). In particular these authors determined that the mean difference in torque values calculated from observed galaxies in their sample of 163, when compared with numerical simulations that were randomly oriented and then "deprojected", is $<\Delta Q_b> = 0.007$. Interacting/merging systems are not dealt with in this thesis.

Assumption (b) is entirely reasonable for the types of galaxies described in this thesis, although would not be valid for dwarf galaxies because of their extensive dark matter halos (Freeman, 1970). Weiner (1998), for example, shows that the inner regions of the disk of NGC 4123 must be near 90% - 100% of the required maximum disk forcing. The M/L assumption is supported by detailed rotation curve studies and multi-band near-infrared surface photometry performed by Freeman (1992) and Mathewson et al. (1992). This suggests that near-infrared light is a representative tracer of mass within the disks of spiral galaxies.

The process of deriving gravitational potentials from near-infrared images is reviewed by Quillen (1996). Given a nearly constant-M/L assumption, the two-dimensional potential can be derived as the Fast Fourier Transform convolution of the mass density with 1/R (Binney & Tremaine, 1987). The gravitational torque method does not require photometric calibrations, since the torques are calculated relative to the mean axisymmetric background gravitational field. The degree to which background effects

influence the analysis is dependent on the location of the relative torque maxima in a galactic disk. Most galaxies exhibit these maxima near the inner regions of the disk, dominated by the high luminosity contribution of the bulge or bar. The GTM manifestly measures torques only due to the luminous contribution of galaxies, and does not take any dark matter considerations into account. The maximum torques however, are usually obtained well towards the inner regions of the disk, where dark matter effects are not important.

The effects of assumption (c), that galactic disks exhibit an exponential scaleheight, as opposed to other functional such as sech (z) dependencies, has been investigated by Laurikainen & Salo (2002) who show the gravitational torque method to be fairly insensitive to different forms of the vertical density distribution. One of the principal uncertainties is that vertical scaleheights are essentially unknown for preferentially face-on galaxies. In the detailed analysis presented in §4.3.3, gravitational torques for 40 nearby galaxies are calculated based upon assumed scaleheights of 225pc, 325pc and 425pc, respectively – values that have been adopted by Gilmore & Reid (1983) and Buta & Block (2001). The effect that the assumed scaleheight variation has on a galaxy is to *increase* the gravitational torque strength for a given *decrease* in scaleheight (and vice versa). Buta & Block (2001) find an average torque uncertainty of ± 13% for a ±100pc uncertainty in scaleheight. i.e.: Uncertainties in the scaleheight range of 225pc/325pc/425pc, move a galaxy by one gravitational torque class at most; most galaxies are shown to remain in the same class through this range in assumed scaleheight. These scaleheights require an exponential vertical density profile lookup table, which has been provided and further modified by Laurikainen & Salo (2002), as used in this thesis.

Future refinements to this assumption can be made by incorporating the scaleheight/Hubble-type dependence on the ratio h_R/h_z, found by de Grijs (1998). Late-type spirals have, on average, thinner disks than their early-type counterparts. As a result, the ratio is larger for late types. De Grijs shows that highly inclined disk galaxies in the K'-band (2.1μm) exhibiting these distributions are more peaked than expected for a *sech(z)* distribution, but are smoother than an exponential one. The strongly asymmetric

red-to-blue (V – K) colour profiles found along the minor axes of a large proportion of spiral galaxies, such as NGC 2841 (Elmegreen & Block, 1999), may be accounted for in disks that are *exponential* in the radial and perpendicular directions. Future studies could furthermore improve the scaleheight determination by scaling from values of the radial scalelength as expressed in Quillen, Frogel and Gonzalez (1994).

2.3.2 Gravitational Potential and Force Ratio Maps

Star cleaned, deprojected images are cropped to a 2^n square pixel array, for use in image processing code written by Quillen, Frogel and Gonzalez (1994) (hereafter, QFG), which transforms near infrared images into a two-dimensional potential. The tangential (F_T) and radial (F_R) components of the forces calculated can hence be calculated. The analysis performed operates on the ratio map $Q(i,j) = F_T(i,j)/F_{0R}(i,j)$, where F_T is the tangential force and F_{0R} is the mean axisymmetric radial force, derived from the $m=0$ component of the potential.

Figure 2.4 shows the force ratio map for M33. The effects of both the spiral arms and the bar are clearly evident. The small, yet clearly defined "butterfly" pattern (Buta & Block, 2001) is a characteristic signature of a (mini)bar and the additional structure is due to the spiral arms. Furthermore, the structure in the force ratio map alternates by quadrants with two positive maxima and two negative maxima at each radius. Buta & Block (2001) allowed for asymmetry in the bar by deriving a value of $|Q_{T(max)}|$ in each quadrant, and then averaging these four values to get a single gravitational torque Q_g for the galaxy. In the case of a bar, a symmetric “butterfly” pattern for these maxima/minima is found. Spiral arms reveal a more complex force ratio signature. At each radius, the values of $|Q_{T(max)}|$ were averaged as before, however the maximum force ratios are typically found at larger radii. The ratio maps are subsequently used to derive a single value that characterizes the gravitational torque strength. To this end, the torque value Q_g, is the maximum of the individual torque ratio maxima computed as a function of radius.

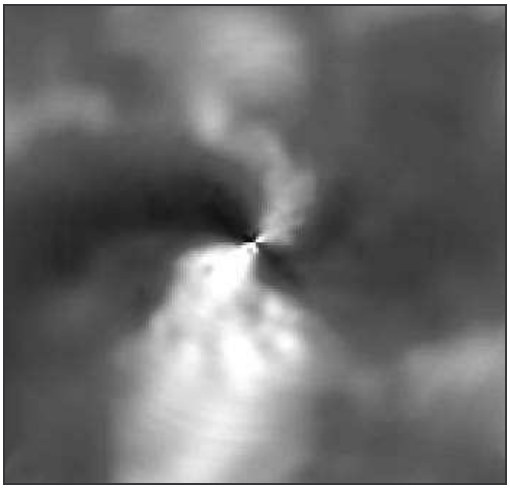

Figure 2.4: *Force ratio map of M33. The butterfly pattern is a distinct signature for the presence of a (mini)bar in the central region of this galaxy. Extreme dark and light areas denote the maxima/minima of the force ratios in each of four quadrants.*

2.3.3 The Gravitational Torque Parameter Q_g

In particular, for a given radius R, the relative gravitational torque is defined as:

$$Q_g(R) = \frac{F_T^{\max}(R)}{< F_R(R) >} \tag{2-1}$$

where

$$F_T^{\max}(R) = [\frac{\partial \Phi(R,\theta)}{\partial \theta}]_{\max} \tag{2-2}$$

$F^{max}{}_T(R)$ represents the maximum amplitude in the tangential force at radius R and

$$< F_R(R) >= R(\frac{d\Phi_0}{dR}) \tag{2-3}$$

is the mean axisymmetric radial force at the same radius, given by the m=0 gravitational potential Fourier component. This method assumes an exponential vertical scale height and a constant mass-to-light ratio, as discussed above.

The resulting gravitational torques can be quantitatively classified into a sequence of contiguous torque classes, where each class {*0,1,2,..,7*} is defined by galaxies having relative torques of Q_g = *0.00, 0.10, 0.20, …, 0.70 ± 0.05*, respectively. e.g.: A Q_g of *0.10±0.05* represents a tangential force reaching 10% of the axisymmetric background radial force. In the particular case where the gravitational torques of bars are calculated, the gravitational torque classes are referred to as *bar classes* and are defined in exactly the same way. It is possible to actually separate the gravitational torque from bars and from spiral arms themselves, as explored later in this thesis (§4.2.2).

Class	Q_g Range
0	<0.05
1	0.05-0.14
2	0.15-0.24
3	0.25-0.34
4	0.35-0.44
5	0.45-0.54
6	0.55-0.64
7	>0.64

Table 2.1

2.3.4 Error Analysis of the GTM

The errors given in the gravitational torque calculation are derived from the relative errors in adjacent quadrants. These are usually small for highly-symmetric bar-like features and progressively get more extreme as the symmetry of a galaxy weakens. The errors quoted on the Q_g measurements are the mean error in the difference of the Q_g values across the quadrants for a given galaxy. Galaxies that are particularly symmetric have intrinsically low errors for their Q_g determination, while correspondingly more lopsided spiral arms introduce a higher mean error. The reader is referred to Buta & Block (2001) for a more detailed description on the error analysis of the GTM.

2.3.5 Gravitational Torques in the Stellar Backbone of Messier 33

Initial deprojection of the deep JHK_s 2MASS mosaic was performed after centering the image with respect to the galaxy centre. The position parameters adopted were $logR_{25} = 0.23$ (RC3) where R is the galactic major/minor axis ratio, and $PA = 23$ degrees (Deul & vd Hulst, 1987 and Regan & Vogel, 1994). The image was furthermore resized (down-sized, due to computer memory constraints) and cropped to a $2^{10} = 1024$ square pixel array before the QFG code was applied.

This analysis confirms the presence of the famous two inner trailing spiral arms. (The winding sense of these arms is opposite to the direction of rotation of the galactic disk.) The Fourier intensity amplitude $m = 2$ component rises sharply as a function of radius to a peak near 80 arcsec, and drops off until about 300 arcsec, indicating the presence of a bar. Higher even harmonics (m = 4 & 6) corroborate well with this feature, although are much smaller in relative amplitude.

The calculated gravitational torque is found to be $Q_g = 0.22$, thus placing M33 into a gravitational torque class of 2. Subsequently, a bar/spiral decomposition (see §4.2.2 for a detailed description of this technique) reveals the presence of a small bar or oval with $Q_b = 0.21$. The separated spiral arms torque has $Q_s = 0.15$. It is a useful cross-check to see that the individual bar and spiral arms torque do not exceed the total gravitational torque Q_g of the galaxy.

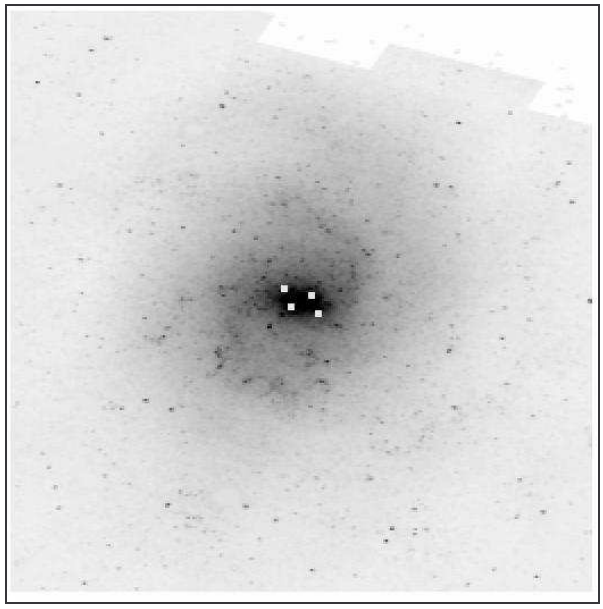

Figure 2.5: *A deep deprojected JHK_s 2MASS image of M33, where the GTM (with further bar/spiral separation – see §4.2.2) reveals a class '2' bar. The gravitational bar torque maxima (white squares) have been superimposed on the inner oval/bar.*

2.4 A Fourier Approach to Calculating Spiral Arm Pitch Angles

2.4.1 A Dust Penetrated Spiral Arm Classification

Optical images of spiral arms invariably show dense ridges of interstellar dust interspersed with hot, blue OB stars. While the focus of the Hubble and de Vaucouleurs schemes are in the *optical* regime, the morphology of the *stellar backbones* can be successfully examined using near-infrared detectors. These near-infrared images can be deprojected and subjected to Fourier methodology, where pitch angles can be determined.

Block & Puerari (1999) proposed classifying evolved stellar disk morphology into three principal dust penetrated archetypes. The bins are designated α, β and γ which correspond to spiral arm opening angles of ~10 degrees, ~25 degrees and ~40 degrees, respectively. This dust penetrated scheme has no correlation with the Hubble scheme, as indeed the Hubble-Jeans tuning fork does not constrain the older Population I stellar disk morphology. This is particularly evident when comparing, for example, the dust penetrated morphology of NGC309 at K´ band with a V-band image of NGC718.

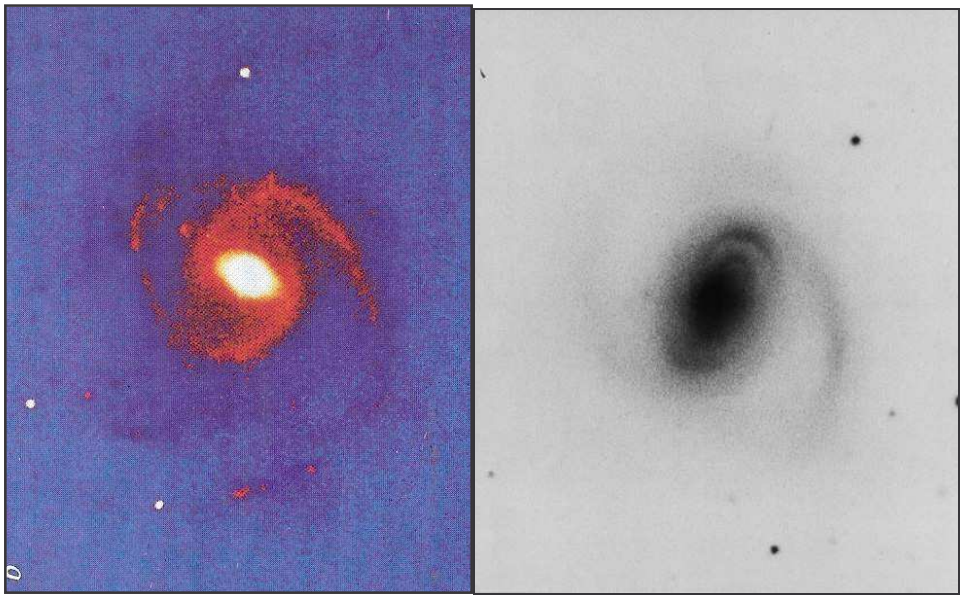

Figure 2.6: *A 2.1μm image of NGC309 (left) and an optical image of NGC718 (right) taken with the 5m Hale reflector. Both exhibit the same number of arms with very similar pitch angles (18° and 24°, respectively), even though they are classified as Sc and Sa in the Hubble scheme, respectively (Block & Puerari 1999).*

The spiral arm pitch angle is related to the mass distribution and rate of shear. Galaxies that have a higher central mass concentration, and hence a higher specific density, together with a higher rate of shear, would exhibit more tightly wound arms. Angular momentum redistribution by large-scale spiral torques will be stronger for stellar arms with a larger pitch angle. Pfenniger et al. (1996) have postulated that this would lead to significant morphological changes in the disk over one Hubble time – which leads to the concept of *secular evolution*.

2.4.2 Description of the Fourier Coefficients A(p,m)

The Fourier method offers an excellent mathematical technique for quantifying spiral structure in terms of modes. Many galaxies exhibit a lopsided m=1 mode in the near infrared. Linear modal theory (Bertin, 1996 and references therein) however is in favour of an m=2 mode being responsible for more efficient outward angular momentum transport. Modes greater than m=2 are prone to suppression in the stellar disk by the inner Lindblad resonance (ILR). A Lindblad resonance occurs when:

$$\Omega_p = \Omega \pm \frac{\kappa}{2}$$

(2-4)

where Ω_p is the precession rate or pattern speed, Ω the angular frequency of circular rotation and κ the radial epicyclic frequency. An inner Lindblad resonance (ILR) occurs when:

$$\Omega_p = \Omega - \frac{\kappa}{2}$$

(2-5)

The gas content of a galaxy is very important in these considerations, because gas-rich spirals can accommodate modes larger than m=2. Multi-armed features are expected to be seen in the optical domain due to the high responsiveness of the gas, but in the near-infrared the stellar disk invariably shows only the dominance of low order modes (m=1 and/or m=2).

In the Fourier method, an image is decomposed into a basis of logarithmic spirals of the following form where r and θ are polar coordinates, m is the mode number or number of spiral arms and p relates to the pitch angle as defined in equation (2-8):

$$r = r_0 e^{\frac{-m(\vartheta)}{p}}$$

(2-6)

Considère & Athanassoula (1988) note that the method does not assume that the observed spiral structures are always logarithmic, but analyses the observed light distribution as a superposition of logarithmic spirals.

Here the Fourier coefficients *A(p,m)* can be expressed as:

$$A(p,m) = \frac{1}{D}\int_{-\pi}^{+\pi}\int_{-\infty}^{+\infty} I(u,\theta)\exp[-i(m\theta + pu)]dud\theta$$

(2-7)

Where r and θ are polar coordinates and $u := ln(r)$. The number of spiral arms is written as m and p relates to the pitch angle P as follows:

$$P = \arctan(\frac{-m}{p}) \tag{2-8}$$

$I(u, \theta)$ is the intensity map from a given (deprojected) galaxy, in $(ln(r), \theta)$ space.

The normalization factor, D, is defined:

$$D = \int_{-\pi}^{+\pi}\int_{-\infty}^{+\infty} I(u,\theta)dud\theta \tag{2-9}$$

The numerical calculation of the integrals in $u := ln(r)$ are performed from a minimum radius (selected to exclude the bulge/bar region) to a maximum (being the outer isophotes from the spiral arms in the images analysed).

The above theory is thus numerically modeled as:

$$A(m,p) = \frac{\sum_{i=1}^{I}\sum_{j=1}^{J} I_{ij}(\ln r,\theta)\exp(-i(m\theta + p\ln r))}{\sum_{i=1}^{I}\sum_{j=1}^{J} I_{ij}(\ln r,\theta)} \tag{2-10}$$

The inverse Fourier transform can be expressed as:

$$S(u,\theta) = \sum_{m} S_m(u)e^{im\theta} \tag{2-11}$$

Where:

$$S_m(u) = \frac{D}{e^{2u}4\pi^2}\int_{p-}^{p+} G_m(p)A(p,m)e^{ipu}dp \tag{2-12}$$

With $G_m(p)$ being a high frequency filter to smooth the $A(p,m)$ spectra at the interval boundaries (Puerari and Dottori, 1992):

$$G_m(p) = \exp[-\frac{1}{2}(\frac{p - p^m_{\max}}{25})^2]$$

(2-13)

Here $p^m{}_{max}$ is the value for p attained for a maximum amplitude for a given m. See Block & Puerari (1999) for detailed examples.

2.4.3 Fourier Detection of a Faint Stellar Arc in the Outer Disk of M33

Fourier analysis confirms the presence of a large northern arc of stars spanning 120 degrees in azimuth about the outer disk. This arc is approximately 5' in radial width, at a galactocentric radius of ~ 14' - 19' (3.4 - 4.7 kpc) north of the bulge. This corresponds to a radius of approximately 2-3 disk scale lengths. (Ferguson et al., 2006, give the V disk scale length to be 0.1 degrees.) There is also a fainter counterpart to this arc in the south. These arcs dominate the Fourier spectra at J, H and K_s even though the mean surface brightness in the arcs at K_s is only 20-21 mag arcsec^{-2}, accounting for their lack of previous detection.

In the near-infrared M33 does not present ten arms as it does in deep optical images. The only dominant modes are m = 1 and m = 2 at J, H and K_s and the decoupling between gaseous and stellar disks is likewise only partial. The two inner 'grand-design' trailing spiral arms seen optically are prominent but are not dominant in the near-infrared regime, with a computed pitch angle of ~ 14 degrees. The inner sets of near-infrared arms are also evident in Regan & Vogel (1994) (see their Figures 1 and 3).

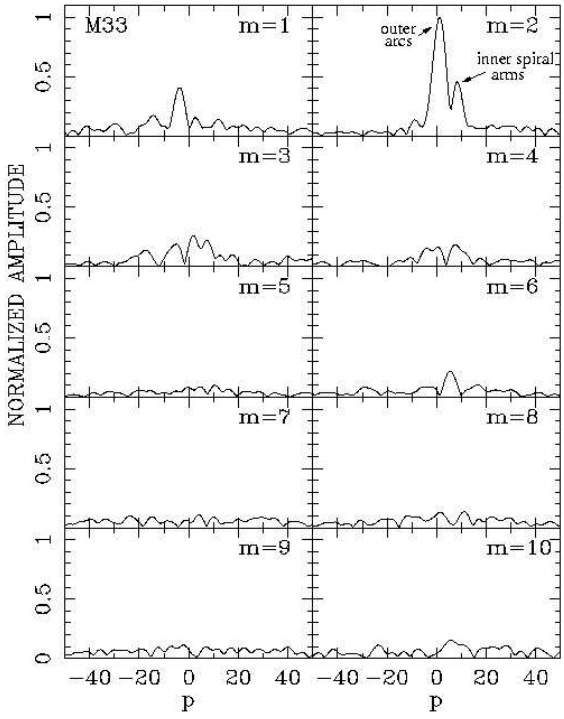

Figure 2.7: *Normalized amplitude versus pitch angle of Fourier modes m=1 through m=10. The dominant peak at m=2, where $P_{max} \neq 0$, reveals the presence of two large open outer arcs hitherto undetected. The smaller peak is a signature of the inner 'grand design' spiral arms.*

Of greatest interest however, is the dominant and very high m=2 peak. The peak does not occur at $P_{max} = 0$ (as expected for bars, for example, with pitch angles of ~ 90 degrees). Rather, the dominant m=2 peak corresponds to a set of giant arcs (very open spiral arm structures) on both the northern and southern regions of the outer disk. The northern arc is the more dominant one, with a pitch angle of ~ 58 degrees. It is these outer arcs which dominate the m=2 Fourier spectra, and not the inner grand design structure for which M33 is so famous.

2.5 The Case for Giant Arcs of Carbon Stars

2.5.1 Colour – Colour Photometry of the Outer Disk of M33

The colour of the arcs are extremely red, ranging from J-K_s = 0.8 magnitude to 1.2 magnitude (Block et al., 2004a). The redness of the arcs cannot however be attributed to extinction by dust. Freedman et al. (1991) obtain E(B- V) = 0.10 ± 0.09 magnitude, which included both foreground (Milky Way) and internal M33 extinction while K_s band extinction is approximately one-tenth that of optical passbands (Rieke & Lebofsky, 1985). Therefore A(K_s) is estimated to be only ~ 0.03 magnitude.

2.5.2 Keck Spectroscopic Verification of Carbon Stars

Of the three largest spirals in the Local Group, Messier 31, the Milky Way and Messier 33, each are known to have a definitive warp. In the case of M33 this warped envelope is prominent in the neutral hydrogen HI-21cm line commencing at a radius of about 5 kpc, with a notable asymmetric extension toward the North-West (e.g.: Corbelli & Schneider, 1997). At a radius of about 10 kpc the neutral hydrogen gas rotation axis is inclined by some 40 degrees with respect to the axis of the inner disk (Rogstad et al., 1976). Corbelli & Schneider (1997) confirm that at a radius of 5 kpc (about 3 disk scalelengths), a distinct change in inclination of the HI distribution in M33 is observed.

The NW extension may be a betrayal of tidal interactions between M33 and M31, which are only ~ 200 kpc distant. In their modeling of the HI envelope, Corbelli & Schneider found the phase to change at a radius of ~ 20 arcmin, which is precisely the outer domain of the arcs. It seems highly plausible from this argument alone, that fresh, low-metallicity gas is being fed to the host galaxy (M33) via external accretion. The outer disk from which mass is accreted is inclined to the inner disk of M33 and has a different angular momentum. While warps may be tidally generated in the proximity of companions, galaxies such as M33 do not have any nearby companions. In this case, warping and gas infall may be inextricably linked, as discussed by Binney (1992). Confirmation of whether the M33 HI-warp is induced by the infall of gas would be provided by the presence of a red, intermediate age (0.6 - 2 Gyr) population of carbon stars. This is because carbon stars are expected to be associated with recent star formation. Tsalmantza

et al. (2006) have found a carbon star population near the centre of the LMC as well as in the spiral arms in M31, the loci of star formation. The carbon star sample size in the SMC and in M33 was too small for these authors to trace their radial distribution. Rowe et al. (2005) however found them relatively more abundant in the outer parts of M33. Block et al. (2004a) propose that formation of the very red stars in the arc was precipitated in the outer disk relatively recently (between 0.6 Gyr and 2 Gyr ago), but the question of whether this occurred in bursts or in a continuous process cannot be differentiated from the J - K_s colours.

While the near-infrared regime is usually exploited in terms of minimal dust extinction, it is precisely here that carbon stars can contribute critically to our understanding of intermediate age clusters as well as the building and accretion processes of galactic disks. The true extent to which carbon stars contribute towards the outer-disk luminosity of evolving spiral galaxies has not hitherto been investigated from a morphological perspective. It is precisely for this reason that M33 serves as a profound Rosetta stone as it reveals spectacular arcs of carbon-rich stars in its outer disk. The reason attributed as to why the Fourier spectra have preferentially identified the large carbon-star-bearing arcs, as opposed to the central regions of the M33 disk, is due to sustained ubiquitous star formation in the arcs. In the first few Myrs, red supergiants dominate the integrated luminosity at near-infrared wavelengths, while carbon stars will dominate later with ages of between 0.6 and 2 Gyr. After that, ordinary red- and asymptotic giant branch stars dominate. In the case of M33 however, the carbon stars clearly dominate and the accreted gas from the outer regions has not had time to be transported to the inner disk. Presumably older populations dominate the inner disk, where the signature of TP-AGB stars at K band weakens considerably.

The methodology by Block et al. (2004a & 2007) differs from conventional ways of photometrically identifying carbon stars using intermediate band filters (such as V, I, 77, 81), as presented by Rowe et al. (2005) for M33, using the Canada-France-Hawaii Telescope (CFHT). The (V, I, 77, 81) photometric method was pioneered by Cook, Aaronson and Norris (1986) and requires a large enough telescope to resolve individual

stars. The three Sloan filters g, r, i, as used by Demers & Battinelli (2005) to identify 361 new carbon star candidates in M31 are another way to identify carbon stars. Resolution of individual stars however remains crucial.

Tsalmantza et al. (2006) identified carbon stars on the basis of their red J-K_s tail. This methodology can potentially be exploited to identify carbon stars in spiral galaxies well outside our Local Group with moderate sized telescopes, where individual stars are not resolved.

Rowe et al. (2005) have identified carbon and M-type stars in AGB populations and traced the carbon star to M-star ratio (C/M) as a function of radius. This spatial C/M-star ratio map reveals striking maxima at exactly the positions of the "arcs", or outer spiral arms of M33. The C/M ratio is an index of both age and of metallicity, whereby age increases in metal-poor regions. These authors' interpretation of the radial distribution of the C/M ratio uniquely as a metallicity indicator leads them to conclude that there is a strong metallicity gradient which spans most of the disk up to and including the outer spiral arcs at 5kpc (20 arcmin). This interpretation is based upon the viscous disk model, whereby the outer shear of the rotation curve drives mixing in these outer parts which are able to diffuse localized abundance gradients.

In M33, the "viscous disk" model applies up to a radius of 5kpc, which is sufficient to include the outside of the arcs, and is the radius up to which the optical disk is exponential. It is also likely to be the mechanism with which the accreted gas from the warped disk is utilized in star, and inner-disk, formation. The flattened metallicity gradient could be linked to the accretion of low-metallicity gas. The viscous accretion disk model is used to build exponential galaxy disks, either with viscous torques for angular momentum exchange, or with gravitational torques due to spiral arms or bars. If the viscous and star formation time scales are of the same order, then the resulting stellar disk has an exponential distribution independent of the disk rotation law and of the assumed viscosity prescription. Tsujimoto et al. (1995) have calculated that the expected metallicity gradient would also be exponential.

The Block et al. (2004a) JHK_s photometric method uses the fact that the colour of the northern arc extends to very red colours of $J\text{-}K_s > 1.1$. These authors argue that while very old M giants of solar abundance can plausibly reach $J\text{-}K_s \sim 1$ (see Figure 2 in Bessell & Brett, 1988) and even redder if they are super-metal-rich (see Frogel & Whitford, 1987), stars with $J\text{-}K_s > 1$ in low-metallicity regions cannot be M-giants but are most likely to be very red carbon stars. A carbon star requires that an oxygen dominated surface be reversed to carbon dominated, due to the dredged-up material from the star's interior. This process is more favourable in cases where the surface is metal-poor.

Searle (1971) and Pagel & Edmunds (1981) find a strong radial abundance gradient in the Triangulum galaxy of -0.09±0.02 dex/kpc in O/H, with the outer regions being metal poor and only reaching solar abundance towards the central region. Beaulieu et al. (2006) confirm an even steeper radial metallicity gradient (-0.16 dex/kpc in O/H over 4-5kpc) evident in HII regions, B-supergiants and planetary nebulae, by detecting beat Cepheids in M33. The presence of TP-AGB stars preferentially enhances the near-infrared surface brightness at these outer radii and could well be responsible for the apparent sharp radial truncation of disks observed optically (Kregel, et al. 2002). The outer regions of M33 are relatively metal-poor, and solar abundance is reached only in the very central domain of M33. For further discussion on the metallicity gradient in M33, see Magrini, Corbelli & Galli (2007).

The arcs are believed to signify the presence of fresh, low-metallicity gas flowing inward along the inclined warp of M33 towards the inner disk. In the absence of the warp, the low- and high-metallicity gases would be expected to be well mixed by the gravitational torques induced in the disk and by the inner oval/minibar. This is not the case however, for low-metallicity gas flowing inward along the observed warp. It might therefore not be surprising to find that the arcs may preferentially be characterized by populations of metal-poor stars.

In the evolutionary cycle of stars which have masses of between 1.3 and 3.5 M_O, there is a period (0.6 to 2 Gyrs) where they reside as Thermally Pulsing Asymptotic Giant Branch (TP-AGB) stars, principally dredging up carbon. These are very luminous giants which have been found to typically double the integrated bolometric luminosity of intermediate age (0.6 to 2 Gyrs) Magellanic Cloud clusters at K (Marigo et al. 2003, Maraston 1998). Mouhcine and Lançon (2003) find that a K-band luminosity enhancement is very prevalent due to the intermediate age stellar population, when considering stellar population synthesis models in Local Group galaxies. The corner of parameter space occupied by individual carbon stars in our Milky Way is presented in Figure 5 in Persson et al. (1983). Ages of young clusters in the SMC have a turnoff mass which generates large populations of carbon stars that are very cool, with very red J-K_s colours in the range of 1.2 - 1.9 magnitude. The integrated J-K_s colours for clusters in the LMC and SMC ranges from ~ 0.4 - 1.2 magnitude.

Persson et al. (1983) suggest the spectral signatures of luminous carbon stars may be prominent enough that metal-poor, intermediate age stellar populations may be detectable in the integrated light of more distant galaxies. Only recently have grids of asymptotic giant branch models become available (Marigo et al., 2003) which include carbon stars. All integrated-light models (e.g.: Worthey, 1994; Bruzual & Charlot, 1993; Leitherer et al., 1996; Vazdekis, 2001) have hitherto not included carbon stars.

The magnitudes and colours of 7 candidate targets in the outer northern arc are listed in Table 2.2. Their positions are detailed in Block et al. (2004a & 2007). A distance modulus of 24.64^m to M33 was assumed in deriving the absolute magnitudes, corresponding to a linear distance of 840 kpc (Freedman et al., 1991).

Star	J	H	K_s	J-K_s	J-H	H-K_s	M_{Ks}
1	17.96	16.76	15.91	2.05	1.20	0.85	-8.74
2	18.49	17.09	16.32	2.16	1.40	0.77	-8.33
3	19.61	18.04	16.66	2.96	1.57	1.39	-7.99
4	18.57	17.26	16.49	2.08	1.31	0.77	-8.16
5	18.82	17.35	16.54	2.28	1.47	0.81	-8.11
6	18.42	17.24	16.46	1.97	1.18	0.78	-8.19
7	18.37	16.91	15.82	2.55	1.46	1.10	-8.83

Table 2.2

LRIS spectra (Oke et al., 1995) of these carbon star candidates were obtained on 2004 Aug 17 UT with the Keck I telescope. The aperture mask slitlets had widths and lengths corresponding to 1.2" and 11.5", respectively. The grating, with 600 grooves per mm, had a resolution of ~8Å per projected slit width and a spectral range from 6825Å – 9415Å for slitlets near the centre of the mask. Each star was dithered along the slitlets between two exposures of 600 seconds each. The spectra from each of the slitlets were extracted and reduced independently, with the wavelength calibration being derived from airglow lines. The spectrophotometric standard G191B2B (Massey et al. 1988) observed near the centre of the mask provided an approximate flux calibration by transferring the system response function found for this slitlet to the same wavelength intervals for the other slitlets. Differential vignetting and other field-dependent variations in response were neglected as they are typically small for the LRIS instrument.

A section of the northern plume of M33 was imaged with the 5m Hale reflector at Mount Palomar using the 2048x2048 array near-infrared camera WIRC (Wilson et al., 2003). Individual stars were resolved in the 8.5' x 8.5' field of view, with a resolution of 0.25 arcsec per pixel. The centre of the field of view was positioned at $01^h34^m28.1^s$, +30°54'00" (J2000). The seeing FWHM for this observation was 0.8 arcsec in J, and 0.7 arcsec in K_s, and had an integration time of 540 seconds. This provided a limiting surface brightness at K_s of 20.2 mag arcsec^{-2}. The point source photometry S/N = 10 limits are 19.0, 18.0, 16.9 magnitude in J, H and K_s, respectively.

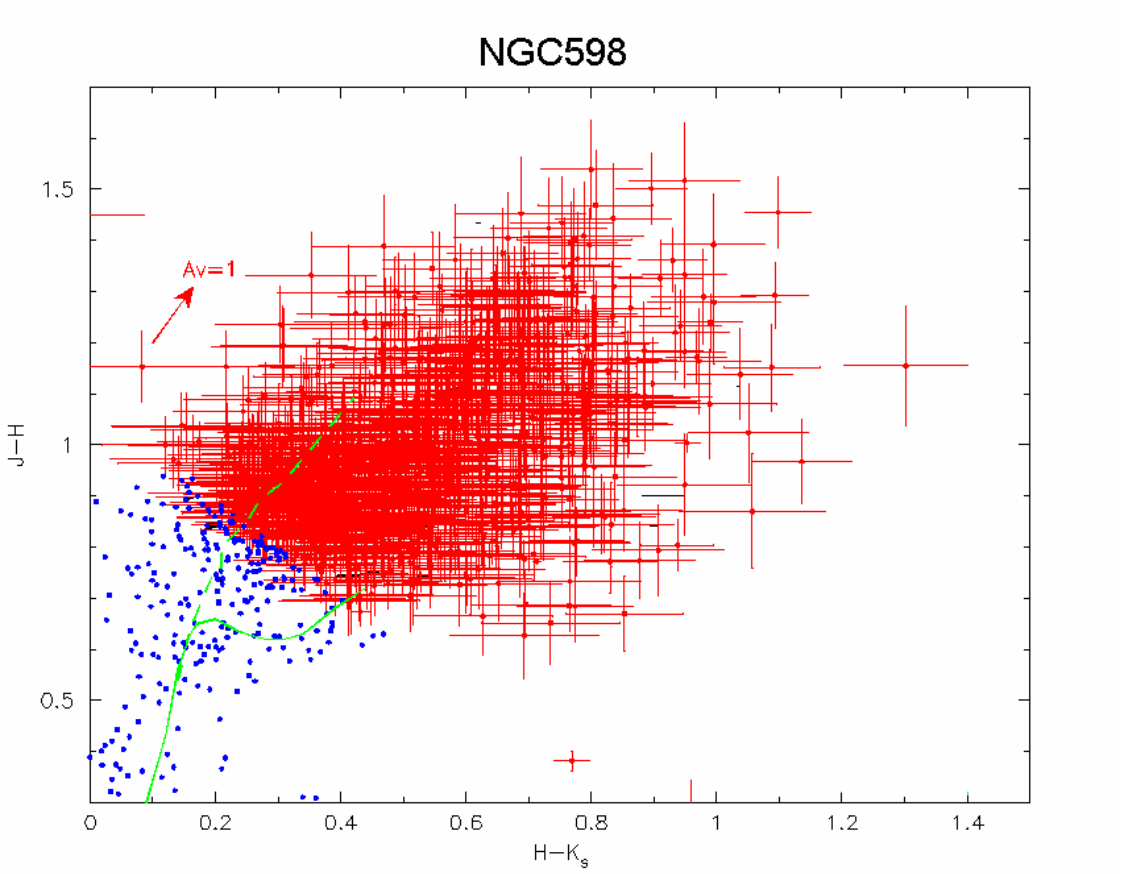

Figure 2.8: *This J-H, H-K_s colour-colour diagram reveals the presence of extremely red stars in the outer arcs. The sample presented has been cleaned of low detection sources, with S/N < 10. The evolved giant and main-sequence dwarf tracks (solid and dashed lines, respectively) are from Bessell and Brett (1988). In this figure, foreground Milky Way stars appear with blue colours of H-K_s < 0.2, J-H < 0.8 and J-K_s < 1.0 magnitude. Most M33 sources in the outer arcs are redder with H-K_s > 0.4, J-H > 0.9 and J-K_s > 1.3 magnitude. Colour uncertainties of the red sources are less than 10%.*

Near-infrared photometry with the Hale reflector had revealed stars with very red (J-K_s > 1.1) colours in the low metallicity outer region, 0.5 degrees away from the centre of M33. Further spectroscopic observations of this area were obtained with the Keck II telescope (see circle in Figure 1, Block et al., 2007). These data were obtained with the Echellette Spectrograph and Imager (ESI; Sheinis et al., 2002) on 2004 July 18 UT and used the Echellette mode which allows a wavelength coverage from 3900Å – 11060Å with a resolution of ~ 56 km s^{-1} with the 1 arcsec slit. The 1200 seconds exposures for each target were obtained at parallactic angle near transit.

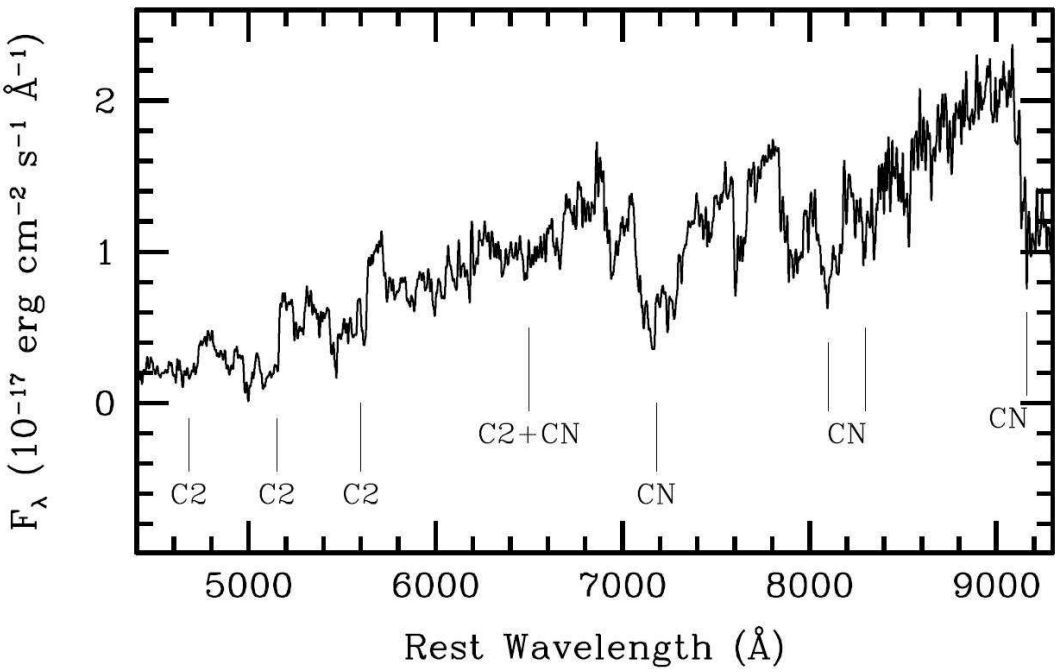

Figure 2.9: *A Keck II Spectrum of a carbon star approximately 5 scalelengths away from the centre of M33. The dominant CN absorption features are clearly evident and are a definitive signature of TP-AGB carbon stars. Carbon stars contain a host of molecular spectral features such as the CN bands and the C2 Swan bands. The conclusive presence of CN bands near 7000Å, 8000Å and 9000Å are indicated above.*

These observations confirm the presence of carbon stars (see Figure 2.9) in the outer disk of M33 exactly where Rowe et al. (2005) find their carbon-star number count function to peak. While the truncation of the outer disk has been estimated to be ~ 5 scalelengths (Ferguson et al. 2006), the carbon-star-bearing arcs occur out to radii of 3.5 – 5 kpc (2 – 3 scalelengths). At these radii, the HI distribution shows a distinct variation in inclination as reported by Corbelli & Schneider (1997).

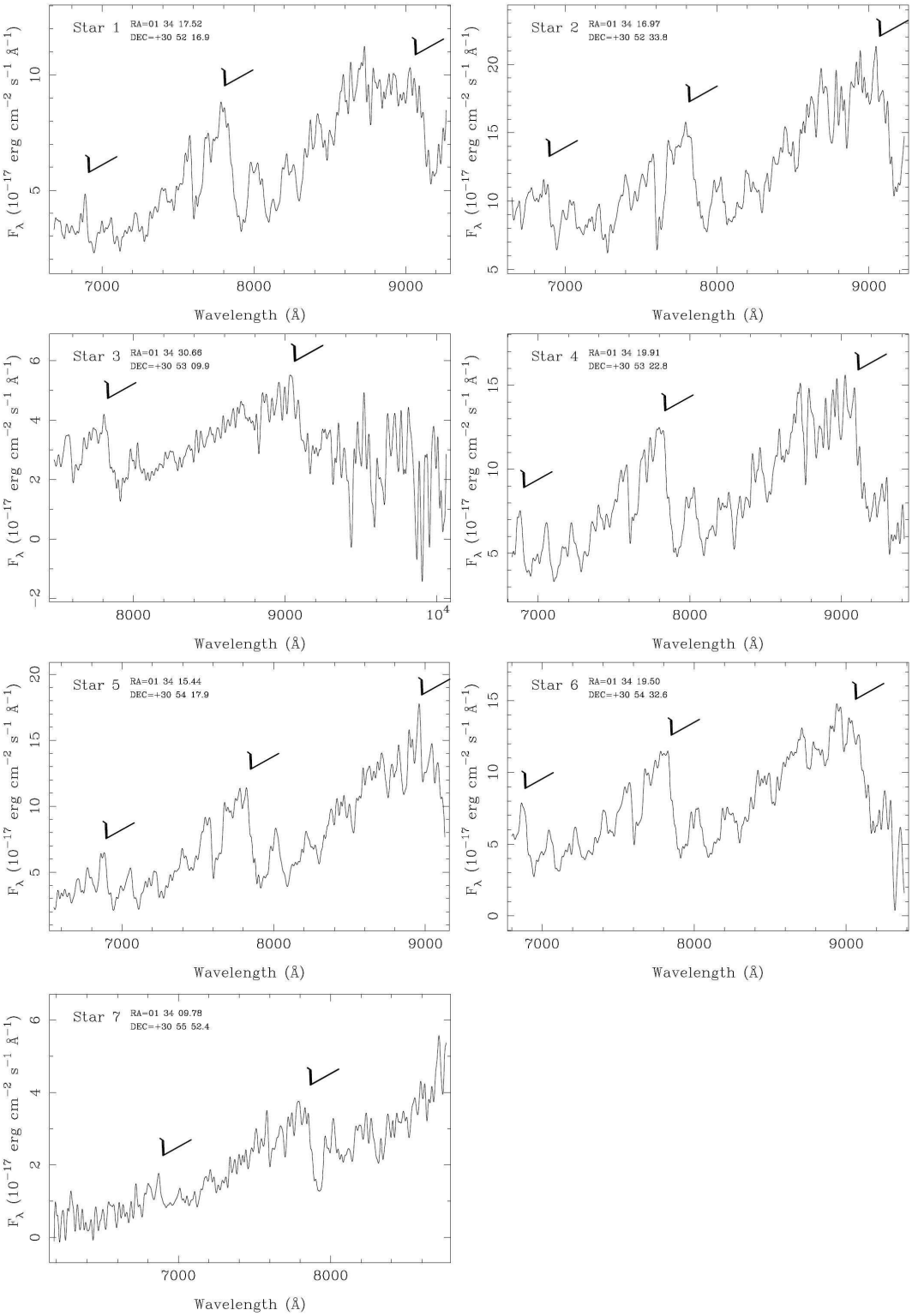

Figure 2.10: *Keck I spectra of targets listed in Table 2.2*

2.5.3 Spitzer IRAC Observations

Further observations of M33 were made in the near-infrared using IRAC on the Spitzer Space Telescope (Werner et al., 2004; Gehrz et al. 2007) on 2005 January 21 UT as part of the Spitzer Guaranteed Time Observing Program (Program ID 5), by Spitzer Science Working Group member, R. D. Gehrz. Due to the extremely large diameter which M33 subtends, the IRAC observation comprises 438 frames per channel, including a 3 point ½ pixel dither for each frame position. Each frame had an integration time of 12 seconds. Processing details of the raw Spitzer data are given in Block et al. (2007). A more comprehensive analysis of these IRAC mosaics will be presented elsewhere (Gehrz et al., in preparation). This section however is dedicated to the dust grain morphology observed in the disk of M33.

Block et al. (2007) report the 8.0μm IRAC image of M33 offers unprecedented insight into the global ISM dust morphology. While the 2MASS JHK_s images clearly show the giant arcs of carbon stars, the global ISM dust morphology can also be effectively traced at 8.0μm. Carbon stars are one of the most important contributors to the replenishment of dust in the interstellar medium. Being thermally pulsating asymptotic giant branch stars, they undergo pulsation modes in their outer atmospheres which become extended and may reach a temperature low enough for some of the constituent elements to condense into very small particles – essentially dust. The stars' radiation pressure produces a progressively expanding circumstellar shell of gas and dust (Le Bertre et al., 2003). The dust emission from carbon star as well as oxygen-rich shells is detected at 8.0μm (Buchanan et al., 2006). These authors note that "most of the C-rich stars have spectra that are dominated by warm dust" and furthermore show that oxygen-rich stars such as MSXLMC587 and carbon stars such as MSXLMC1488 both show emission at 8.0μm.

The Spitzer IRAC mosaics of M33 were deprojected with the same position parameters as used on the 2MASS subsample by adopting $\log R_{25} = 0.23$ (RC3, de Vaucouleurs et al., 1991) where R is the ratio of the major to minor axis, with a position angle of 23 degrees (Deul & van der Hulst, 1987; Regan & Vogel, 1994). The Rayleigh-Jeans starlight distribution tail was removed from the 8.0μm image, by subtracting a scaled version of

the IRAC 3.6μm mosaic. This resulted in a 'non-stellar' pure dust map from 8.0μm - κ 3.6μm, where the constant κ is set to be 0.25. The contribution from stellar photospheres is removed by this subtraction and leaves only the emission from dust grains tracing the ISM morphology. There are various uncertainties in determining the precise value of κ such as taking the extended aperture correction into account, and the exact mid-infrared colour of the stellar population which is modeled by scaling the 3.6μm emission. Other authors such as Helou et al. (2004) suggest a value of 0.232 instead of 0.25 for κ. The choice of κ is only accurate at the 10-15% level, so the use of a slightly brighter photospheric contribution is well within the correction uncertainties.

Observing photospheric emission at 3.6μm as opposed to ISM dust emission is another alternative. At these shorter wavelengths carbon star photospheres would certainly be detected, but photospheres of oxygen rich stars would however also be included.

Inferring upper and lower age limits for carbon stars is not trivial because no calibrating SMC or LMC clusters exist in the two separate age regimes of 0.2 – 0.6 Gyr and 2 – 4 Gyr (see Figure 1 in Marigo et al., 1996). Age limits for carbon stars are uncertain because of the unknown efficiency of the third dredge-up and hot bottom burning in the envelope of most massive AGB stars. Carbon stars are very populous in the observed range of 0.6 – 2 Gyr. They could be populous in a wider range of 0.2 – 4 Gyr, but there are currently no observations to compare the models with. Stellar evolution theory cannot help due to numerous uncertainties in the TP-AGB phases for the models to be *a-priori* predictive.

Marigo et al. (2003) suggest the upper age limit for Carbon stars is 4 Gyr (for a 1.3 solar mass star of half-solar metallicity). They set a lower age limit of only a few hundred Myr, for a 3.5 solar mass carbon star. If there is a significant carbon-rich stellar population, it may well lie in the 0.6 – 2 Gyr age regime. This intermediate-age, carbon-rich population together with its accompanying main sequence turnoff stars and oxygen-rich giants should effectively outshine any *older* populations present in the disk, at all wavelengths.

2.6 Insights into Building of Galactic Disks

2.6.1 Origin of Carbon Star-Bearing Arcs

Spiral galaxies are believed to be dynamically open systems whose constituent disks continue to form even at present (Block et al., 2002). From a cosmological perspective, this accretion is reported to be fed from large scale structure filaments (Kereš et al. 2005). The rate of accretion may be of such significance that the mass of spiral disks could double every ~10 Gyrs. The source of the accreting gas is very likely to originate from reservoirs which Sancisi (1983) reports enshroud nearly all spiral disks. This supports a "bottom-up" galactic disk formation scenario, where disks appear to form from the inside out. The outer regions of disk galaxies are significantly younger than the inner regions, and are correspondingly metal deficient (Bell & de Jong, 2000). Cosmological simulations of galaxy formation predict that the outer parts are predominantly composed of a young–intermediate age population (Weil, Eke & Efstathiou 1998) and suggest that intermediate age stars (0.6 – 2 Gyrs) should represent the dominant contribution in these outer regions. Models of isolated, non-accreting galaxies are ruled out.

Due it its relatively close proximity, M33 with its prominent HI warp, provides an excellent example of studying gas accretion in the outer domains of spiral disks. Furthermore, the photometric technique used to identify carbon stars based *exclusively* on their J, H and K_s integrated luminosity colours could possibly be used for detecting similar TP-AGB populations in more distant galaxies, where individual stars cannot be resolved.

Star formation in the early universe was already well underway at a redshift of z~6. This leads to the plausible contention that 0.6 Gyrs later (at z~4), we should observe a proliferation of carbon stars. At these redshifts, the carbon stars' luminosity peak will be observed in mid-infrared passbands. Maraston (2005) advocates the use of carbon stars to provide an age indicator of high-redshift stellar populations. The JSWT will be well suited to address these questions, and low metallicity carbon star populations in the outer disks of high-redshift galaxies would furthermore be powerful indicators of galactic gas accretion at earlier times.

In summary, Keck spectroscopy of individual stars has confirmed the presence of an enhanced abundance of carbon stars in the outer spiral arms of M33. These two "arcs" were identified previously from their red colour by Block et al. (2004a). Furthermore, these conclusions are in very good agreement with spatial C/M-star ratio map of M33 produced by Rowe et al. (2005), revealing the outer arms conspicuously. These outer spiral arms are also prevalent in the Fourier m=2 component of the IRAC 8.0μm dust emission mosaic. It is at precisely the radius of these outer arms where the HI-21cm warp starts, which acts as a reservoir for gas fueling star formation. Magrini, Corbelli & Galli (2007) propose a similar conclusion regarding gas accretion in M33 on the basis of O/H, S/H and [Fe/H] abundances.

2.6.2 Inferring Carbon Star Populations in the Outer Disks of High-Z Galaxies

Nearly all spiral galaxies reveal HI gas reservoirs in their outer disks (Sancisi, 1983). Such conspicuous warped morphology, even in the absence of any perturbation or companions, implies that gas is being almost continuously accreted, with a different angular momentum to that of the inner disk (Binney, 1992). Furthermore, systems of gas accretion need not necessarily show any signs of accretion of the luminous stellar component as is revealed by the presence of tidal tails, stellar loops or close companions.

The presence of carbon stars in the outer disk of M33 leads to the questions of just how ubiquitous such intermediate age populations may be in the outer regions of other spiral disks. The photometric technique used to identify thermally-pulsing asymptotic giant branch carbon stars may well be applied to more distant spirals on the basis of their red J-K_s colours in low metallicity domains. Maraston (2005) indeed proposes using carbon stars as age indicators for high-redshift stellar populations. Tsalmantza et al. (2006) have also proposed such a methodology.

Carbon stars could possibly provide and important contribution to the infrared luminosity of high-redshift galaxies. Carbon star populations in the Large Magellanic Cloud are produced in large numbers with ages of about 0.6 to 2 Gyr. This implies that galaxies which undergo a burst of star formation will present an enhancement to their infrared

light flux 0.6 Gyr later and will decay after about 2 Gyr. Bouwens et al. (2003) report that star formation in the early universe was already proceeding at a redshift of at least z ~ 6. It is therefore plausible that the earliest carbon stars in the universe may already be observed at a redshift of z ~ 4, after about 0.6 Gyr since initial star formation. These carbons stars would likely have doubled their rest frame near-infrared output, which will be detectable with mid-infrared instruments on telescopes such as JWST. However, it is a sobering thought that ground based 10m class telescopes are required to resolve individual carbon star spectra in the outer disk of our second nearest spiral, M33. This accentuates the urgent and immediate need to identify unresolved sets of carbon stars in distant spiral galaxies on the basis of their colours alone. Such a methodology will be independent of the need to first resolve such populations with very large (30m class) telescopes and imaging them through Sloan or (V, I, 77, 81) filters.

– CHAPTER 3 –

SPITZER MORPHOLOGY OF THE GREAT NEBULA IN ANDROMEDA – LORD OF THE RINGS

White whorls of stars slow turning in the sky,
Across the borders of the measured night,
On, on beyond the treasures of the eye,
Where only magic lenses garner sight:
Transparent reapers of dim sheaves of light.
– George Brewster Gallup

Based on:

An almost head-on collision as the origin of two off-centre rings in the Andromeda galaxy

D. L. Block, F. Bournaud, F. Combes, **R. Groess**, P. Barmby, M.L.N. Ashby, G.G. Fazio, M.A. Pahre & S.P. Willner

***NATURE**, Vol. 443, 832, 19 October 2006*

3.1 Introduction

3.1.1 Early Descriptions of Messier 31

The Persian astronomer Abd-al-Rahman Al-Sufi, who observed the Andromeda Galaxy in 964, described it as a "small cloud". The first description of this conspicuous galaxy in the constellation of Andromeda, based on telescopic observation, was given by Simon Marius in 1612. The Andromeda Galaxy (Messier 31=NGC224) is the nearest and also the most massive giant spiral galaxy to us with a mass at least 1.5 that of the Milky Way; the Empress in the Local Group of Galaxies. Edwin Hubble classified the “Great Nebula in Andromeda” as Sb, and referred to it as a prototype of an unbarred spiral. Hubble also identified extragalactic Cepheid variables for the first time on astronomical photographs of this galaxy, providing the first truly reliable indications of its distance. Modern values (Stanek & Garnavich, 1998) place Messier 31 at a distance of approximately 780 kpc.

Early wide-field blue-sensitive photographic images suggested that the 120 000 light-year diameter of the Andromeda Galaxy was only marginally larger than our Milky Way, estimated at approximately 100 000 light years across. Recent studies by Ibata et al. (2005) with one of the Keck telescopes however, has revealed a tenuous population of stars extending far beyond M31's initial diameter estimates, stars which Ibata and collaborators argue are part of the main disk itself. This extended stellar disk makes the Andromeda Galaxy more than 220,000 light-years in diameter.

In 1991, the Hubble Space Telescope Planetary Camera imaged the central region of the Andromeda Spiral (Lauer et al., 1993). Its nucleus revealed a double structure with two nuclear hot-spots located within a few kpc of each other. The nuclei of many galaxies are known to be violent places and Messier 31 is no exception with the existence of a supermassive black hole at its centre (Kormendy, 1988).

3.1.2 Optical Morphology of Messier M31

High spatial resolution near-infrared studies of the entire Andromeda Spiral have been hugely restricted by the very large angular diameter which this galaxy subtends, over 190 arcminutes (3.2 degrees). As a consequence, early morphological studies of the entire galaxy have historically been confined to photographs imaged through wide-field Schmidt telescopes. Sections of the galaxy have been very carefully studied using larger telescopes; for example, in 1943, Walter Baade was the first to resolve stars in the central region of M31 and he later (Baade & Payne-Gaposchkin, 1963) also very perceptively noted that the two inner spiral arms (N1 and S1 in his terminology) began at projected distances of 3.4 arcmin and 1.7 arcmin, respectively, from the centre of the galaxy. Baade described N1 and S1 as "dust arms; no supergiants or HII regions visible".

Messier 31 has two dominant elliptical satellite galaxies, Messier 110 (NGC 205) and Messier 32, as well as multitudes of smaller ones. In his early pioneering spectroscopic work, Vesto M. Slipher (1913) remarked upon repeatedly getting negative redshifts from the Andromeda nebula, "The magnitude of this velocity, which is the greatest hitherto

observed, raises the question whether the velocity-like displacement might not be due to some other cause, but I believe we have at the present no other interpretation for it. Hence we may conclude that the Andromeda Nebula is approaching the solar system with a velocity of about 300 kilometers per second." A collision between the two galaxies will indeed occur several Gyrs hence.



Figure 3.1: *The Great Nebula in Andromeda (the Andromeda Spiral Galaxy), is situated at a distance of approximately 780 kpc, is inclined at 77.5 degrees to the line of sight (Rubin and Ford 1971, Nieten et al. 2005) and has a position angle (PA) of 37.7 degrees east of north (Nieten et al. 2005).*

(Image Credit: NOAO/AURA/NSF)

3.2 Spitzer Observations of M31 with IRAC

3.2.1 Introduction

The Spitzer Space Telescope is a multi platform, high sensitivity near- and mid-infrared detector, operating in an earth-trailing heliocentric orbit. Designed with a "warm-launch" mission objective, it utilizes passive radiative cooling along with a small (360 litre) super-fluid helium cryostat to achieve background limited observations. Launched in August 2003, Spitzer is expected to have a 5 year nominal operational lifetime.

The Infrared Array Camera (IRAC), the Multiband Imaging Photometer for Spitzer (MIPS) and the Infrared Spectrograph (IRS) comprise the three instruments onboard the Spitzer Space Telescope. This thesis presents analysis performed on data generously supplied from IRAC principal investigator, Giovanni G. Fazio.

3.2.2 Spitzer's Infrared Array Camera

IRAC explores the near infrared universe in a completely new parameter space, incorporating high spatial resolution studies free from atmospheric absorption. IRAC is a four-channel camera (Fazio et al. 2004a) capable of simultaneous broad-band images at 3.6μm, 4.5μm, 5.8μm and 8.0μm. These are often referred to as channels 1-4, respectively. Two nearly adjacent 5.2 x 5.2 arcmin^2 fields of view in the focal plane are viewed by the four channels in pairs (3.6μm and 5.8μm; 4.5μm and 8.0μm), resampled to 0.8600 arcsec per pixel. The 5.8μm and much more predominantly the 8.0μm channel on IRAC detects small, warm dust grains in emission and provides first time dust maps of a large sample of galaxies. Analysis is performed on a subsample of these in this thesis.

3.2.3 Wide Field IRAC Mosaic of M31

In order to observe the entire Andromeda galaxy with IRAC, a total of 3000 individual images in each of the four IRAC channels were required, facilitated by some 700 pointing requests (Barmby et. al, 2006). The final mosaics were created with a pixel scale of (nominally) 0.8600pix/arcsec. Fifteen Astronomical Observation Requests (AORs)

were used to map a region approximately 3.7 x 1.6 degrees. The long dimension is along the galaxy major axis, with an extension to the NW to include the companion galaxy NGC 205. The central 1.6 x 0.4 degrees region was covered by three AORs. Full details are contained in Barmby et al. (2006).

3.3 Dust Penetrated 8.0μm IRAC Morphology

3.3.1 PAHs in Emission

The unusual morphology of the Andromeda Spiral has long been an enigma. Although regarded for decades as showing little evidence of a violent history, M31 has a well-known outer ring of star formation (Pellet et al. 1978; Brinks & Shane 1984; Dame et al. 1993; Haas et al. 1998; Nieten et al. 2005) at a radius of 10 kpc whose centre is offset by 10% from the galaxy nucleus. In addition, the outer disk is warped as seen at optical (Ibata et. al. 2001) and radio (Braun 1991) wavelengths and the halo contains numerous loops and ripples. It is however the striking morphological composition of Messier 31, as visible at 8.0μm, which forms the basis of this chapter. Here bulge starlight is suppressed while the emission of warm tiny dust grains is delineated.

These warm dust grains reveal two prominent rings which appear to be density waves propagating in the disk. The Baade dust arms N1 and S1 (Baade & Payne-Gaposchkin, 1963), when seen in emission, also begin diametrically opposite each other from the centre of the galaxy. It is important not to confuse the Baade dust arms with a morphologically but distinct “turbulent spiral who aspect ratio appears significantly more face-on than does the disk of stars and gas in M31” (Ciardullo et al., 1998). Existence of this structure was already indicated in the early photographic investigation of Johnson & Hanna (1972). It is associated with ionized gas (Devereux et al. 1994) and most likely involves ISM ejection via a galactic wind (see e.g. Mathews & Baker 1971). Rubin & Ford (1971) note that the velocities along the near side of the minor axis of Messier 31 are not zero but negative, indicative of an outflow i.e. both rotation and expansion are required to reproduce the observed velocity fields of the inner mini-spiral.

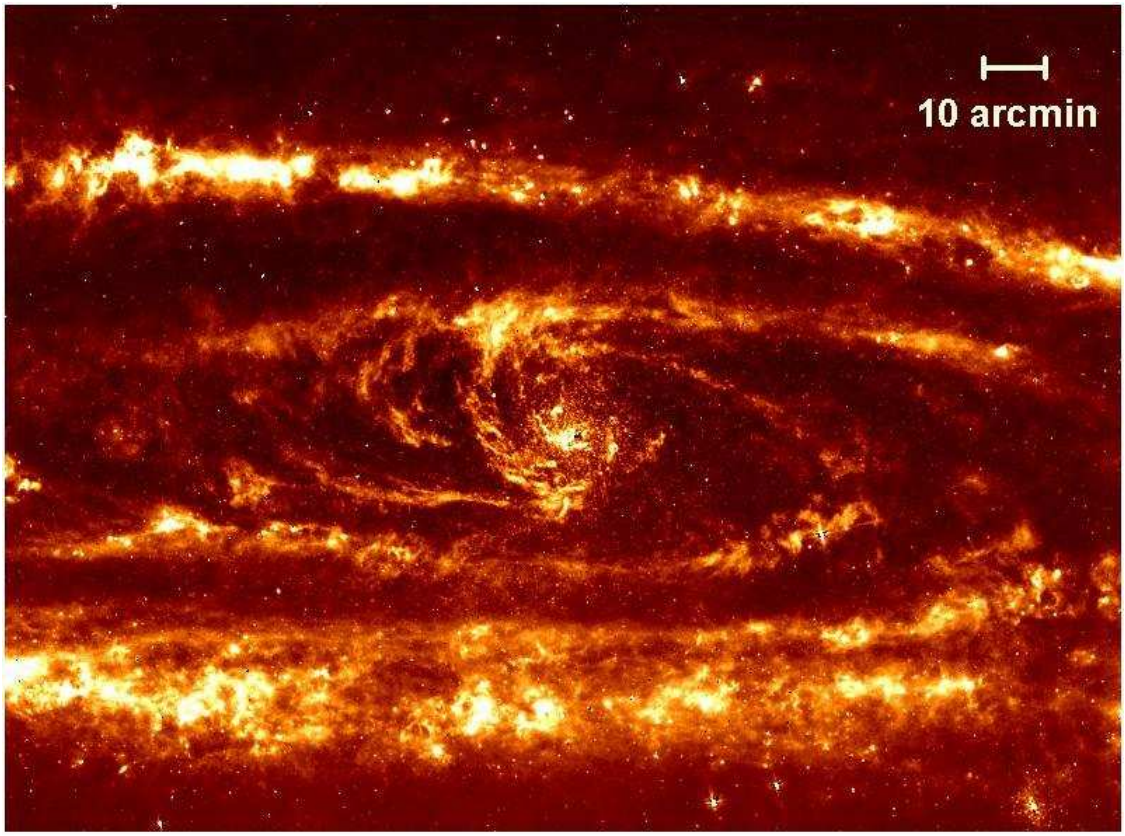

Figure 3.2: *A non-stellar Spitzer IRAC image of the central region of the Andromeda Spiral at 8.0μm, shows the distribution of very small grains as well as macromolecules, all seen in emission.*

3.3.2 A non-stellar 8.0μm Dust Map of M31

The starlight flux itself at 8.0μm is less than 25% compared to that of the 3.6μm emission, since the Rayleigh-Jeans tail at 8.0μm has already experienced a significant drop-off. Bulges show up strikingly in 3.6μm, as they are heavily dominated by emission from late-type stars. The contribution of the bulge light at 8.0μm was subtracted with a 0.28-times scaled 3.6μm stellar emission map. (See §2.5.3 for more details on this procedure.) This procedure enabled the careful first time exploration of the inner M31 morphology at unprecedented spatial resolution.

The contention that Messier 31 may contain a central bar has been the subject of investigation for over 50 years. Lindblad (1956) argues in "*On a Barred Spiral Structure in the Andromeda Nebula*", that: "The run of the isophotes in the central region from microphotometric records shows a certain skewness against the major axis as drawn for

the nebula as a whole … it is possible that this skewness is connected with … the central line of the 'bar'". He continues, "Reconstructing the main features of the nebula in its own plane, one finds that the run of the spiral arms in relation to the bar is of a type which is very characteristic for the barred spirals." Rubin & Ford (1971) showed that the gas velocity distribution deviates from axisymmetry about the minor axis. Stark & Binney (1994) concluded that "the tilt of the inner isophotes, gas velocities in the inner kiloparsec and the 'face-on spiral' pattern seen in dust and ionized gas", are "explained by a central bar." More recently, Athanassoula & Beaton (2006) have argued on the basis of near-infrared photometry for the presence of a bar and Gordon et al. (2006) have shown striking evidence at 160 μm for bright ansae (handles) on two ends of the minor axis along which a proposed bar is suggested to reside. In this case it should be noted that deprojected images of M31 were used and the stretch for such a highly inclined spiral can be severe.

The morphological difficulties of definitively detecting the remnants of a dissolved bar are overcome by going to that domain of the electromagnetic spectrum where the *bulge light* no longer dominates; the domain where dust grains themselves are the principal source of light emission, rather than starlight.

If a bar were to be present and extend from N1 to S1, its projected length would be 326.8", or a linear distance of about ~1200pc (at an assumed distance to M31 of 780kpc). The in-plane inter-Baade arm distance is derived by taking the effects of M31's 77.5º inclination into account, yielding a linear "bar length" of ~6 kpc. This compares to the bar length in our Milky Way of 4.4 kpc (Benjamin et al. 2005). Note that the original, un-deprojected, images of Messier 31 were used to estimate this bar length, mitigating complications due to deprojection stretch. The absence of actually seeing the bar itself at 8.0 μm or longer wavelengths in no way precludes the absence of a stellar bar. While bars of many galaxies are seen in both starlight (3.6μm) and dust emission (8.0μm), there is a family of barred galaxies containing bars which are devoid of dust (see §5.4.1). In other words, while such galaxies show a distinct bar in starlight, no central bar is visible at 8.0μm, the wavelength at which very small, warm dust grains radiate.

That no bar-like structure is directly evident in the IRAC 3.6μm image suggests some possibilities. First and foremost is that the bar could be overwhelmed by the brightness of the large bulge in this highly inclined early-type spiral galaxy. There are a number of mathematical methodologies to subtract away a bulge of stars, but each has its set of limitations, as subtraction of a synthetically generated bulge depends on a number of inherent assumptions. Moreover, the bulge in Messier 31 is not spherical but triaxial, having three non-equal perpendicular axes. This dramatically complicates any synthetic bulge subtraction at 3.6μm, without removing any central and fainter stellar features, such as a bar, for example.

A second, more speculative possibility, is that the bar itself may be in a state of bar dissolution. Bournaud & Combes (2002) have argued that the bar phenomenon is transient – episodic – and that bars form/dissolve/reform as a function of time. These authors argue that a galaxy may undergo 4-5 bar episodes in one Hubble time. Driving this process is principally the accretion of gas from outside the disk. While we cannot prove that this has happened in the central region of M31, this is an intriguing possibility; the kinematic signatures in the central regions of M31 would then be suggestive of a central bar which once was there a few Gyr ago, but which has now largely dissolved. In this scenario, the bar's remnant evidence, such as the diametrical positioning of the Baade arms, is still apparent today. Of-course the bar may be incipient, and in the process of reformation.

Thirdly, there may not be a bar at all.

3.3.3 Two off-centre rings of dust

Messier 31 is famous for a conspicuous outer ring observed at a radius of approximately 10kpc, consisting of gas and dust with associated star formation. There are several tracers of this outer ring, such as the HI 21cm line for atomic gas (Brinks & Shane, 1984), the CO lines for molecular gas (Dame et al. 1993, Nieten et al. 2005) and the dust morphology at far-infrared wavelengths (IRAS, ISO Haas et al. 1998, and Spitzer-MIPS,

Gordon et al. 2006). The 10 kpc ring is also observed in radio-continuum (Beck et al. 1998) and in the Hα line (Pellet et al. 1978), tracing current star formation. The peculiar morphology of M31, composed of a warped outer disk, is spectacular in atomic gas (Henderson 1979), at visible wavelengths, as well as in molecular gas (Casoli et al. 1987, Nieten et al. 2005). Furthermore, there are myriad stellar loops in the outer disk (Ibata et al., 2001).

The warping of the gas disk in the central kpc appears to be seen much more face-on (Jacoby et al. 1985). The high inclination of the disk (77.5 degrees to the line of sight; Rubin and Ford 1971, Nieten et al. 2005) allows for many interpretations, from a leading one-armed spiral (Simien et al. 1978) to a non-planar trailing two-armed spiral (Braun 1991), also with ring-like structures (Haas et al. 1998, Gordon et al. 2006). The pitch angle of the assumed spiral features is small (less than 10 degrees), which explains why it is possible to propose both leading and trailing spiral arms to generate the ring morphology. As noted earlier, it is exceedingly difficult to deproject the various features in the disk, since deviations from a planar geometry are huge.

Subtraction of the 3.6 μm bulge contribution has strikingly revealed the presence of an inner ring comprising small, warm, dust grains, straddled at either ends by the Baade dust arms (Baade & Payne-Gaposchkin, 1963). The inner ring is elongated towards the minor axis, and most likely belongs to the warped central gas disk. It is therefore not possible to know its ellipticity exactly, but it is unlikely to be circular. Even more remarkable is that the centre of this central ring is offset from the galaxy centre (see Figure 3.4). The inner dust ring's dimensions are calculated to be 1.5 kpc by 1 kpc, and it is offset by a huge 40 percent of the ring radius, at a projected distance of 1.8 arcmin (400 pc) from the centre of the galaxy. Messier 31 thus contains two offset rings; the well-known outer ring being offset by approximately 10% (see Figure 3.3). Both rings are plausibly interpreted to be density waves induced by an almost head-on collision, with the dwarf companion galaxy M32 being the most likely candidate. In the case of resonance-induced rings, the degree of off-centering increases with radius in stark contrast to the scenario in M31 where the degree of off-centering *decreases* with radius. Andromeda therefore bears a striking

resemblance to the double-ringed Cartwheel Galaxy, the archetypal galaxy formed by a head-on collision.

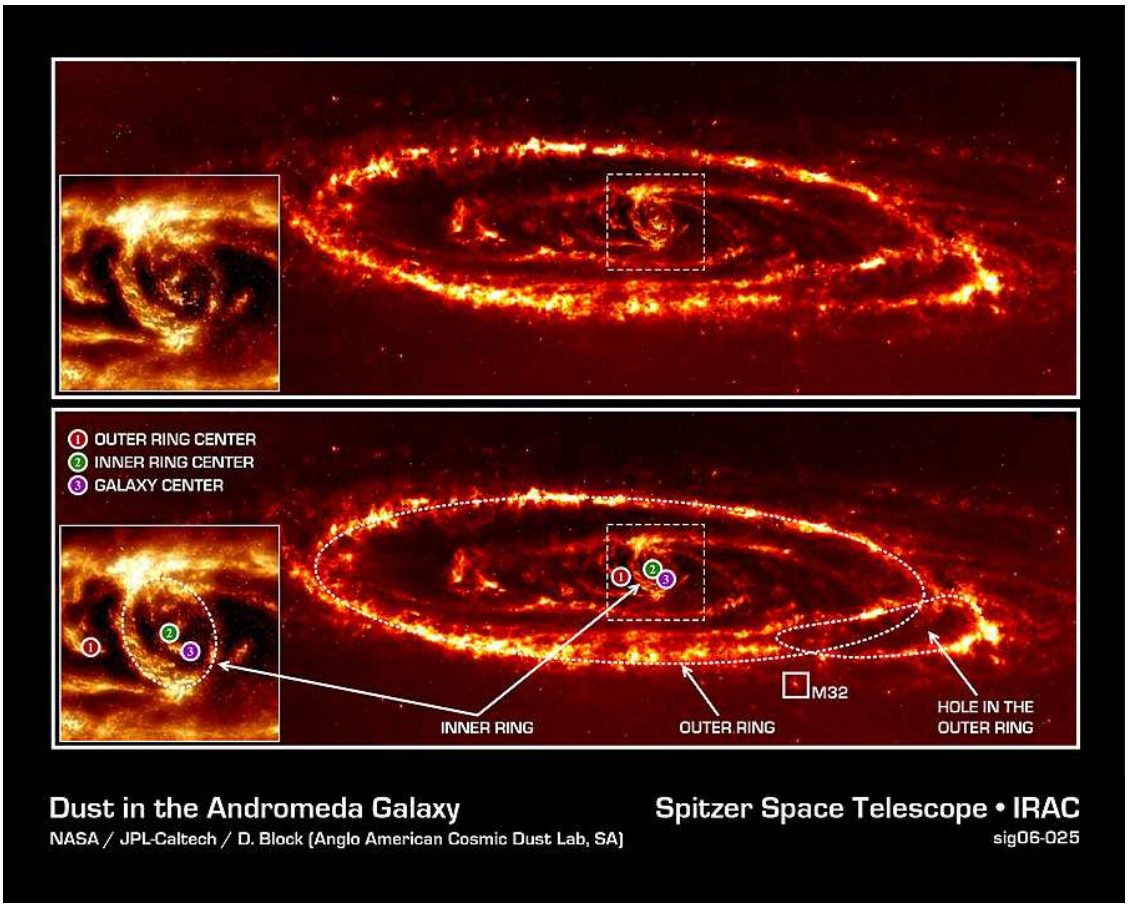

Figure 3.3: *Spitzer IRAC imaging of the Andromeda galaxy at 8.0μm reveals the presence of two off-centre rings of dust. Both rings are interpreted to be density waves induced by an almost head-on collision. The famous outer 10kpc ring has an offset of ~10% from the centre of the galaxy, while the first time discovery of an inner 1.5kpc by 1.0kpc ring is off-centre by about 40%. A scaled subtraction of the 3.6μm map was used to reveal the underlying dust morphology by removing light from stellar photospheres. The remaining luminosity therefore traces the emission of warm dust grains and macromolecules in the interstellar medium. The most likely impactor candidate is the elliptical dwarf companion galaxy M32, seen to the lower right in the white square. M32 appears faint in this image because its dust content is relatively low and much of the prominent starlight at 3.6μm has been subtracted away.*

3.4 Collisional Interpretation

3.4.1 Introduction

Simulations of a near head-on collision in Messier 31, by Bournaud & Combes (Block et al, 2006), suggest that the numerical models corroborate that the observed double ring morphology of the Andromeda spiral is indeed the result of a recent head-on collision, having taken place about 200 Myrs ago. The head-on collision, most likely with M32, produced major global morphological features, and induced the formation of the two offset expanding density wave rings.

In the Hubble Atlas, Messier 31 is classified as a striking prototype of a 'grand-design' spiral galaxy, with no obvious signs of interaction with any of its companions. The passage of a companion has however been suggested to explain the warps seen in the outer disk of M31 at both optical wavelengths (Ibata et. al. 2001, 2005 and by Ferguson et. al. 2002) as well as in observations of radiation from neutral hydrogen gas. Sato & Sawa (1986) identify NGC205 as being responsible. As far as the inner disk is concerned, Byrd (1978, 1983) has suggested that the spiral arms themselves have been locally perturbed by tidal interactions with M32, producing spurs.

It is instructive to examine whether the passage of a companion in the disk of M31 merely caused localized features (e.g. spurs, holes) or major global features, like density-waves resulting in star formation.

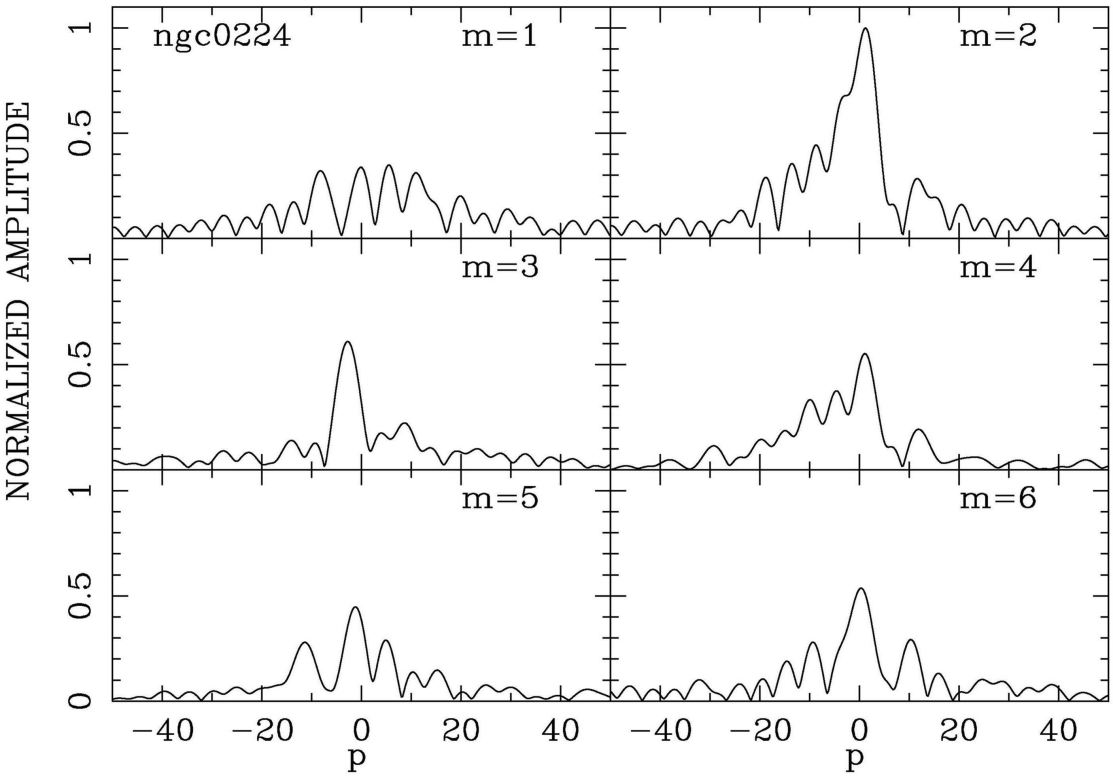

Figure 3.4: *Fourier spectra generated from a deprojected 8.0μm image of the central region of Messier 31. The Fourier spectra confirms that the dominant Fourier mode is m=2, indicative of the two inner Baade dust arms, whose pitch angle is computed from the m=2 spectral panel to be 57 degrees.*

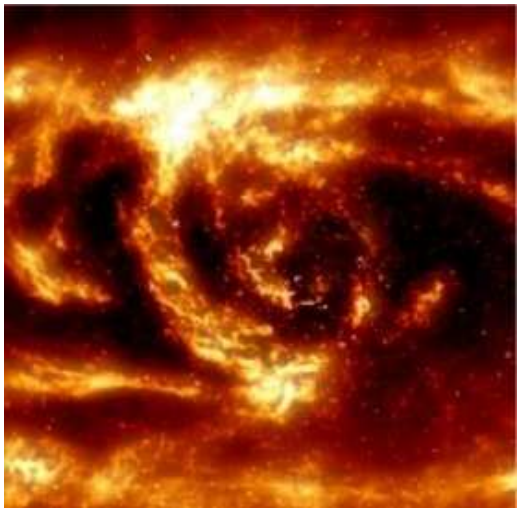

Figure 3.5: *The central region of the Andromeda Spiral Galaxy secured at non-stellar 8.0μm with the Spitzer Space Telescope. Full observing details in Block et al. NATURE (2006). This is a close up of the 1.5 by 1 kpc inner ring of M31. The ring is off-centre by approximately 40%, from the centre of the nuclear bulge position and the two inner dust arms identified by Baade (Baade & Payne-Gaposchkin, 1963) commence at the bright regions along the apparent major axis of the ring as seen here. The image shown here was subjected to Fourier spectral analysis and a 0.28 scaled subtraction of the 3.6μm image carefully revealed where the Baade arms of dust themselves actually begin. A distinct morphological component – a central mini-spiral of dust identified by Rubin and Ford (1971), Johnson and Hanna (1972) and Ciardullo et al. (1998) whose aspect ratio is significantly different and more face-on than the highly inclined disk of M31 itself, lies within the ring.*

Published Spitzer MIPS images of the Andromeda Galaxy (Gordon et al. 2006) at 24μm reveal emission from other sources (possibly from AGB stars) near the centre of the galaxy. The inner ring morphology is therefore contaminated at these longer wavelengths. It is only by exploiting the high spatial resolution of IRAC that the complete inner ring is best seen to full advantage and its morphological properties have been resolved. There are two viable scenarios in which two rings in disk systems such as M31 are formed. The first is by head-on galaxy collisions. Such collisions produce expanding ringed density waves (see Lynds & Toomre 1976, Appleton & Struck-Marcell 1996), as in the Cartwheel galaxy. The second scenario describes rings whose formation is induced by rotating bars in spiral disks. The inner, outer and nuclear rings in barred spiral galaxies identify orbital resonances and arise from the galaxy's internal dynamics (unlike collisional rings).

The ring offsets strongly supports the interpretation of a collision. Resonance rings, related to bars, never reveal such a large degree of offset (40% for the inner ring) from galaxy centres and the relative brightness of the inner and outer rings further supports a collision origin (Block et al., 2006). When a bar induces a strong pair of rings, the most prominent one is generally the inner, located just beyond the bar at the 4:1 resonance. In M31 however, the outer ring is much brighter than the inner one and thus the evidence for the double set of rings in M31 being produced by collision is highly compelling.

3.4.2 The Prevalence of Ringed Galaxies at High-z

High-z investigations, such as the Hubble Deep Field (HDF) – north and south – along with the Ultra Deep Field (UDF) and more recently, the GOODS survey, have revealed a striking number of galaxies which fall outside traditional classification bins, when observed at optical wavelengths. As such, galaxies at $z \approx 0.5 – 1.0$ and higher, secured even with HST's NICMOS array, are not dust penetrated. Radiation at H (1.65μm) band is received from 4,000Å *rest frame* emission at $z \approx 3$.

While some work has been done to explore the morphological mix of such field galaxies as a function of redshift (Glazebrook, et al., 1995; Abraham et al., 1996a; Driver, et al. 1998), not much quantitative analysis has been reported in the literature regarding the near-infrared rest-wavelength regime. A number of investigations have indeed considered possible systematic changes in galaxy morphology as a function of rest-wavelength (Abraham, et al., 1996b; Giavalisco, et al., 1996; Bouwens, et al., 1998), with reference to morphological "k-corrections" which reveal optical rest frame systems with near-ultraviolet filters.

Block et al. (2001), however, suggest near-infrared rest-wavelength observations of high-z galaxies may unlock key secrets. Near-infrared morphology traces the underlying stellar mass distribution (Charlot, 1996; Frogel, et al., 1996; Kauffmann & Charlot, 1998) because dust extinction at K_s is only $1/10^{th}$ that of optical images. For this reason, Block et al. (2001) have simulated rest-frame near-infrared morphology studies on high-z galaxies as will be observed through the James Webb Space Telescope (JWST), formerly

designated the Next Generation Space Telescope (NGST). Many galaxies observed optically at high-z exhibit peculiar/chaotic morphology, such as HDF 2-86 (van den Bergh, 1998) at z=0.749. Indeed van den Bergh et al. (1996) propose that this HDF galaxy is still in the process of initial formation. Block et al. (2001) have suggested that these optically peculiar galaxies may appear far more symmetric when studied in the dust penetrated regime with JWST. The masks of these high redshift systems have, however, not yet been penetrated because studies of z=3 systems with an H band filter (1.65 μm) only will show the morphology of these systems at a rest wavelength of 4000Å.

3.4.3 Comparison with the Cartwheel galaxy

The provenance of Andromeda's multiple ring morphology is highly in favour of expanding ring-like density waves triggered by a near head-on galaxy collision, much like that observed in the Cartwheel Galaxy. The Cartwheel is the archetype of a double-ringed morphology produced by a collision with a smaller neighbour. As with the observed M31 morphology, the Cartwheel shows two distinct density wave rings: a conspicuous outer ring, associated with massive star formation, and an elliptical inner ring, offset from the centre of the galaxy. In between the two rings lie several filamentary spiral arms, termed "spokes", which have developed a trailing pattern terminating at the inner ring. Several models have been computed of the Cartwheel galaxy, simulating the almost head-on collision with one of its companions (e.g. Struck-Marcell & Higdon 1993, Horellou & Combes 2001).

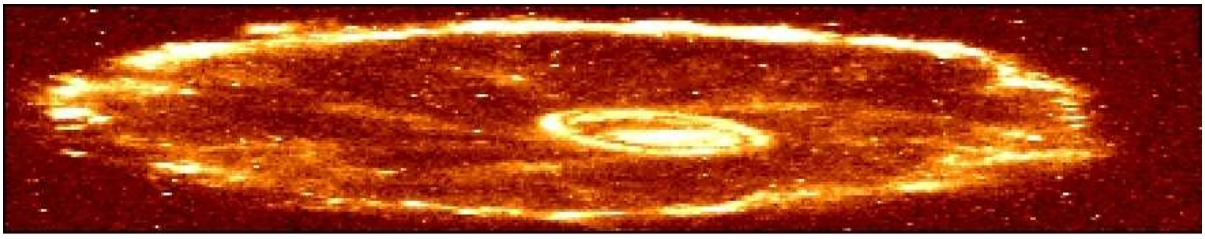

Figure 3.6: *A Hubble Space Telescope (HST) blue-band image of the Cartwheel galaxy (ESO 350-40) (Borne et al. 1994) has revealed massive star formation taking place in the outer ring of the Cartwheel. Evident are blazing OB associations, as well as the dusty structure of the elongated and off-centered inner ring. As in M31, the Hα, radio-continuum and HI 21cm emissions trace the outer ring (Higdon 1996). The HST image of the Cartwheel is projected with the same inclination as Andromeda in Figure 3.6 and the similarity of the double-ringed eccentricity is highly compelling in that this B band image of the Cartwheel gives the closest analogue to the double-ringed 8.0μm IRAC morphology of M31.*

To investigate whether the passage of M32 through the disk of Andromeda is capable of forming the two offset density wave rings identified in the IRAC images, N-body simulations of the type described in Bournaud & Combes (2003) were performed.

3.4.4 N-body Simulations by Bournaud & Combes

Numerical simulations by Bournaud & Combes (Bournaud & Combes, 2003; Block et al, 2006), offer a completely new interpretation for the morphology of M31. Both rings result from a companion galaxy plunging nearly head-on through the centre of the disk of M31. The most likely candidate is M32. Head-on collisions between galaxies are rare, but it appears nonetheless that one took place 210 million years ago in the Local Group. The simulations these authors performed included the gravitational effects of stars, gas and dark matter in M31 and M32, simulating one million particles and having a spatial resolution of 350 parsecs. An initial mass ratio for M32 of $1/10^{th}$ that of M31 (including dark matter) was assumed. Current epoch mass estimates of M32 are lower, consistent with gas and stars likely to have been stripped during the collision (Bekki et al. 2001). The results of the simulations, which fully incorporate the dark matter content in both galaxies, are shown in Figure 3.7. These simulations account for the orbit of the disrupting galaxy close to the polar axis of M31, and the mass ratio takes the dark matter into account, as well as the mass stripped in the collision. The simulations of a head-on collision beautifully reproduce the observed global morphologies of the Andromeda spiral and strikingly reveal two density wave rings resulting from a collision with a M32-like companion that occurred 210 million years ago.

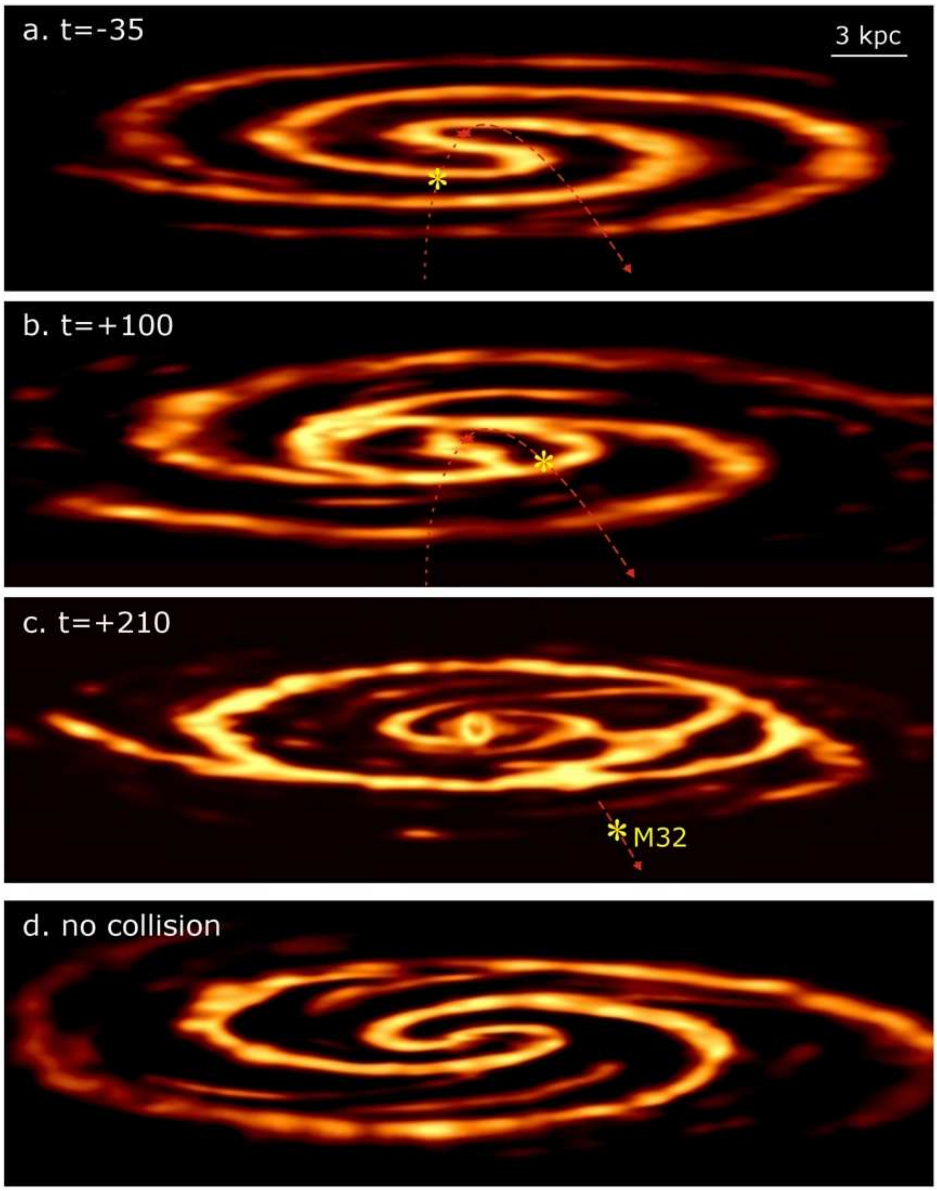

Figure 3.7*: Numerical simulation by Bournaud & Combes (Block et al., 2006) of a head-on encounter between M31 and M32 forming two ring-like density-waves, both of which are offset from the galaxy centre. The mass we invoke for the companion (a ratio 1/13th in stellar mass with M31, or 1/10th including dark matter) is compatible with the present mass of M32. The collision is not exactly head-on, but the companion path is inclined with respect to the perpendicular of the M31 plane by 35 degrees. The companion crosses the M31 disk at a velocity of 265km/s, with an impact parameter of 4 kpc, 210 Myr ago. It would now be located at a distance of 35kpc and at a galactic latitude of about 45 degrees, which is fully compatible with the present position of M32.*

Both density wave rings are offset from the galaxy centre in the simulations. The outer density wave in M31 propagates through the disk, resulting in a perturbed interlacing of spiral features with an outer ring. This produces the extremely conspicuous hole observed in the outer 10 kpc ring of M31 (compare ***c*** and ***d*** in Figure 3.7; see also Figure 3.3).

The gas morphology produced by the simulations (Bournaud & Combes, 2003) of a nearly head-on encounter of M32 with the central region of M31 are seen in Figure 3.7. The N-body models by these authors include the gravitational dynamics of stars, interstellar matter, as well as dark matter in both M31 and M32. A "sticky-particle" scheme accounts for the dissipative nature of the interstellar medium. The dashed red line demarcates the orbit of M32 with the impact trajectory closely aligned to the polar axis of M31. Snapshots a, b, and c occur at t = 35 Myr prior to the collision and at 100 and 210 Myr post impact, respectively. The latter represents the position of M31 as we see it today. All snapshots are viewed with the disk at an inclination angle of 77 degrees for direct comparison with Figure 3.3. Snapshot c shows the central region of M31 warped by a tilt angle of 30 degrees with respect to the main disk plane in accordance with observations (Jacoby et al. 1985). The two ring-like density-waves (both offset from the galaxy centre) as well as the hole in the outer ring are seen. Snapshot d shows the gas morphology at t = 210 Myr starting from the same initial disk conditions but without a collision scenario. In this case the dynamics without a collision do not produce double rings. The initial mass ratio for M32 (including dark matter) is assumed to be $1/10^{th}$ that of M31. The companion is assumed to impact the M31 disk at a velocity of 265 km/s with an impact parameter of 4 kpc. It would now be located at a distance of 35 kpc and at a galactic latitude of about 45 degrees, which is fully compatible with the present position of M32 (Mateo, 1998).

In comparison with the Cartwheel galaxy, the two rings in M31 are less contrasted, and are interlaced with prominent spiral arm features. Ring contrasts are highly dependent upon the mass of the companion involved in the collision process. These contrasts are indeed reproduced in our numerical model, resulting from the smaller mass of the colliding companion. The Cartwheel Galaxy has clearly undergone a much more violent

collision which makes the density wave rings much more contrasted compared to its spokes (spiral arms). The simulation by Bournaud & Combes confirms that the spiral disk in M31 can still be observed beyond the primary ring wave. In addition, the second elongated density wave ring begins to propagate in the central regions of the galaxy, most likely in a tilted central disk. The non-zero impact parameter produces the off-centering of the inner ring, and the inclination of the orbit with respect to the perpendicular produces the ring elongation. It is interesting to note that the collision does not destroy the boxy bar that pre-existed in the target disk in the simulation and that the inner ring has a random orientation with respect to the triaxial bulge, which is oriented at 15 degrees from the major axis.

3.4.5 Dynamics of the induced velocity field

Specific velocity perturbations are produced by induced ring-waves in a disk galaxy by a near head-on collision, which serve as confirming signatures of the event. These perturbations are very complex when modeled in all three dimensions (Appleton & Struck-Marcell, 1996). In addition to the perturbation of the rotational (tangential) as well as radial velocities, there are characteristic velocities perpendicular to the disk plane, which becomes warped and corrugated. However, due to the high inclination of Messier 31, the velocity perturbations perpendicular to the galactic plane will have a negligible effect on the Doppler velocities as observed from our point of view. For the case of small perturbations, such as the one suggested where the interacting companion has a mass less than $1/10^{th}$ of the target mass, it is possible to model the perturbation analytically with first order epicyclic theory. Once receiving a velocity impulse due to the brief passage of the companion through the target galaxy, the particles in the target galactic disk perform small oscillations around a guiding centre in a circular orbit. The effect is dominated by the resulting kinematic wave at the beginning of the perturbation, while the self-gravity of the perturbation only becomes more important at later epochs.

At a particular epoch, a density wave appears where particles propagate outwards in their epicyclic oscillation and encounter particles in other orbits flowing inward. The sense of

the dominating radial velocity of most particles in the ring depends on the precise potential and variation of the epicyclic frequency with radius.

The epicyclic approximation predicts larger perturbations in the tangential velocities for a flat rotation curve (as is the case for M31) by a factor of 1.4. In the numerical model, tangential streaming motions are indeed seen ranging between 15 and 20 km/s at the 10 kpc ring radius. The sense of the dominating velocities in the ring wave depends on the potential, and a velocity gradient is predicted at the ring boundaries.

After the companion has crossed the target galactic disk, the particles experience an inward tidal pull, and the conservation of angular momentum requires that tangential velocities increase with respect to the circular velocity. When particles then propagate outwards in their epicycle, their tangential velocity reaches a minimum at their apocentre.

The kinematic signature of a resulting positive radial velocity in the ring will thus be associated with a decreased rotational velocity towards the outer parts of the ring and a corresponding increased rotational velocity in the inner parts of the ring. This signature is very significant since the predicted tangential streaming motions are opposite in direction to that expected for spiral arm density waves. A spiral arm exhibits a tangential velocity increase just outside the arm and a decrease on the inner side (Shu et al., 1973).

Both neutral hydrogen gas (Brinks & Shane, 1984) and CO molecular traces (Dame et al. 1993, Nieten et al. 2005) reveal streaming motions in M31. These are more readily determined in the diffuse neutral component, because the molecular gas is generally patchier. The perturbations in the galactocentric radial and tangential directions are blended in various proportions in the observed Doppler velocities, depending on the position with respect to the major or minor axis. Only tangential velocities are measured on the major axis while only radials ones are measured on the minor axis. The 77.5 degree inclination of M31 however, makes it more difficult to disentangle the radial rings and spiral arms velocity components, since both are compressed in projection along the minor axis. Near the major axis where tangential perturbations are expected to dominate,

the inclination effects are less severe. The observed isovelocity curves (Unwin, 1983) favour a depression of tangential velocity in the outer parts of the arm/ring. This results in a consistent interpretation in terms of a ring induced by collision rather than secular-evolution spiral density waves. In other regions of M31, the streaming motions correspond to density-wave features, fully consistent with the underlying spiral structure. For a more quantitative discussion on the dynamics of the induced velocity field, see the appendix to the online edition of Block et al. (2006) at www.nature.com/nature

– CHAPTER 4 –

SEPARATION OF BAR AND SPIRAL ARM TORQUES IN NEARBY DISK GALAXIES

The essential fact is that all the pictures,
which science now draws of nature,
and which alone seem capable of according
with observational facts,
are mathematical pictures.

– Sir James Jeans

4.1 Introduction

4.1.1 The Hubble-Jeans Tuning Fork Revisited

Central elongated features in disk galaxies, known as bars, were first recognized by Curtis (1918a). The percentage of ovals and bars cannot be estimated from blue-light images, because young Population I dust masks are very efficient in obscuring them. The Hubble classification scheme already recognized the morphological differences between barred and unbarred spiral galaxies, such as those listed in '*A Revised Shapley Ames Catalogue of Bright Galaxies*' (commonly, the RSA, Sandage & Tammann, 1981) and in the '*Carnegie Atlas of Galaxies*' (commonly, the Carnegie Atlas, Sandage & Bedke, 1994). It is very significant that there are a greater proportion of galaxies classified as 'barred' in the '*Third Reference Catalogue of Bright Galaxies*' (commonly, the RC3, de Vaucouleurs et al., 1991) as compared with the RSA, being a forerunner of the Carnegie Atlas. The reason for this refinement is credited to de Vaucouleurs who took careful cognizance of the nebulous divide between barred and unbarred galaxies by introducing the notation (SA, S<u>A</u>B, SAB, SA<u>B</u>, SB). SA galaxies are prototypical unbarred spirals while SB's are strongly barred. Underlined letters specify the dominant contribution in the intermediate cases.

It should be borne in mind that these atlases are all constrained to optical photography. The ubiquity of bars in our local universe has only recently been fully appreciated – a direct result of near-infrared imaging. In particular, 70% of spirals classified in the *Carnegie Atlas* are classified as unbarred using the Hubble scheme, a number which reduces to 27% when these galaxies are imaged in the near-infrared (Eskridge & Frogel, 1999). Similarly, 40 galaxies with a wide range in Hubble type, out of a sample of 45 by Seigar & James (1998) are barred in the J and K bands. Nine of these galaxies are classified as unbarred in optical wavelengths. Block et al. (2001) estimate that over 80% of disk galaxies in the local universe are barred in the near-infrared. As such, bars are a far more integral feature of disk galaxies than was previously thought.

4.1.2 Quantitative Bar Strength Classification

Bar strength measurements have taken on a variety of different quantitative approaches. One of the most readily amenable, as investigated by Martin (1995), is the isophotal deprojected bar axis ratio $(b/a)_{bar}$. This is usually written as a bar ellipticity index: ($\varepsilon_{bi} = 10[1 - (b/a)_i]$). This parameter is not a complete description of bar strength, but serves as a readily accessible one and relates to bar strength based on analytic models by Athanassoula (1992a). Abraham & Merrifield (2000) refine the bar axis ratio parameter by considering "the minimum fraction [F_{Bar}] of the bar's stars that one would have to rearrange in order to transform the structure into an axisymmetric distribution", which they quantify as:

$$F_{Bar} = \frac{2}{\pi}[\arctan(\frac{b}{a})^{-\frac{1}{2}} - \arctan(\frac{b}{a})^{\frac{1}{2}}] \tag{4-1}$$

Bar-interbar contrast was investigated by Elmegreen & Elmegreen (1985) who derive relative bar luminosities in terms of the m = 2 and m = 4 components of Fourier intensity amplitudes. The bar luminosity fraction ranges from between 1% to 20% relative to the total luminosity of the disk given a standard isophote of $\mu_B = 25.0$ mag arcsec^{-2}. Although a distinction can be made between strong and weak bars, the method only indirectly links to their gravitational torques. The maximum bar-interbar contrast may lie inside the

radius of the bar, but instances where it is outside the bar have been found by Buta (1986), such as in NGC 1433. The bar-interbar contrast is also sensitive to resolution and seeing effects (Seigar & James, 1998).

4.2 Bar and Spiral Arm Torque Classification using the Modified GTM

4.2.1 Introduction

Buta & Block (2001), as well as Block et al. (2001) have pioneered an alternative approach to quantifying the observed bar strengths of galaxies. These authors implemented the proposal by Combes & Sanders (1981) that gravitational potentials could be investigated by assuming a nearly constant mass-to-light ratio in dust-penetrated near-infrared disk galaxies. The Gravitational Torque Method (hereafter, GTM) described in detail in §2.3, provides a quantitative handle on the prominence of bars in disk galaxies in the near-infrared. Advantages of the GTM over previous methods are that it is not dependant on surface photometry, spectroscopic data, deprojected bar ellipticities, nor a rigorous definition of the bar. The modified GTM or "bar torque method" has exhibited considerable robustness in the presence of noise and takes full cognizance of the disk in which the bar is embedded (see, for example, NGC 922 in Block et al. 2001). This method of bar description has been recently used by Rozas et al. (1998), Knapen et al. (2000), and Abraham & Merrifield (2000). This thesis builds on the analysis performed by these authors with the aid of an excellent data set of Spitzer IRAC as well as IRIS2 K_s band images secured with the 3.9m Anglo Australian Telescope (AAT).

The correlation between spiral arm torque and bar torque in spiral disk galaxies has remained an open question. Laurikainen et al. (2001) and Block et al. (2002) have suggested that the GTM could be modified so as to determine, separately, the contribution of bar and spiral torques. If the bar and spiral arms are well enough separated, then the maximum torque obtained by the original GTM will be a good approximation to the bar strength. However, many barred spirals have strong spiral arms that break directly from the ends of the bar, and these arms can significantly affect the bar strength as determined by the GTM. For this reason, the GTM was modified by

introducing Fourier-based image processing methods which aid in the separation of the torque contributed by bars and spiral arms. With such a separation analysis, the question as to whether bars with larger torques drive spirals with larger amplitudes can be properly addressed.

4.2.2 A Fourier Technique to Separate Bars and Spiral Arms

Bar-spiral decomposition involves subjecting a star-cleaned, deprojected near-infrared image of a disk galaxy, to a two-dimensional Fast Fourier Transform analysis. For each barred galaxy which has been image processed in this thesis, the following prescription was used:

Since the GTM calculates a relative gravitational torque, being the ratio between the tangential and radial components, foreground (Milky Way) sources and very strong star-forming regions need to be removed. These objects can cause local maxima or minima in the force ratio maps that may be unreliable if the mass-to-light ratios of these regions differ from the dominant old stellar background. Luminous red supergiants impact the K-band (Rhoads 1998) and can influence luminosity flux by as much as 30%. However, the precise contribution of obscured HII regions and red supergiants to K-band luminosity is still to be properly addressed. For all galaxies listed in this chapter, removal of such sources was achieved using the IRAF routine IMEDIT. (See §2.2.2 for a detailed discussion on foreground source removal for dense fields, such as those through which M33 is imaged.)

In order to correctly account for the effects of inclination, galaxies need to be deprojected. Preparation for deprojection involves centering of each galaxy so that the image pixel with the highest intensity in the bulge (determined using the IRAF routine IMEXAM) corresponds with the centre of a square image frame. Both of these manipulations (centering and cropping) are performed simultaneously using the IRAF routine IMLINTRAN. The next step is the actual deprojection.

For approximately half of the galaxies analysed in this chapter, position angles and axis ratios have been sourced from individual papers (see table 4.1) while the remainder come from the '*Third Reference Catalogue of Bright Galaxies*' (RC3, de Vaucouleurs et al. 1991). The deprojection is subsequently performed using the IRAF routine IMLINTRAN and the images are cropped to a 2^n square array, where n is typically 8, 9 or 10, to be processed by the QFG code (see §2.3.2).

The bar-spiral decomposition technique requires an accurate identification of the bar. Such an identification is made with reference to the phase of the m=2 Fourier component, which readily identifies the presence of a bar as a locus of constant phase for an extended region in radius space.

Mathematically, the separation involves scaling the sine and cosine amplitudes of the bar-dominating even Fourier terms, according to the ratio of the m=0 amplitudes at different radii. Since the Fourier phases are approximately constant in the case of a bar, this scaling works particularly well as a first order approximation.

Relative Fourier amplitudes calculated by Ohta et al. (1990) for six early-type barred systems, showed three characteristics of the relative Fourier amplitudes of bars:

i. higher order even-terms are significant for strong bars (this thesis uses up to m=10);
ii. relative amplitudes of bars rise and decline radially past a maximum, that lies symmetric with respect to the middle of each side of the apparent bar;
iii. for high resolution images, it is feasible to consider the radii of the maxima for higher order terms (m = 4, 6, 8, …)

The relative Fourier intensity amplitudes I_m/I_0 are computed, and it is assumed that the even ($m \geq 2$) term's (i.e. the bar's) relative intensity increases radially outward, until reaching a maximum at which point they declines in a similar and often identical way (i.e.: a mirror image about the maximum) as per the Ohta et al. prescription. In order to

determine the extent of the extrapolation of the bar, the I_m/I_0 ratio is plotted as a function of radius and shows a distinct peak at small radii for mostly pure bar plus disk systems. These are traced out to a specified radius where the bar is assumed to be well mixed with the ends of spiral arms. There is also usually an inner radius where the bar is assumed to go to zero, thereby avoiding the inner nuclear regions of galaxies which always have high intensity, and avoids convolution uncertainties in processing the 'central pixels'. In cases where the bar and spiral are well enough separated, their individual signatures are easily determined.

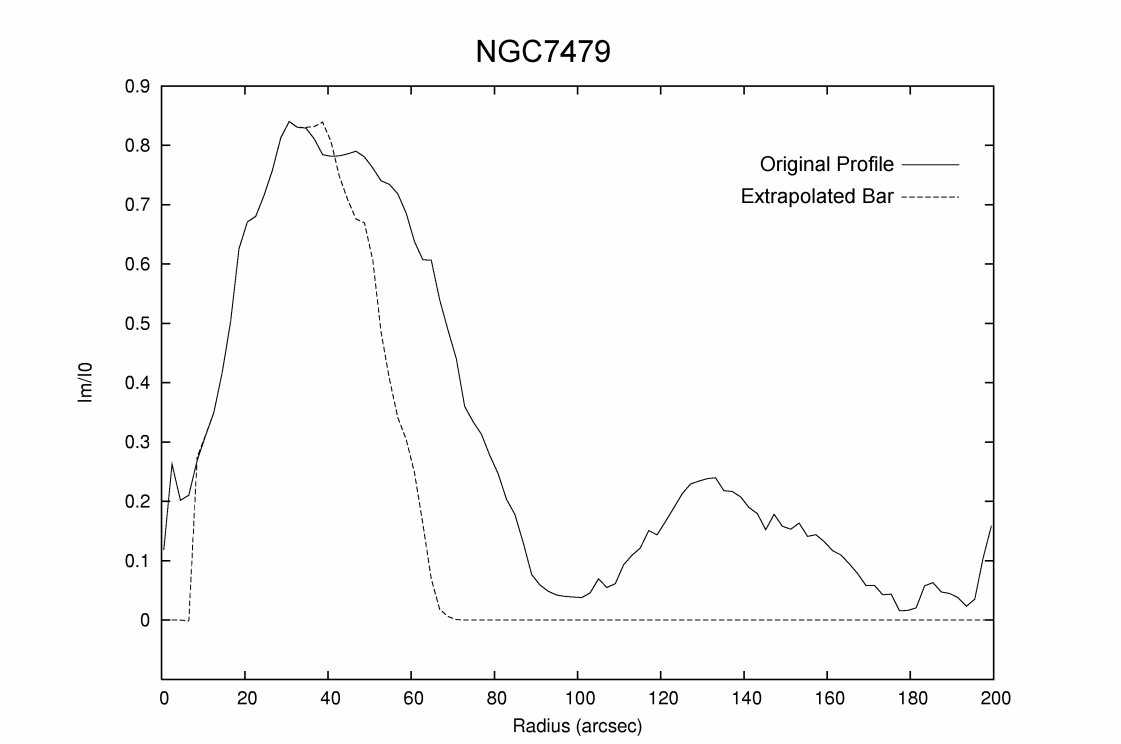

Figure 4.1: *The NGC7479 relative Fourier intensity amplitude for m=2 is plotted as a function of radius (solid line). The extrapolated synthetic bar profile is represented by the dashed line. The bar profile is reflected about a radius of 37 arcsec, and it is assumed not to end abruptly but that it decays to zero similarly to the way in which the profile slope reached a maximum. The "double-hump" near the bar profile "centre" is an artifact of this method, but the alternative of modeling the original profile slope to ~100 arcsec did not result in a satisfactory bar decomposition in the case of NGC7479. All galaxies that have been bar/spiral separated in this thesis have been selected using this prescription.*

For each bar-spiral separated galaxy in this thesis the radius of the maxima of the bars were individually determined, along with the minimum radius (the extent of the nuclear region) as well as deciding whether the decay of the I_m/I_0 curves for the even m terms, follows the profile of the bar, or if it needed to be synthetically extrapolated as a mirror image about the maximum. In practice, this is an iterative process whereby the parameters are individually judged, and are then verified by Inverse Fourier transform. This results in a synthetic image of the galaxy which can be compared with the original.

4.2.3 Synthetic Bar/Spiral Arm Generation through Inverse Fourier Transforms

By selecting the appropriate m terms, an Inverse Fourier Transform provides a graphic representation of the galaxy, where, in the case of this thesis, terms with m>10 have been excluded. The technique thus provides a full 'Fourier smoothed' image.

The power of this technique is exploited by selectively choosing only the even m terms, i.e., m=2, 4, … 10 to extract the bar-only light intensity contribution. This in turn can be subtracted from a smoothed image with all terms from m = 0 to 10 present, so that only the axisymmetric disk as well as the spiral arms remain, to provide the spiral arm contribution.

This method effectively isolates the contribution to the overall gravitational torque from the bar, and as such, provides a way to compute the maximum relative bar torque Q_b and the maximum relative spiral torque Q_s separately.

The method is illustrated for NGC 4593 in Figure 4.2. The prominent bar dominates the relative Fourier amplitudes near the inner region. It is assumed the bar does not end abruptly, but in the absence of the spiral, the even relative Fourier amplitudes due to the bar decline in the same manner as they rose to the bar maximum.

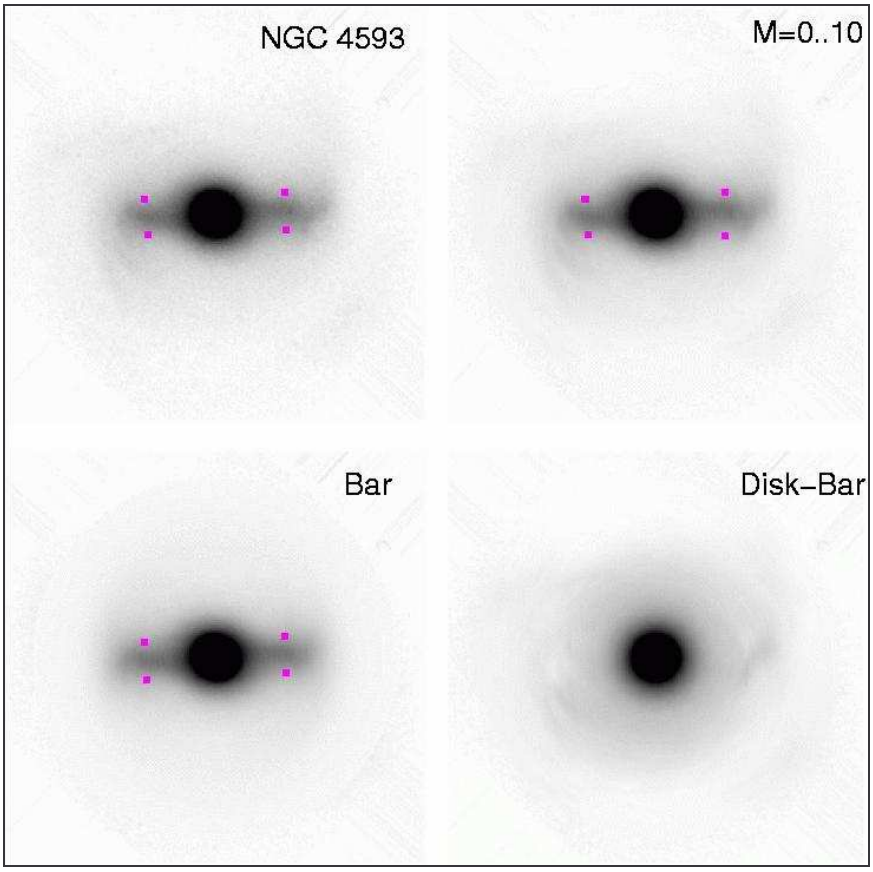

Figure 4.2: *This K_s band image of NGC4593, secured with the IRIS2 instrument on the 3.9m AAT, reveals the power of the bar spiral decomposition technique. All four quadrants have the same orientation, with the bar rotated to horizontal. Top left is the deprojected AAT image. The image at top right was generated by displaying only the terms (m=0, 1, 2,…10). This "Fourier-smoothed" version of the full image demonstrates that the first 10 m terms are sufficient to retain essentially all the large scale morphological detail. The image at lower left was generated using only the terms m = 2, 4, 6, 8, 10. This effectively selects the bar-only contribution to the light intensity distribution of the galaxy. The lower right image shows the axisymmetric disk plus spiral arms, generated by subtracting the "bar-only" contribution from the m=0..10 smoothed image. The positions of the torque maxima are indicated by the four squares on each of the images containing the bar.*

In cases where bars are not completely symmetric about the galaxy's centre, the extrapolations result in residual over/under subtractions. This occurs in particular cases where the bar relative intensity profiles may not be as symmetric as initially assumed and is correspondingly treated by incorporating the shape of the decline past the maximum as far as possible, with minimal extrapolation thereafter.

It is believed that for most disk galaxies, the analysis can be realistically cut at m=10 without losing much additional information. To verify this, Buta et al. (2003) have computed potentials from both the full image at maximum resolution, and a Fourier-smoothed image based on the sum of all even and odd terms up to m=20. These authors find that the Fourier-smoothed m=0-20 images generally give the same result as the full (unsmoothed) images, with any differences being attributable to noise and the occasional bright star-forming region, and is not reliant on the morphology of the galaxy as a whole.

4.3 A Combined Sample of 40 Nearby Barred Galaxies

4.3.1 Details of the Spitzer IRAC Sample

The sample investigated here consists of 40 galaxies listed in Table 4.1. These were loosely selected which span a broad range of Hubble type and inclination < ~65°. These galaxies also span a large range of optical apparent bar strengths covering the de Vaucouleurs families SA, SAB, and SB.

Of the sample galaxies, 17 were observed with IRAC onboard the Spitzer Space telescope (see §3.2.2). The Spitzer images were taken at 3.6μm, and have a pixel scale of 0.8600 arcsec/pixel. Further details are provided in table 4.1.

GALAXY	PA(deg)	Incl.(deg)	PA/Incl.Source	D(Mpc)	DSource
NGC0266	162	29	Grosbøl (1985)	61.9	T&F
NGC3198	36	72	Corradi (1991)	10.8	T&F
NGC3351	11	46	Grosbøl (1985)	8.1	T&F
NGC3368	135	48	Moiseev (2005)	8.1	T&F
NGC3627	173	63	RC3	6.6	T&F
NGC4303	7	25	Warmels(1988)	15.2	T&F
NGC4314	95	23	Grosbøl (1985)	9.7	T&F
NGC4321	58	25	Grosbøl (1985)	16.8	T&F
NGC4421	20	41	RC3	16.8	T&F
NGC4450	170	50	Grosbøl (1985)	16.8	T&F
NGC4536	130	65	RC3	13.3	T&F
NGC4579	89	39	Grosbøl (1985)	16.8	T&F
NGC4725	37	49	Grosbøl (1985)	12.4	T&F
NGC5371	5	51	Grosbøl (1985)	37.8	T&F
NGC5377	37	57	Grosbøl (1985)	31	T&F
NGC7479	25	41	RC3	29.1	T&F
NGC7741	163	38	Grosbøl (1985)	12.3	T&F

Table 4.1: *Position angle, inclination and distances to 17 galaxies of the Fazio GTO sample of Spitzer IRAC galaxies. The Spitzer data used in this chapter are exclusively 3.6μm (Channel 1) images. All distances assume the Hubble parameter as used in Tully & Fisher as 75km/s/Mpc*

While calibrations to the Spitzer data are available (in MJy/steradian relative to Vega) these calibrations are not required for a gravitational torque analysis because bar and spiral torques are measured relative to the axisymmetric radial force.

4.3.2 Details of the AAT IRIS2 Sample

K-band observations of 23 galaxies were secured by Johan Knapen with the 3.9m AAT, with a nominal resolution of 0.441 arcsec/pixel. The GTM is not critically dependent on sky subtraction for the AAT images, as only relative gravitational torques are calculated and the spiral and bar torque maxima tend to occur in the fairly bright inner regions of the disk where sky subtraction uncertainties have particularly little influence. Position parameters for each galaxy were sourced preferentially from Grosbøl (1985) as well as the RC3. These included position angle (PA) and inclination. The distances to each galaxy were taken preferentially from Tully & Fisher (1987), and were calculated from

the RC3 using a Hubble parameter of 75km/s/Mpc. Further details are provided in table 4.2.

GALAXY	PA	Incl.	PA/Incl.Source	D	DSource
IC1438	–	32	RC3	33.8	T&F
IC4290	98	36	RC3	64.88	RC3(75)
NGC1300	103	51	Grosbøl (1985)	18.79	T&F
NGC1566	60	37	RC3	13.43	T&F
NGC175	36	0	Grosbøl (1985)	50.99	RC3(75)
NGC4593	89	47	Grosbøl (1985)	39.45	T&F
NGC5101	–	32	RC3	27.42	T&F
NGC521	30	23	Grosbøl (1985)	67.04	RC3(75)
NGC5335	90	49	RC3	62.53	RC3(75)
NGC5365	4	51	RC3	33	T&F
NGC613	113	46	Grosbøl (1985)	17.46	T&F
NGC6221	5	46	RC3	19.4	T&F
NGC6384	31	50	Grosbøl (1985)	26.6	T&F
NGC6782	45	49	RC3	51.89	RC3(75)
NGC6907	57	32	Grosbøl (1985)	41.67	RC3(75)
NGC7155	4	36	RC3	23.5	T&F
NGC7329	107	47	RC3	42.12	RC3(75)
NGC7513	114	48	Grosbøl (1985)	20.85	RC3(75)
NGC7552	1	37	RC3	19.5	T&F
NGC7582	157	65	RC3	17.6	T&F
NGC7690	132	67	RC3	16.4	T&F
NGC986	150	41	RC3	23.23	T&F
UGC10862	–	24	RC3	26.9	T&F

Table 4.2: *Position angle, inclination and distances to 23 galaxies of the Knapen 3.9m AAT sample of IRIS2 K_s band galaxies. Distances determined from the RC3 use the Tully & Fisher value for the Hubble parameter as 75km/s/Mpc.*

4.3.3 Calculated Bar and Spiral Arm Torques

This procedure was conducted on the full sample of galaxies listed and revealed a variety of bar and spiral arm strengths, as well as variety in the Fourier extrapolations. In this sample, the highest mean error is quoted as 0.14 for NGC7741 (Q_g=0.54+/-0.14) which has the effect of misclassifying the galaxy by a single torque class at most. For a more detailed description of the error determinations in the GTM, see §2.3.4 and Buta & Block (2001).

The gravitational torque calculated for each galaxy of the sample of 40, is compared with the torque calculated for the full Fourier smoothed (m=0,1,2,…10) image. (See figure 4.3). The straight line graph has a very good fit, and the torque of the smoothed image is very similar to that of the original, in all cases, as is expected.

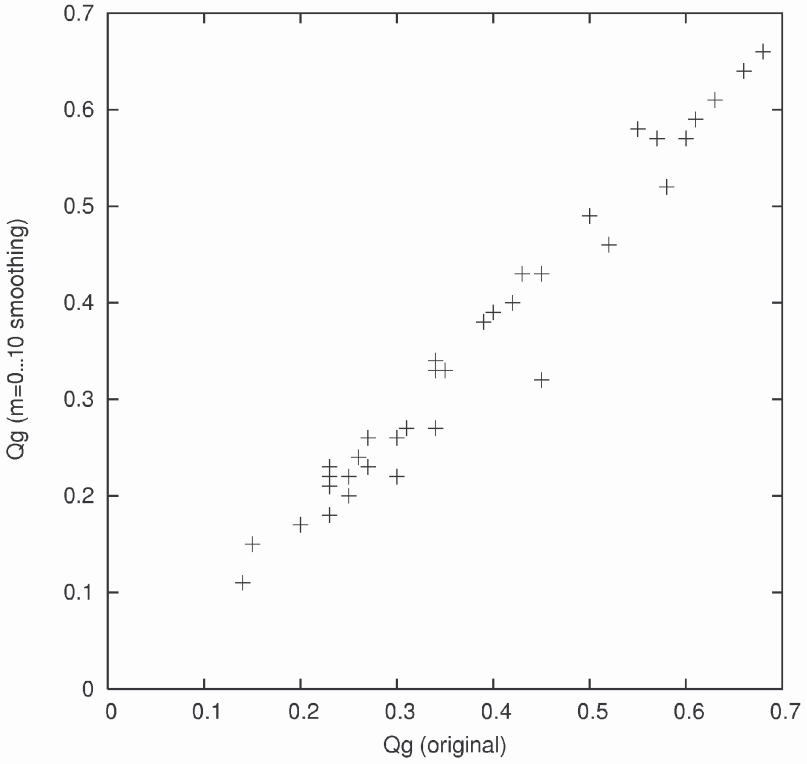

Figure 4.3: *The effect of determining gravitational torques from images generated using only the terms m = 0, 1, …, 10 as compared with "unprocessed" images, for 17 Spitzer IRAC and 23 IRIS2 AAT galaxies combined. The greatest source for scatter is attributed to mildly prominent star forming regions which are smoothed out in the m = 0, 1, …, 10 Inverse Fourier transform.*

Furthermore, the GTM necessarily presents the maximum torque prevalent in any given image, and so even if a barred galaxy has a strong spiral arm component (such as NGC7479), the value for the gravitational torque is taken to be the maximum, and not the sum, of the bar and spiral components.

The effect of assuming values of scaleheights with such a wide range (425pc is almost double that of 225pc), was shown to affect the determined gravitational torque by at most one gravitational torque class (i.e.: 10% of the relative torque calculation). This corroborates well with Buta & Block (2001).

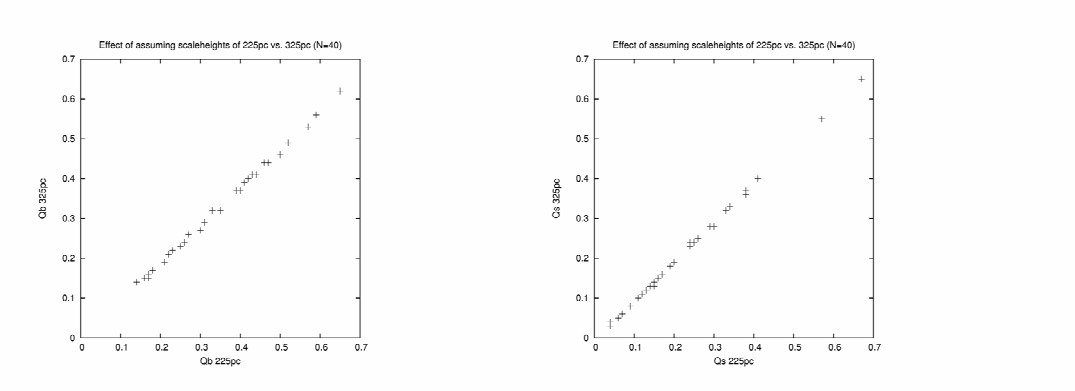

Figure 4.4: *Assuming scaleheights of 225pc and 325pc for each galaxy in the combined sample of 40, reveals a negligible change in the classification of bar and spiral arm torque class. Bar torques (seen in the panel on the left), have a minimum value of Q_b ~ 0.14, compared with spiral arm torques, which are down to Q_s ~ 0.04*

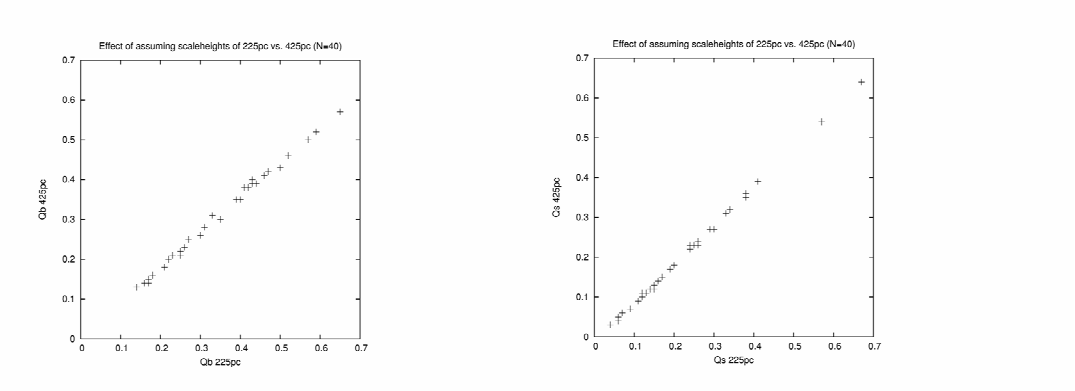

Figure 4.5: *Similar to Figure 4.4 above, but with assumed scaleheights of 225pc and 425pc. A change of a single bar strength class is the most severe deviation, and only when torque values are high, Q_b >0.5. Spiral arm torques are far less affected due to their radial distance from the bulge, where the exponential form of the scaleheight function has tapered off, thereby representing a thinner disk.*

The straight line plots in Figure 4.4 and Figure 4.5 reveal the relative insensitivity of a moderate change in scaleheight on the calculated value for gravitational torques. Tables 4.2.1, 4.2.2 and 4.2.3 summarize the results of the separations. The errors listed for Q_b and Q_s are internal to the procedure and do not include the uncertainties due to sky subtraction (as in the case for the AAT data), vertical scaleheight, bulge shape, mass-to-light ratio, or the bar extrapolation. The error in Q_s is particularly instructive since it shows the variation in the spiral arm morphology. If Q_s were based only on a single maximum or minimum, it would risk being biased by a single star-forming region or complex. Averaging over four quadrants smoothes such biases and a large error in Q_s provides an indication of the asymmetry of the spiral. A comprehensive listing of all torque values calculated on the discussed sample of 40 galaxies is tabulated in tables 4.2.1 – 4.2.3.

In summary, the preparation for each torque calculation, with its associated error, was individually performed using the following procedure: (1) The galaxy was centred, (2) foreground stars were removed, (3) the galaxy was deprojected, (4) in the case of barred galaxies – the bar was rotated horizontally, (5) a Fourier smoothed image was generated using the m=0, 1, … 10 Fourier terms, (6) the initial Fourier intensity amplitude plot was generated, (7) the parameters for the extrapolated bar were determined, (8) a synthetic bar was generated, (9) the subtraction was verified to be sensible and adequate, (10) if it was not, different extrapolation parameters were attempted, (11) the successful bar separation parameters were then stored for use with individual scaleheight values of 225, 325 and 425pc. i.e.: Each scaleheight value has an associated deprojected image, a Fourier smoothed image, a "bar only" image and a subtracted bar or "spiral only" image. The QFG code was run on each image individually to determine the maximum relative gravitational torques observed. i.e.: 40 galaxies, with 4 separate images each, were analysed with the QFG and GTM – resulting in a total of 160 calculations for *each* of the three scaleheight values assumed. Thus the above procedure was performed a grand total of 480 times for this chapter, the results of which are listed in the tables that follow.

Tables 4.2.1 – 4.2.3: *Gravitational torques as computed on the combine sample of 17 IRAC Spitzer and 23 IRIS2 AAT galaxies. Q_g represents the relative gravitational torque of correctly deprojected images of each galaxy, with no further processing. Q_t is the torque value for synthetic recreation of the entire galaxy using only the lower Fourier terms, m = 0, 1, …, 10. Q_b is the separated bar torque (m = 2, 4, 6, 8) and Q_s is the spiral arm only component.*

Galaxy	Q_g	Error (Q_g)	Q_t	Error (Q_t)	Q_b	Error (Q_b)	Q_s	Error (Q_s)
IC1438	0.27	0.02	0.26	0.02	0.27	0.03	0.16	0.05
IC4290	0.63	0.06	0.61	0.06	0.65	0.05	0.24	0.08
NGC0266	0.45	0.04	0.32	0.04	0.42	0.04	0.20	0.11
NGC1300	0.68	0.13	0.66	0.13	0.72	0.01	0.38	0.16
NGC1566	0.23	0.02	0.23	0.02	0.18	0.01	0.27	0.05
NGC175	0.60	0.06	0.57	0.05	0.46	0.06	0.34	0.02
NGC3198	0.34	0.05	0.27	0.05	0.35	0.05	0.24	0.13
NGC3351	0.30	0.01	0.26	0.01	0.25	0.03	0.13	0.01
NGC3368	0.25	0.01	0.22	0.01	0.25	0.02	0.04	0.01
NGC3627	0.31	0.03	0.27	0.03	0.17	0.03	0.17	0.03
NGC4303	0.57	0.12	0.57	0.11	0.40	0.01	0.41	0.16
NGC4314	0.52	0.04	0.46	0.04	0.50	0.04	0.13	0.06
NGC4321	0.27	0.07	0.23	0.06	0.17	0.03	0.38	0.06
NGC4421	0.30	0.03	0.22	0.02	0.30	0.03	0.19	0.16
NGC4450	0.20	0.02	0.17	0.02	0.18	0.04	0.06	0.01
NGC4536	0.25	0.02	0.20	0.02	0.18	0.02	0.25	0.04
NGC4579	0.23	0.01	0.18	0.01	0.21	0.04	0.09	0.01
NGC4593	0.40	0.04	0.39	0.04	0.41	0.01	0.15	0.03
NGC4725	0.23	0.02	0.21	0.02	0.22	0.01	0.15	0.03
NGC5101	0.43	0.02	0.43	0.01	0.43	0.01	0.06	0.03
NGC521	0.26	0.05	0.24	0.04	0.26	0.05	0.12	0.02
NGC5335	0.73	0.08	0.71	0.07	0.76	0.05	0.19	0.04
NGC5365	0.23	0.02	0.22	0.02	0.23	0.02	0.04	0.01
NGC5371	0.34	0.13	0.34	0.09	0.31	0.04	0.33	0.14
NGC5377	0.14	0.03	0.11	0.03	0.14	0.03	0.11	0.08
NGC613	0.50	0.04	0.49	0.04	0.47	0.01	0.34	0.23
NGC6221	0.43	0.07	0.43	0.07	0.44	0.03	0.30	0.12
NGC6384	0.15	0.01	0.15	0.01	0.16	0.01	0.07	0.01
NGC6782	0.34	0.02	0.33	0.02	0.33	0.02	0.14	0.03
NGC6907	0.42	0.16	0.40	0.14	0.43	0.02	0.38	0.19
NGC7155	0.35	0.02	0.33	0.01	0.35	0.03	0.06	0.02
NGC7329	0.39	0.02	0.38	0.02	0.39	0.03	0.12	0.03
NGC7479	0.55	0.12	0.58	0.09	0.52	0.03	0.57	0.21
NGC7513	0.66	0.25	0.64	0.26	0.78	0.03	0.26	0.09
NGC7552	0.61	0.03	0.59	0.03	0.59	0.01	0.29	0.04
NGC7582	0.45	0.03	0.43	0.03	0.43	0.01	0.15	0.05
NGC7690	0.23	0.04	0.21	0.04	0.17	0.12	0.15	0.01
NGC7741	0.58	0.11	0.52	0.10	0.57	0.11	0.29	0.06
NGC986	0.75	0.10	0.74	0.10	0.72	0.02	0.58	0.21
UGC10862	0.79	0.05	0.77	0.05	0.79	0.05	0.67	0.28

Table 4.2.1: *Scaleheight ~ 225pc*

Galaxy	Q_g	Error (Q_g)	Q_t	Error (Q_t)	Q_b	Error (Q_b)	Q_s	Error (Q_s)
IC1438	0.26	0.02	0.24	0.02	0.26	0.03	0.15	0.05
IC4290	0.60	0.06	0.57	0.06	0.62	0.05	0.23	0.08
NGC0266	0.42	0.06	0.30	0.04	0.40	0.02	0.19	0.11
NGC1300	0.64	0.12	0.63	0.12	0.68	0.01	0.37	0.15
NGC1566	0.23	0.02	0.22	0.02	0.17	0.01	0.25	0.05
NGC175	0.56	0.06	0.53	0.06	0.44	0.05	0.33	0.02
NGC3198	0.32	0.05	0.25	0.04	0.32	0.05	0.24	0.12
NGC3351	0.27	0.01	0.24	0.01	0.23	0.03	0.12	0.01
NGC3368	0.24	0.01	0.21	0.01	0.23	0.02	0.04	0.01
NGC3627	0.29	0.03	0.25	0.03	0.16	0.03	0.16	0.03
NGC4303	0.55	0.12	0.53	0.11	0.37	0.01	0.40	0.15
NGC4314	0.48	0.05	0.42	0.04	0.46	0.04	0.12	0.04
NGC4321	0.25	0.06	0.22	0.05	0.15	0.03	0.36	0.04
NGC4421	0.28	0.03	0.20	0.02	0.27	0.03	0.18	0.16
NGC4450	0.19	0.02	0.15	0.01	0.17	0.04	0.05	0.01
NGC4536	0.24	0.02	0.19	0.02	0.17	0.02	0.24	0.03
NGC4579	0.22	0.01	0.17	0.01	0.19	0.04	0.08	0.01
NGC4593	0.38	0.04	0.37	0.04	0.39	0.02	0.14	0.03
NGC4725	0.22	0.03	0.20	0.02	0.21	0.01	0.13	0.03
NGC5101	0.41	0.02	0.40	0.01	0.41	0.01	0.03	0.02
NGC521	0.24	0.04	0.23	0.04	0.24	0.05	0.11	0.03
NGC5335	0.69	0.07	0.67	0.07	0.71	0.04	0.18	0.03
NGC5365	0.22	0.02	0.21	0.02	0.22	0.02	0.04	0.01
NGC5371	0.33	0.13	0.32	0.09	0.29	0.04	0.32	0.14
NGC5377	0.13	0.03	0.11	0.03	0.14	0.03	0.10	0.07
NGC613	0.47	0.06	0.47	0.04	0.44	0.01	0.33	0.21
NGC6221	0.41	0.07	0.40	0.08	0.41	0.03	0.28	0.12
NGC6384	0.14	0.01	0.13	0.01	0.15	0.01	0.06	0.01
NGC6782	0.33	0.02	0.32	0.02	0.32	0.02	0.13	0.02
NGC6907	0.40	0.15	0.39	0.13	0.41	0.03	0.37	0.17
NGC7155	0.32	0.02	0.31	0.02	0.32	0.03	0.05	0.01
NGC7329	0.37	0.01	0.36	0.01	0.37	0.03	0.11	0.03
NGC7479	0.53	0.10	0.54	0.08	0.49	0.03	0.55	0.20
NGC7513	0.63	0.22	0.61	0.23	0.72	0.02	0.25	0.08
NGC7552	0.57	0.03	0.56	0.02	0.56	0.01	0.28	0.04
NGC7582	0.42	0.02	0.41	0.02	0.41	0.01	0.14	0.04
NGC7690	0.22	0.04	0.20	0.04	0.16	0.11	0.13	0.01
NGC7741	0.54	0.14	0.48	0.11	0.53	0.12	0.28	0.08
NGC986	0.71	0.10	0.70	0.10	0.68	0.02	0.55	0.21
UGC10862	0.75	0.05	0.73	0.06	0.74	0.05	0.65	0.27

Table 4.2.2: *Scaleheight ~ 325pc*

Galaxy	Q_g	Error (Q_g)	Q_t	Error (Q_t)	Q_b	Error (Q_b)	Q_s	Error (Q_s)
IC1438	0.24	0.02	0.23	0.02	0.25	0.03	0.14	0.05
IC4290	0.57	0.06	0.55	0.06	0.57	0.05	0.22	0.08
NGC0266	0.41	0.06	0.29	0.04	0.38	0.02	0.18	0.11
NGC1300	0.62	0.13	0.60	0.12	0.65	0.01	0.36	0.15
NGC1566	0.22	0.02	0.22	0.02	0.16	0.01	0.24	0.05
NGC175	0.53	0.06	0.50	0.06	0.41	0.05	0.32	0.02
NGC3198	0.30	0.05	0.24	0.05	0.30	0.05	0.23	0.12
NGC3351	0.26	0.01	0.23	0.01	0.21	0.03	0.11	0.01
NGC3368	0.22	0.01	0.20	0.01	0.22	0.02	0.03	0.01
NGC3627	0.27	0.03	0.24	0.03	0.15	0.03	0.15	0.03
NGC4303	0.49	0.12	0.50	0.10	0.35	0.01	0.39	0.15
NGC4314	0.45	0.05	0.39	0.04	0.43	0.04	0.11	0.04
NGC4321	0.24	0.05	0.21	0.04	0.14	0.03	0.35	0.04
NGC4421	0.26	0.03	0.19	0.02	0.26	0.03	0.17	0.15
NGC4450	0.18	0.02	0.15	0.01	0.16	0.04	0.04	0.01
NGC4536	0.23	0.02	0.18	0.02	0.16	0.02	0.23	0.02
NGC4579	0.20	0.01	0.16	0.01	0.18	0.04	0.07	0.01
NGC4593	0.37	0.04	0.36	0.04	0.38	0.02	0.13	0.02
NGC4725	0.21	0.02	0.19	0.02	0.20	0.01	0.12	0.03
NGC5101	0.39	0.02	0.38	0.02	0.39	0.01	0.03	0.02
NGC521	0.23	0.04	0.21	0.04	0.23	0.05	0.10	0.03
NGC5335	0.66	0.06	0.63	0.06	0.67	0.04	0.17	0.02
NGC5365	0.21	0.02	0.20	0.02	0.21	0.02	0.03	0.01
NGC5371	0.31	0.13	0.31	0.11	0.28	0.04	0.31	0.13
NGC5377	0.13	0.03	0.10	0.03	0.13	0.03	0.09	0.07
NGC613	0.45	0.06	0.44	0.04	0.42	0.01	0.32	0.21
NGC6221	0.39	0.08	0.38	0.08	0.39	0.02	0.27	0.11
NGC6384	0.13	0.01	0.13	0.01	0.14	0.01	0.06	0.01
NGC6782	0.32	0.01	0.31	0.02	0.31	0.02	0.12	0.02
NGC6907	0.38	0.14	0.38	0.13	0.40	0.03	0.36	0.16
NGC7155	0.30	0.02	0.28	0.02	0.30	0.03	0.05	0.01
NGC7329	0.35	0.01	0.33	0.01	0.35	0.03	0.11	0.03
NGC7479	0.50	0.09	0.50	0.07	0.46	0.04	0.54	0.20
NGC7513	0.60	0.19	0.59	0.20	0.68	0.02	0.23	0.07
NGC7552	0.54	0.02	0.53	0.02	0.52	0.01	0.27	0.04
NGC7582	0.40	0.02	0.38	0.02	0.40	0.01	0.13	0.04
NGC7690	0.21	0.04	0.19	0.04	0.15	0.11	0.12	0.01
NGC7741	0.51	0.16	0.45	0.12	0.50	0.14	0.27	0.06
NGC986	0.68	0.07	0.67	0.10	0.64	0.02	0.54	0.20
UGC10862	0.70	0.06	0.68	0.06	0.69	0.05	0.64	0.26

Table 4.2.3: *Scaleheight ~ 425pc*

4.4 Relationship between Bar and Spiral Arm Torques

4.4.1 Do Stronger Bars Drive Stronger Spirals?

The principal goal of this chapter was to test theoretical predictions that bars with larger torques could possibly drive spirals with larger spiral arm torques. The correlation between spiral arm torque and bar torque is presented in figures 4.7 and 4.8. There are three distinct scenarios that can be looked at in closer detail; (a) weak bars with a significant spiral arms torque contribution, (b) strong bars, but weak or no spiral arms and (c) strong bars that drive strong spiral arms.

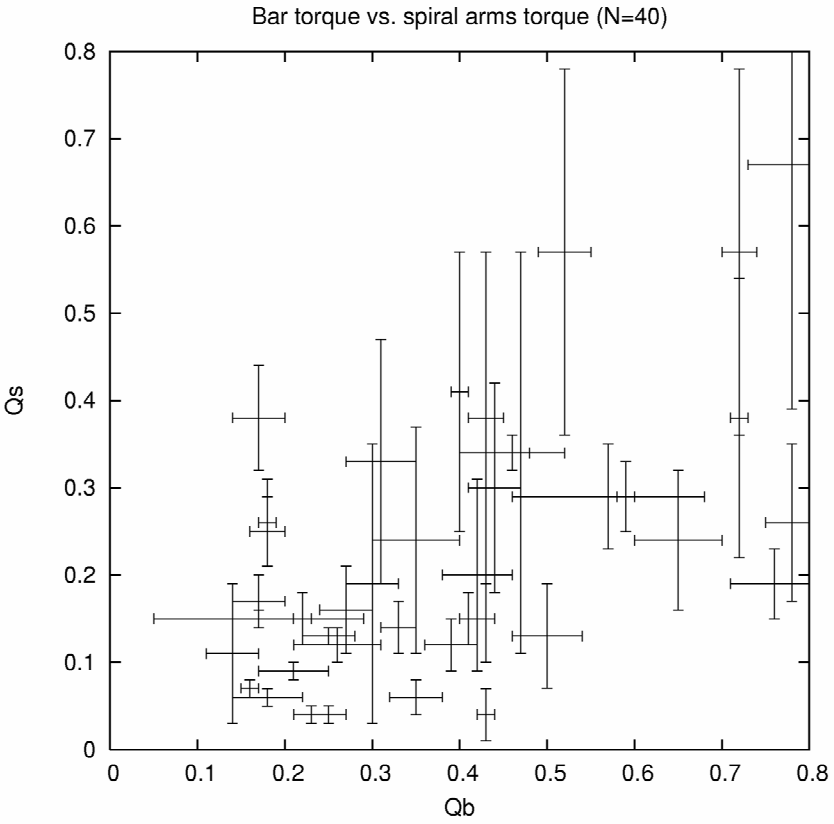

Figure 4.6: *Relative gravitational torques for separated bars and spiral arms for the full sample of 40 galaxies reveal that stronger spirals are not necessarily driven by stronger bars. Bars are not the universal excitation mechanism by which spiral structure is induced, with bar strengths revealing a broad range of values for given spiral arm torques. Error bars represent the relative errors as determined from the GTM.*

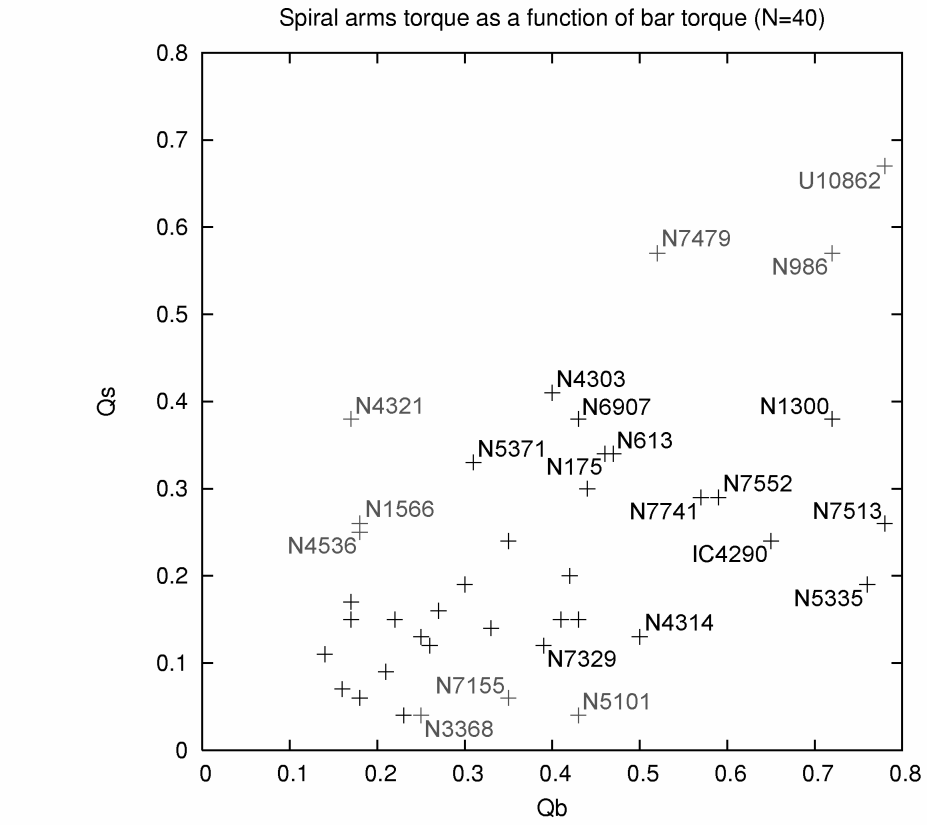

Figure 4.7: *Figure 4.6 without error bars allows specific cases of galaxies which represent the outlying regions of Q_s – Q_b space, to be discussed in detail.*

Galaxies that occupy the lower region of the graph – stronger Q_b, weak Q_s, such as NGC3368, NGC7155, and NGC5101, show a prominent bar, but have very weak or very tightly wound arms, and even rings, which contribute very little to the non-axisymmetric torque of the galaxy. The upper-left corner, most notably NGC4321, NGC1566 and also NGC4536, display a diffuse bar, but strong, prominent grand design spiral arms. These arms contribute to the bulk of the torque and show that the bar component is weak. Examples such as NGC4321 definitively show that galaxies may have strong spiral torques in the presence of relatively weak bars.

Statistically, approximately half of the sample does suggest that stronger bars may drive stronger spirals, but this conclusion needs to be accepted with caution, due to the diluting effect a bar-subtraction may have on the remainder of the galaxy, which in turn weakens the radial axisymmetric contribution by which the tangential component is divided. This would result in an inflated value for the spiral arms torque, as is indeed evident with galaxies such as NGC5371 and NGC4303. Table 4.3 summarizes the observed torques, and provides their Hubble type for optical morphology comparison.

Galaxy	Type	Q_b	Error (Q_b)	Q_s	Error (Q_s)
$Q_b < Q_s$					
NGC1566	Sbc(s)I.2	0.18	0.01	0.27	0.05
NGC4321	Sc(s)I	0.17	0.03	0.38	0.06
NGC4536	Sbc(s)I-II	0.18	0.02	0.25	0.04
$Q_b > Q_s$					
NGC3368	Sab(s)II	0.25	0.02	0.04	0.01
NGC5101	SBa	0.43	0.01	0.06	0.02
NGC7155	SB0	0.35	0.03	0.06	0.02
$Q_b \sim Q_s$					
NGC7479	SBbc(s)I-II	0.52	0.03	0.57	0.21
NGC986	SBb(rs)I-II	0.72	0.02	0.58	0.21
UGC10862	–	0.79	0.05	0.67	0.28

Table 4.3: *Examples of galaxies in the three difference regions of $Q_s - Q_b$ space. These scenarios for the distribution of bar and spiral arms torques are discussed in detail below.*

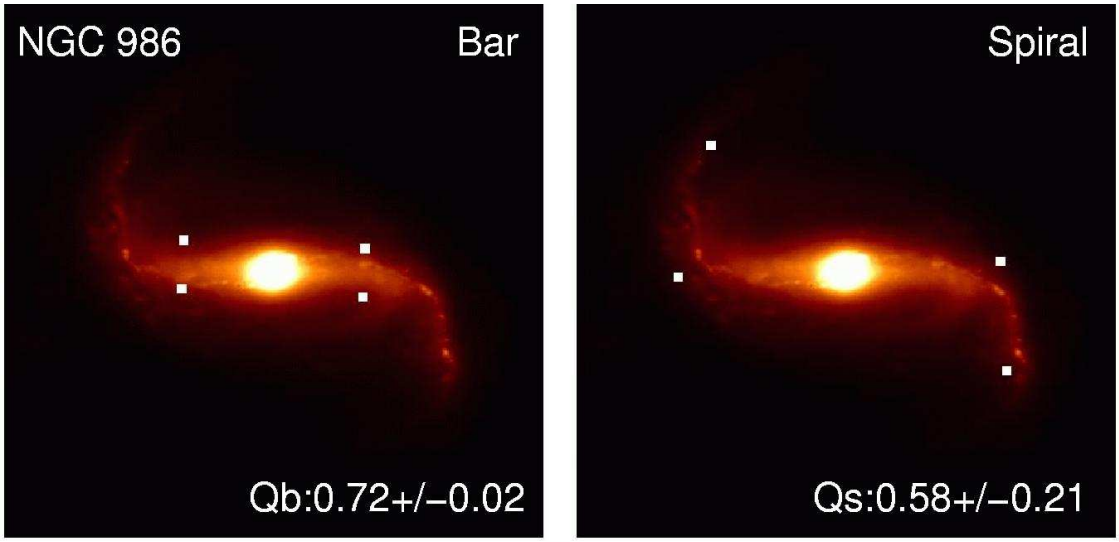

Figure 4.8

NGC986 (**SBb(rs)I-II**) reveals a very prominent bar. Morphologically, it is quite narrow in comparison with the size of the disk, and reveals two prominent straight dust lanes. These dust lanes are accompanied by older Population I stars, strikingly evident in the 3.6 μm images. Two definitive arms emerge from the ends of the bar at a sharp angle, similar to the pattern in NGC1300. Although not visible at the contrast used, in Figure 4.8 these nearly overlap after 180 degrees, thereby forming a nearly complete inner ring.

Elmegreen & Elmegreen (1987) recognized two grand design outer arms, which emerge from the bar at a shallower angle than the inner arms. They are brightest for about 30 degrees of revolution, after which their surface brightness drops off rapidly. Some star formation regions are readily visible in the 3.6 μm images and occur near the ends of the bar and in the parts of the outer arms nearest the bar. The pattern is very typical of many strongly-barred spirals, such as NGC1300.

The outer arms are highly axisymmetric, as evident from the very low relative error of Q_b ~ ±0.02 despite revealing a very high bar torque. Two very prominent dust lanes at the bar's leading edges (relative to the direction of the rotation determined by the winding sense of the spiral pattern) are evident in optical images as well as the 3.6 μm images above. See §5.4.2 for a discussion on models of the hydrodynamic response of gas to a

rotating bar, reproducing the patterns of filamentary dust lanes, as well as the central flattened oval around the bar, and the distinct outer spiral arms.

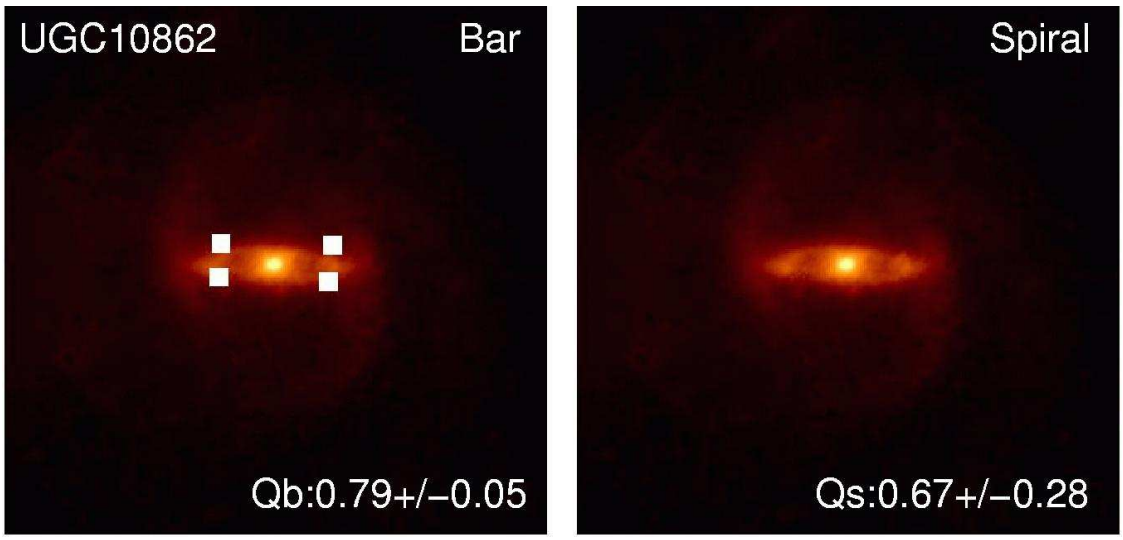

Figure 4.9

With a bar strength of Q_b=0.79+/-0.05, UGC 10862 (Figure 4.9) has the strongest relative bar torque in the entire sample of 40 galaxies observed. Two very bright ansae are evident at the ends of the bar.

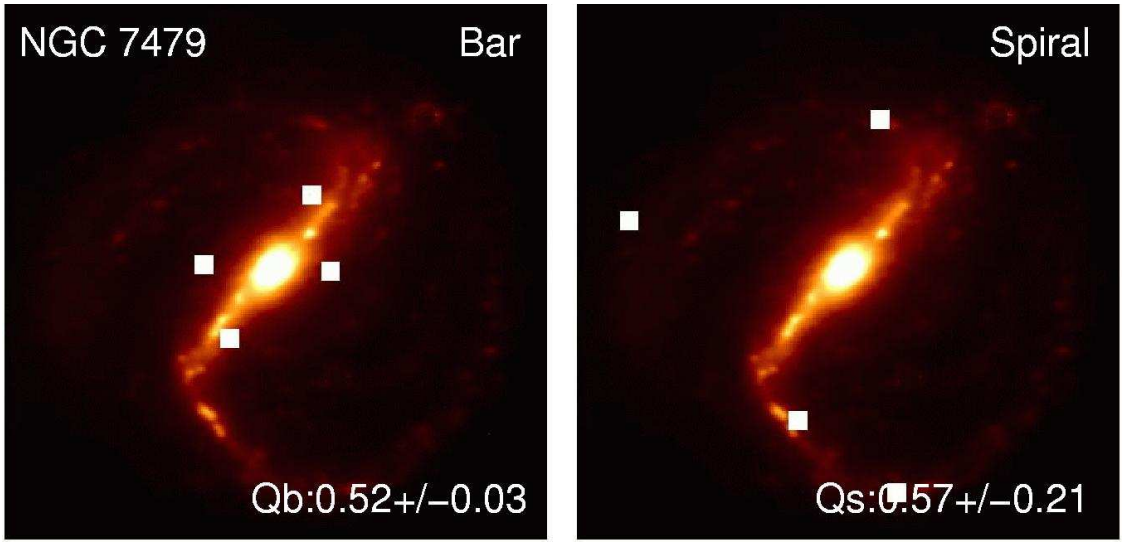

Figure 4.10

NGC7479 (**SBbc(s)I-II**) is likewise an archetypical barred galaxy. Optical images reveal a very strong bar, and characteristic dust lanes associated with it. NGC7479 retains its bar-like morphology across the near-infrared spectrum, even deep into the 8.0μm regime. Elmegreen & Elmegreen (1987) note 'two symmetric inner arms' and 'multiple long and continuous outer arms' which places NGC7479 into a category 9 bin. Low-surface-brightness fragments branch off on the inner side of the two principal arms, which terminate at the ends of the bar, and are not quite as regular when compared with NGC1365 for example.

4.4.2 Prominent Bars with Weak Spiral Arms

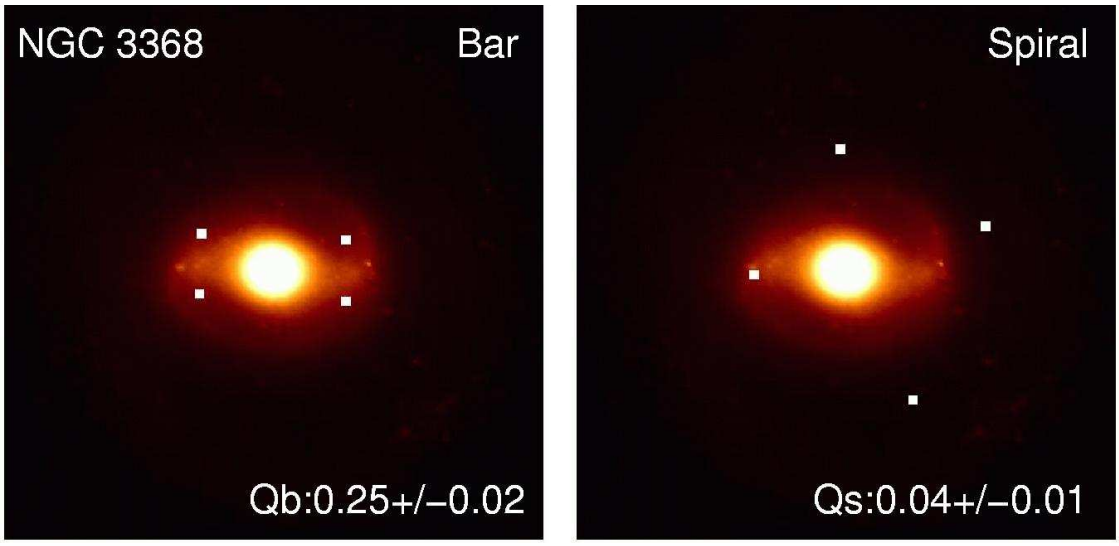

Figure 4.11

NGC3368 (**Sab(s)II**) is given an Elmegreen & Elmegreen (1987) class of 8, signifying "tightly wrapped ringlike arms" and is considered as having a borderline class-3 bar.

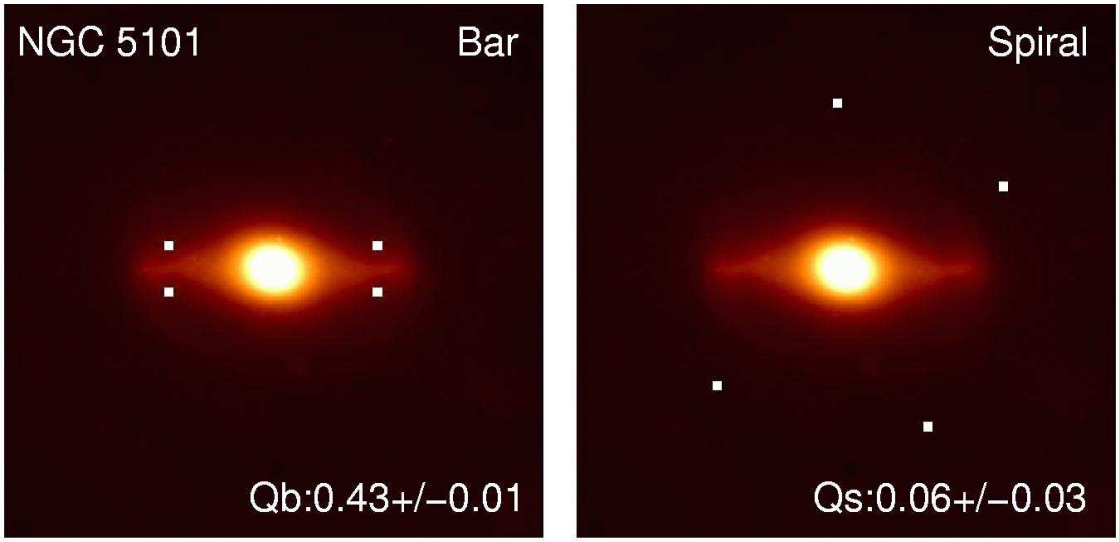

Figure 4.12

NGC5101 (**SBa**) is a very early Hubble type SBa. It would have been placed in the SBa category of Hubble's original scheme because of the broken-ring nature of the inner disk, particularly where the ansae (at the ends of the bars), terminate. Sandage & Bedke (1994) note, "The transition classifications of RSB0/a (with an external ring) in the RC2, and of SB0/SBa in the Hubble Atlas, both based on a 200-inch plate, are inappropriate." The galaxy is a definite SBa.

Optical images also reveal a high star formation rate, evident in the thin, well-defined outer arms. While not visible at the contrast used for the 3.6μm images, there are faint arms that make up the outer external broken-ring, as well as the pattern of "massive" smooth inner disk rims. NGC5101 shows a very symmetric bar, with a very low relative error cross torque quadrants.

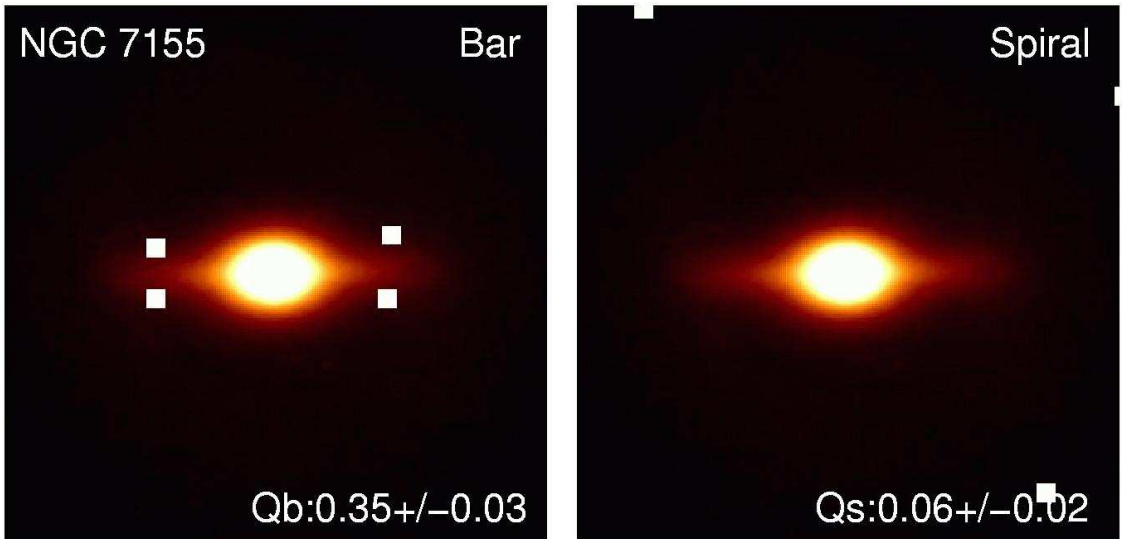

Figure 4.13

Very similar in near-infrared morphology, the bar in NGC7155 (**SB0**) is also very definite and symmetric. Sandage and Bedke (1994) write, "the isophotes of the envelope squeeze down into a peanut shape; the two opposite indentations of the peanut are at the place in the envelope reached by the end of the bar." This would appear to be the case for the near-infrared image too.

4.4.3 Grand Design Structure with Relatively Weak Bars

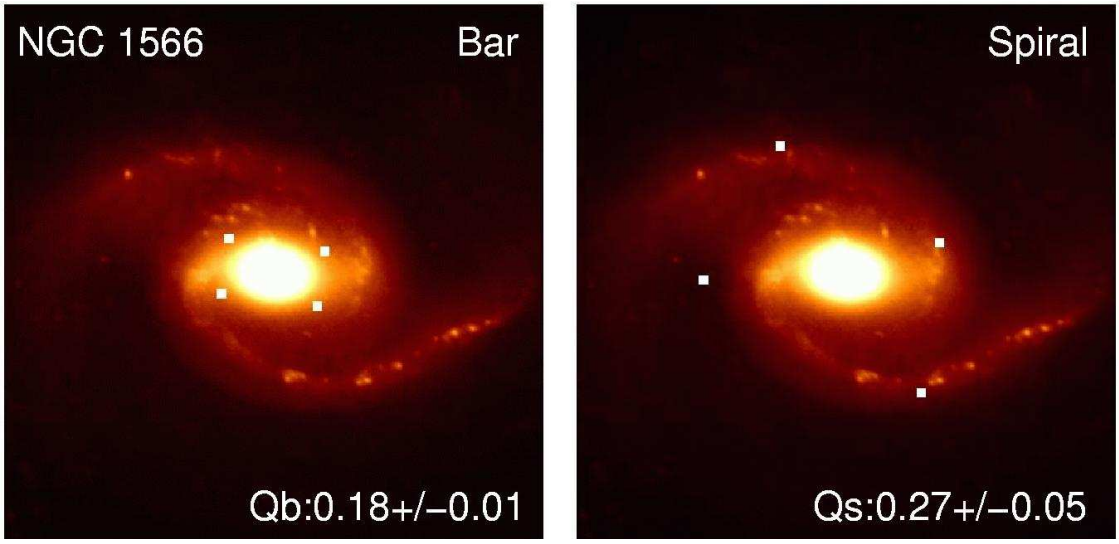

Figure 4.14

Sandage and Bedke (1994) write, “NGC1566 [**Sbc(s)I.2**] is an awesome sight. No written description is adequate to convey the scene when the galaxy is viewed through an eyepiece at the focus of a telescope rather than on an electronic screen.”

Elmegreen & Elmegreen (1987) classify the inner arms as “grand design”, which are of very high surface brightness and reveal copious HII regions. The high surface brightness arms continue to unwind about 180 degrees, each beginning on opposite sides of the bar. Optical images reveal dust lanes closer to the centre compared with the position where the luminous arms begin.

Low surface brightness outer arms exist outside the two main grand design inner arms and reveal fragmented branches. These outermost arms reveal a very pronounced axisymmetry and can each be traced for another 180 degrees.

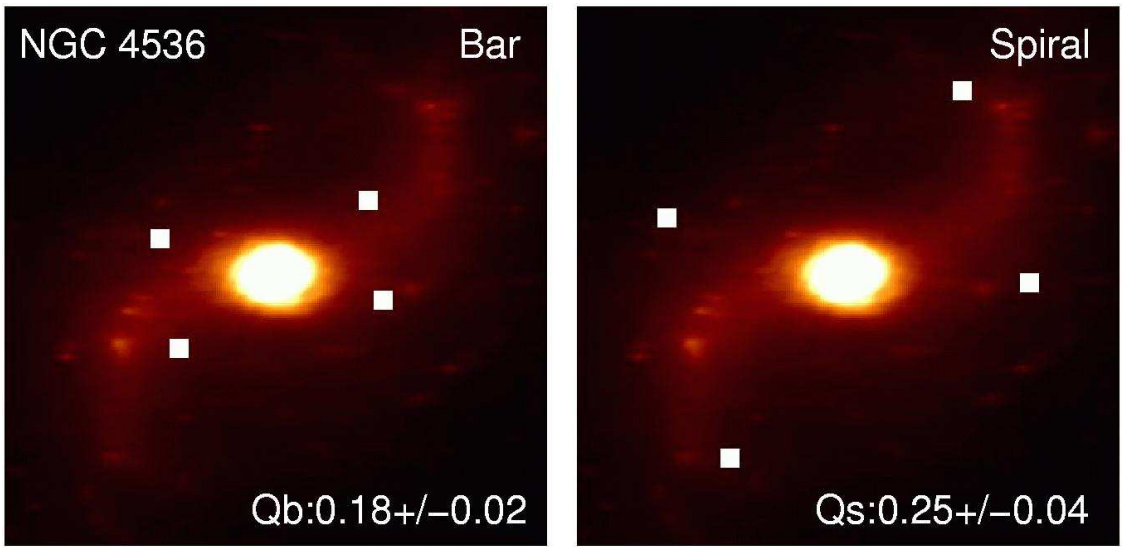

Figure 4.15

NGC4536 (**Sbc(s)I-II**) is one of the largest spirals in the Virgo cluster region. Elmegreen & Elmegreen (1987) classify the spiral pattern as being clearly of the grand design type. There are numerous HII regions evident in the arms, the largest of which are easily detected in the above 3.6 μm images.

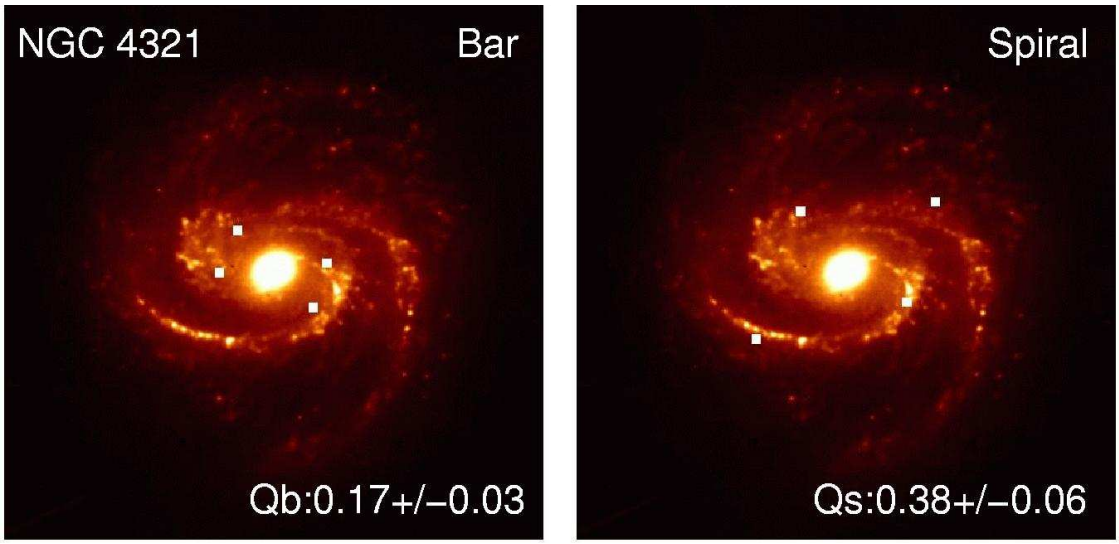

Figure 4.16

Near-infrared as well as optical images reveal two grand design arms in NGC4321 (**Sc(s)I**), beginning near the bulge. Optically, two dust lanes are clearly visible in the central regions, which are accompanied by copious late-type stellar populations, evident at 3.6μm. One side of a dust lane terminates smoothly at the beginning of the first luminous arm. Elmegreen & Elmegreen (1987) classify this prototypically grand design spiral as a category 12 in arms strength due to its 'two long symmetric arms dominating the optical disk'.

4.4.4 Bars as Transient Morphological Features – Further Evidence for Accretion?

In order to find interpretations of these results which are compatible with Figure 4.6, it is necessary to understand the evolution of the bar phenomenon in spiral disks. Bars are formed (via external gas accretion mechanisms) – they dissolve (under their own self influence) – and are reformed again (via further gas accretion). They are the very instability which leads to their destruction and reformation in the presence of gas, in a time frame typically less than 5 Gyrs. This implies that bars are transient morphological features and that there is a life-cycle associated with their influence on galactic disks as a whole. The prevalence of a life-cycle for barred galaxies is fully compatible with the observed scatter in the Q_b versus Q_s plots. Bournaud and Combes (2002) note that gas

accretion radically changes the temporal evolution of the strength of bars. Galaxies with strong bars exist, without the presence of strong spiral arms, as is expected for incipient bars. On the other hand, bars that were once very prominent that have undergone dissolution, may well reveal strong spiral arm torques with only a weak bar component remaining. i.e.: If strong spiral arms were present during the bar dissolution episode, their (spiral arm) torques need not necessarily be greatly reduced. There are also cases where strong bars exist in the presence of strong spiral torques.

The shape of the histogram of galaxy number versus maximum torque (Block et al., 2002; Figure 4.17 in this thesis) is particularly revealing in terms of the time-fraction that a bar spends with a particular strength, in its life cycle. It is striking that very few galaxies exist with a zero bar strength. In the temporal interpretation, this means very few galaxies exist for extended periods without bars. Block et al. (2002) verify that that steep decline towards zero bar strength is in fact a robust conclusion and not dependant on selection biases, such as limiting galaxy inclination to 65º~70º and not considering any interacting systems. It is thus a physical interpretation that disks rarely reside in axisymmetric states, and even between bar episodes, spiral arms retain a significant torque. N-body simulations performed by Bournaud and Combes (2002) find that in the absence of gas accretion, galaxies maintain their axisymmetric shapes, and that bars and spiral arms eventually disappear. The very existence of bars with well defined life cycles strongly argues in favour of continuous gas accretion. Block et al. (2002) have determined this implies galaxies may as much as double their mass in one Hubble time.

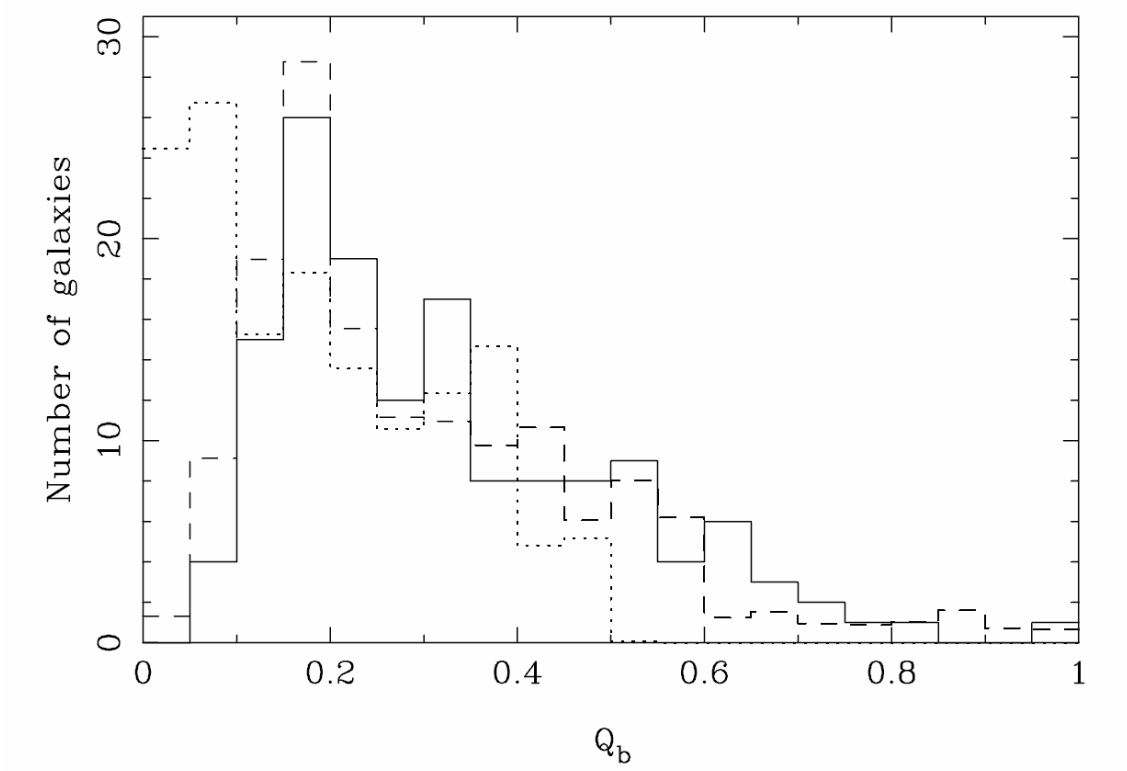

Figure 4.17: *Histogram of gravitational bar torques for a sample of 163 near-infrared disk galaxies investigated by Block et al. (2002). The solid line indicates actual observations. The dashed line is derived from galaxy simulations which double their disk mass due to gas accretion in a Hubble time. The dotted line represents simulations without accretion. The non-observation of galaxies with zero bar torques, as the non-accreting models suggest, argues strongly in favor of the external gas accretion scenario and is fully compatible with the observed distribution of spiral torques in Figure 4.6 and Figure 4.7.*

Further dynamic considerations strengthen this argument. The self-destruction of a bar causes the galactic disk to heat up, introducing stability. This stability is due to the velocity dispersion in the disk, and in the absence of accretion, would suppress any bar formation as well as weaken what spiral structure remains. Gas accretion is a powerful cooling mechanism in galactic disks, making them far more susceptible to bar reformation and aids in the maintenance of spiral structure.

The maintenance of spiral structure has been attributed to various mechanisms, such as density wave propagation with reflections off resonance rings and the central bulge, possibly feedback enhanced. Bertin et al. (1989a) and (1989b) suggest that turbulent

dissipation and shock formation of the young Population I component could well act as moderating processes for the preservation of spiral structure.

The source of external accreting gas has already been mentioned in Chapter 2; Sancisi (1983) reports on vast reservoirs of gas in the outer regions of spiral disks. Pfenniger et al. (1994) have suggested that dark matter in the outer disks may also be in the form of gas. However, in-falling dwarf galaxy accretion rates, as investigated by Toth & Ostriker (1992), cannot account for the observed rates required.

Interacting systems are also ruled out as the origin for barred structure since accretion is a far more efficient mechanism in maintaining gravitational torques. The effect of interactions on gravitational torques remains yet to be investigated, however should not impact on the conclusions derived above in the case of galaxies undergoing secular evolution.

Theoretical considerations that stronger bars may driver stronger spirals are not ruled out by these observations. There is a continuous sequence of galaxies on the $Q_b \sim Q_s$ line, from very weak torque values right up to the strongest observed. There is a dearth of galaxies with very strong bars and weak spiral arms. Similarly, very strong spiral torques are not found in galaxies with very weak bars. However, it is clear that stronger spirals are not necessarily driven by stronger bars. Therefore bars are not the only mechanism which drives spiral structure in disk galaxies.

Future dust penetrated near-infrared rest-wavelength observations with the JWST and other mid-infrared detectors will open up the high-z universe. These will detail bar formation and galactic disk accretion scenarios at earlier epochs, determining whether spiral arm forcing is a product of a Hubble time worth of evolution.

– CHAPTER 5 –

BAR MORPHOLOGY AS SEEN IN DUST EMISSION AT 8.0μm

"A good notation has a subtlety
and suggestiveness
which at times make it seem
almost like a live teacher."
– Bertrand Russell

5.1 Introduction

5.1.1 Dust Morphology Characteristics of Barred Spirals

In 1918, Heber D. Curtis already made the observation that, "There is one fairly common type of spiral… Its main characteristic is a band of matter extending diametrically across the nucleus and inner parts of the spiral. Frequently the whorls in this type form a nearly complete ring; in other examples the whorls appear to begin at the ends of this cross-arm." Today we know at least 80% of spiral galaxies present bars in the near-infrared, and that the bar-morphology is an intimate feature of the structure of spiral galaxies.

A very characteristic feature of strongly barred galaxies such as NGC986, NGC5383, NGC1365 and NGC1300 (see Figure 5.1) is the presence of two prominent dust lanes on each of the two leading edges of the bar. In the case of NGC1300, two strong tightly wound grand-design inner spiral arms begin at the ends of the bar. The two inner arms wrap so tightly that they present the appearance of an almost complete ring. There is a definite indication of a high star formation rate in the region where the arms/bar terminate. The two inner arms wind outwards counter-clockwise, and branch into two sets of outer arms which have a significantly reduced surface brightness.

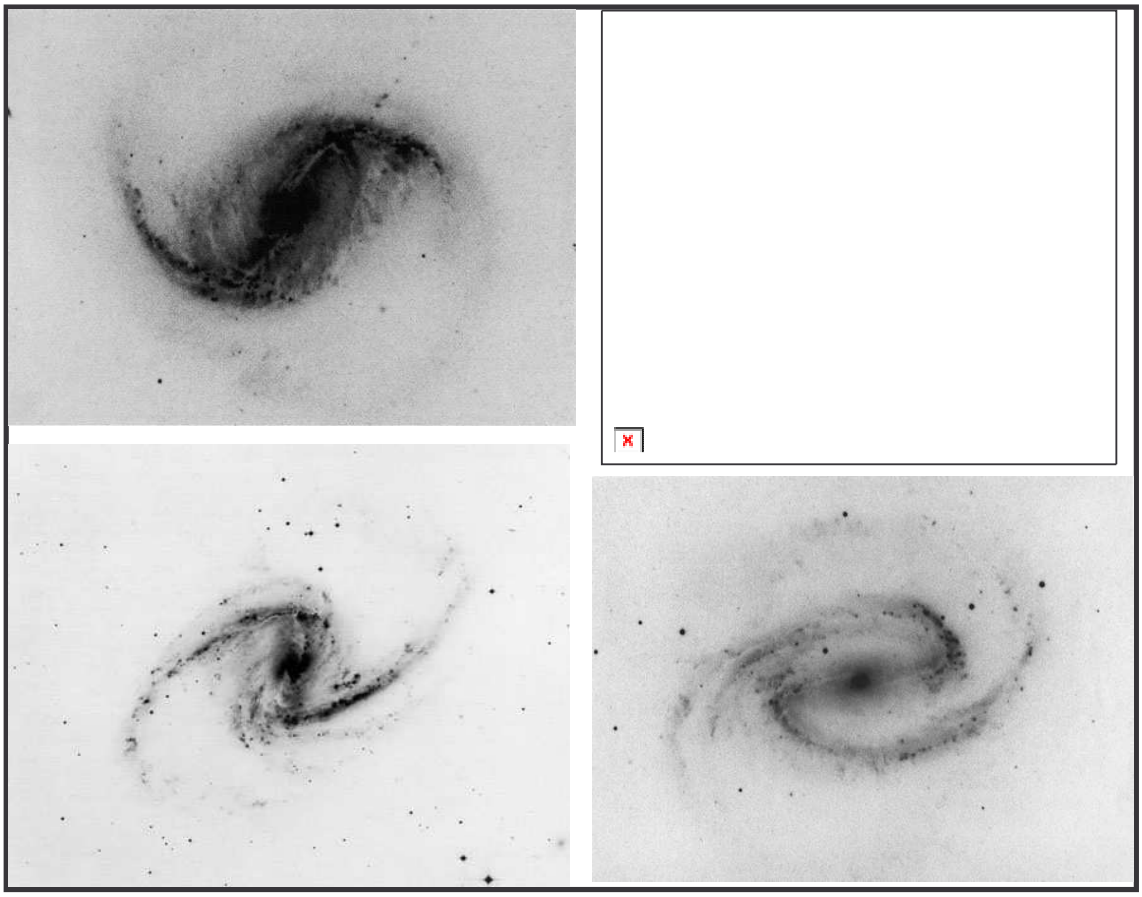

Figure 5.1: *Barred spiral galaxies, NGC986 (top left), NGC5383 (top right), NGC1365 (lower left) and NGC1300 (lower right) each show very prominent dust lanes (seen as white filaments in the images above). These dust lanes are the signature of shock loci at the leading edges of bars. The presence of flocculent dust spurs emanating from the dust lanes at the shock positions reveal a well ordered but intricate velocity field along the shock loci. The fainter dust wisps are along the trailing edge of the bars, and are nearly perpendicular to the resulting prominent dust lanes.*

Bars are believed to be direct evidence of external gas accretion in the majority of nearby galaxies (Bournaud & Combes, 2002; Block et al., 2002; also see §4.4.4 for further discussion) – possibly extending to the high-z domain as well. While bar formation scenarios are still a very active field of research, gas flows in and around the bar region have been investigated extensively by Athanassoula (1992a; 1992b). Furthermore, Sandage & Humphreys (1980) note that most barred galaxies whose spiral arms terminate at the ends of the bar, have grand design arm morphology, rather than being filamentary.

A well known prototype for this pattern is NGC1300, which belongs to the SBb(s) category, denoting a strong and well developed bar. In such instances it is common to find two straight dust lanes towards the edges of the bar. The lanes are on symmetrically opposite sides of the bar and on the leading edges as defined by the sense of the trailing spiral arms. Star formation is also more prevalent on the ends of the bar, as can be clearly seen in the case of NGC1300 (see Figure 5.1) where the arms and outer tips of the bar are shown by many bright knots most likely indicating localized HII regions.

In 1991, Block & Wainscoat presented a case revealing the strong decoupling between optical and infrared images of spiral galaxies. The morphological classification of such is highly dependent upon the wavelength of observation. These authors used the example of NGC309 which optically presents a classic grand design Sc morphology, reveals a SBa type morphology at K band (see §2.4.1 and Figure 2.6). With recent data received from the Spitzer Space Telescope (see discussion below), further decoupling is evident between wavelengths of 3.6μm and 8.0μm. Just as Strom, Strom & Jensen (1976) have commented, "Detailed study of the underlying density wave in late type spirals is considerably complicated by the dominance of the bright population I tracers near the wave crests. This problem can be avoided, in part, by photographing these galaxies at near infrared wavelengths.", so too can the dust distribution in emission now be analysed in the bars of spiral galaxies.

5.2 Surprising insights from quantitative dust emission analyses

5.2.1 Three Distinct Bar Form Families

The GTM was designed to provide a quantitative classification to spiral galaxies as observed in their stellar backbones at J, H, K_s and 3.6μm. The stars trace the mass distribution in the disk and therefore the relative gravitational torques can be calculated. It is very surprising that applying the GTM to 8.0μm images of *some* barred galaxies, reveals a very similar value for the calculated corresponding 3.6μm "torque". In the case of the 8.0μm images, the "torque" values are of-course not gravitational torques, but instead provide a quantitative measure to compare the similarity between the stellar backbone mass distribution with the degree to which the dust traces it.

The selected sample of Spitzer images were chosen to span the de Vaucouleurs scheme (SA, SAB, SB), as well as the Elmegreen & Elmegreen (1987) Arm class range from 1 through 12 (skipping only classes 4,10 and 11 – with the latter two no longer being used). It is very surprising that there exist galaxies which contain a very definitive bar, but which are *devoid* of detectable dust at 8.0μm. For prototypical barred galaxies we expect to find a clear delineation of gas and dust in emission particularly along the leading edges of bars, as described by Athanassoula (1992b, 2000). Prominent dust lanes are observed in examples such as NGC1300, NGC1365 and NGC5383 (see Figure 5.3, section 5.3.2) which extend across the full length from the nuclear region up the ends of the bar. These dust lanes are associated with the shock fronts of gas along the leading edges of bars and appear in optical images of a large number of spiral galaxies (see for example Sandage, 1961).

Dust morphologies induced by stars are therefore expected to be widespread and particularly prevalent in the dust emission bands such as 8.0μm onboard Spitzer. However not all barred galaxies reveal such structure when observed at 8.0μm. There are three distinct families of barred galaxies which can be described as comprising two fundamentally different classes, one showing two different variations as subclasses:

(i) Dusty bars. These bars are seen in both the stellar 3.6μm and warm dust emission 8.0μm bands. We have discovered that there are two distinct classes of barred galaxies within this form family. These are:
   a. The 8.0μm dust morphology is tightly coupled to the 3.6μm morphology.
   b. Dust *spirals* are evident in the proximity of the stellar bar, but do not delineate the bar shape itself. i.e.: The 8.0μm morphology is decoupled from the morphology at 3.6μm.

(ii) Bars which only contain stars with no associated dust. This is very surprising since the prototypical barred galaxies, such as NGC1300 and NGC7479 for example, have a very pronounced stellar population in the bar with distinct dust lanes on the leading edges of the bar. That some barred galaxies exist

which are completely devoid of dust in the bar region provides the basis for the classification of barred spirals into these three distinct families.

While we expect that dust would be found in the presence of the older Population I stellar backbone, is it very surprising to find that applying the GTM to 8.0μm images for some barred galaxies reveals calculated "torque" values which are very similar to those at 3.6μm. NGC7479 for example, reveals a relative gravitational torque of Q_g ~ 0.65 at 3.6μm while the calculated "torque" at 8.0μm is "Q_g" ~ 0.65. This implies that not only does the gas and dust distribution mimic the 3.6μm Population I very well, but also the relative intensity of the 8.0μm component is very similar to that at 3.6μm.

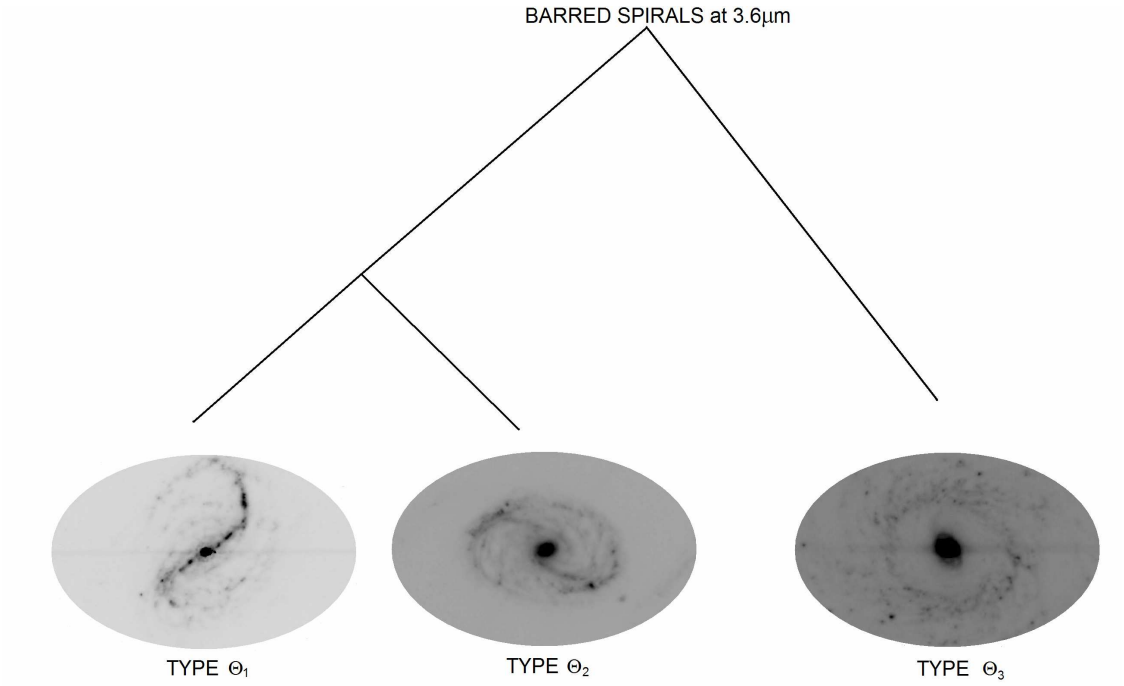

Figure 5.2: *Three distinct "form families" of barred spiral galaxies: Type Θ_1 reveal 8.0μm dust morphologies induced by stars, type Θ_2 have 8.0μm dust morphologies induced by gas only, and type Θ_3 are bars (and possibly even spiral arms) completely devoid of gas and dust. All three families show prominent bars in stars at 3.6μm.*

It is particularly interesting to note that many of the prototypical barred galaxies, such as those first observed and catalogued by Curtis and Hubble, indeed do have very similar values for their 3.6μm and 8.0μm "torques". In cases like these, knowing the warm dust distribution at 8.0μm gives a very good indication of the 3.6μm morphology. These galaxies have been classified as having bars with stars and gas/dust. This is not true of all barred galaxies. Examples, such as NGC0266, and very strikingly NGC4421, show no indication of the presence of stellar bars at 8.0μm, even though they are true SB-type barred galaxies at optical wavelengths and at 3.6μm.

5.3 Type Θ_1 Stellar Bars – as seen through the eyes of Spitzer

5.3.1 The *Coupling* of 3.6μm and 8.0μm images

Four examples of SB-type galaxies listed below present 8.0μm "torques" and morphology which are very similar to their 3.6μm counterparts. NGC7479 (**SBbc(s)I-II**) is such an archetypical barred galaxy and retains its bar-like morphology across the near-infrared spectrum. De Vaucouleurs classified it as type SB(s)c and $Q_{g(3.6)}$ is calculated to be 0.65+/-0.09 – the strongest bar in this sample. The non-stellar 8.0μm Spitzer image reveals a torque value $Q_{g(8.0ns)}$ = 0.65+/-0.17. The added uncertainty in the error for the non-stellar image is derived from less prominent stellar features that off-set the slight general asymmetry of the galaxy. Elmegreen & Elmegreen (1987) place NGC7479 into a category 9 bin with its 'two symmetric inner arms' and 'multiple long and continuous outer arms'. When compared with NGC1365, the arms in NGC7479 are not quite as regular. Low-surface-brightness fragments branch off on the inner side of the two principal arms that terminate at the ends of the bar. NGC7479 has two characteristic, nearly-straight dust lanes along the leading edges of the bar which extend all the way into the high-surface-brightness regions of the grand design spiral arms. The near-side spiral arm shows a prominent central dust lane in the optical image (as seen by the enhanced silhouetting of near-side dust features) and there are large HII regions present in the opposite, elongated arm.

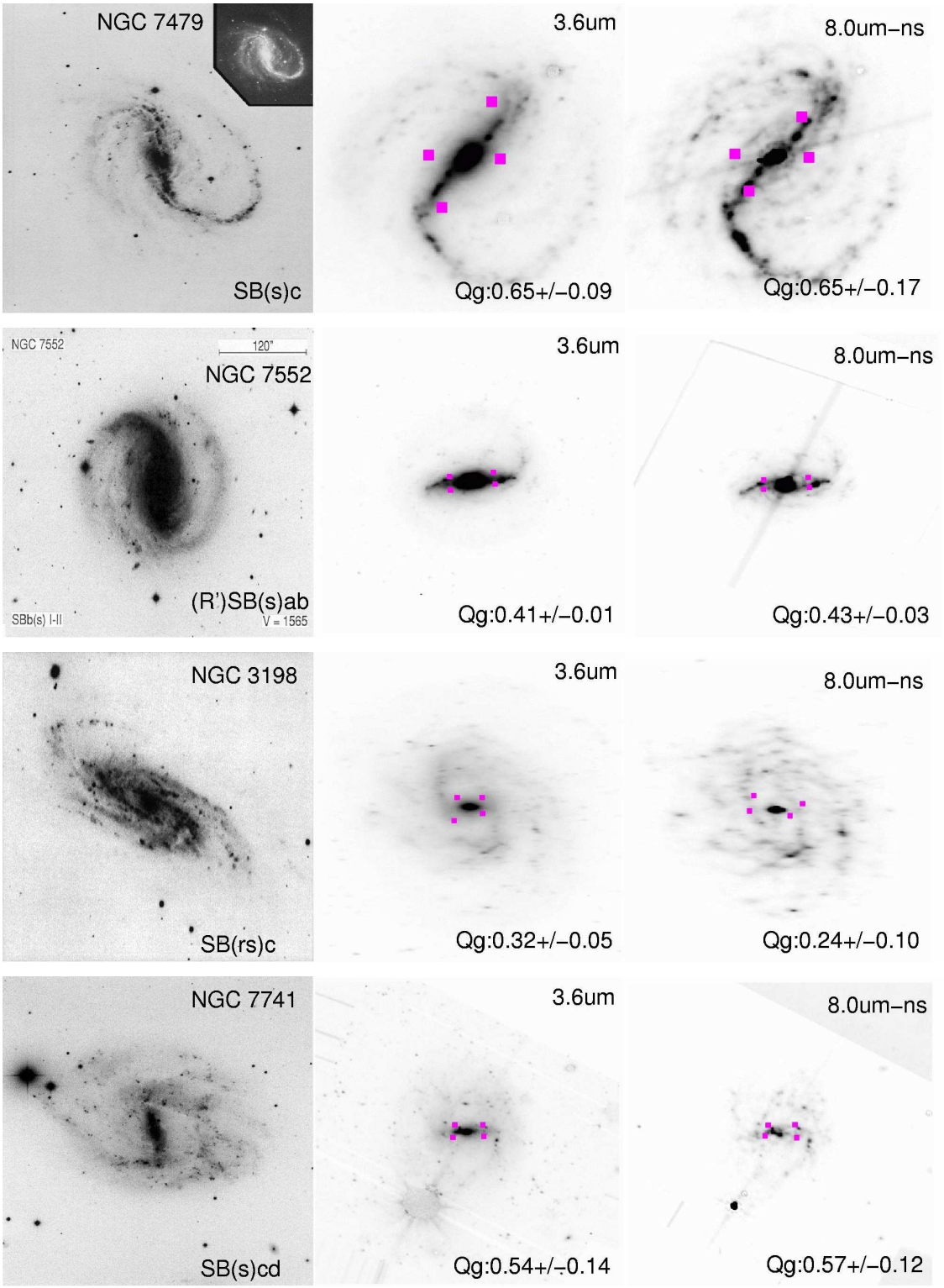

Figure 5.3: *Type Θ_1 Barred Spirals – Dust which delineates the bar morphology induced by stars. These bars contain both stars and dust, with the dust distribution being a very good tracer of the underlying stellar morphology. A scaleheight of 325pc was assumed for all galaxies in determining Q_g.*

NGC7552 (**SBb(s)I-II**) is denoted (R')SB(s)ab with its outer pseudo-ring and has a bar which yields a $Q_{g(3.6)}$ of 0.41+/-0.01 at 3.6µm. The 8.0µm image retains a similar strength with a value of $Q_{g(8.0ns)}$ = 0.43+/-0.03. An intricate dust pattern is revealed in low-contrast optical images inside the central oval/bar. These dust lanes curve into spiral fragments which branch out from two straight lanes characteristic of SBb galaxies on the opposite sides of the bar/oval. The dust shock loci start from opposite sides of the bulge and are straight almost to the end of the bar/oval. While they are not as well defined as is the case for NGC1300, their presence signifies hydrodynamic shocks in the gas due to the gravitational perturbation of the rotating bar/oval. In the case of strong bars, the shock lanes are generally very prominent (see §5.4.2). The luminous outer arms terminate at the ends of the bar/oval. The optical low-surface-brightness spiral pattern of NGC7552 is the reason for its (s) type classification, where the spiral arms terminate at the ends of the bar. Elmegreen & Elmegreen did not classify NGC7552 in their 1987 paper.

The spiral arms in NGC3198 (**SBc(s)I-II**) are thin yet generally well defined. With a calculated 3.6µm torque of $Q_{g(3.6)}$ = 0.32+/-0.05, NGC3198 retains a moderate "strength" of $Q_{g(8.0ns)}$ = 0.24+/-0.05 at 8.0µm. NGC7741 (**SBc(s)II.2**) has a strong bar with many star formation regions, and is classified as SB(s)cd by de Vaucouleurs. The 3.6µm image reveals a gravitational torque of $Q_{g(3.6)}$ = 0.54+/-0.14 and similarly $Q_{g(8.0ns)}$ = 0.57+/-0.12 at 8.0µm. Star formation occurs ubiquitously throughout the arms of NGC 7741 which Reynolds (1927a,b) classifies as being massive. Elmegreen & Elmegreen (1987) place this galaxy in class 5 with 'two symmetric, short arms in the inner regions' and 'irregular outer arms.'

GALAXY	3.6µm	+/-	8.0µm	+/-	8.0µm n-stell.	+/-	De Vauc.	E&E
NGC3198	0.32	0.05	0.20	0.06	0.24	0.10	SB(rs)c	–
NGC4536	0.24	0.02	0.21	0.13	0.22	0.13	SAB(rs)bc	12
NGC7479	0.65	0.09	0.61	0.14	0.65	0.17	SB(s)c	9
NGC7552	0.41	0.01	0.41	0.05	0.43	0.03	(R')SB(s)ab	–
NGC7741	0.54	0.14	0.47	0.18	0.57	0.12	SB(s)cd	5

Table 5.1: Type Θ_1 Barred spiral galaxies

5.4 Type Θ_2 Stellar Bars – S-shaped Dust Shock-Fronts

5.4.1 The *Decoupling* of 3.6µm and 8.0µm bar morphologies

NGC3368 (**Sab(s)II**) is a prototype for the case of stellar bars at 3.6µm and dust spirals at 8.0µm. The central stellar structure remains present at 8.0µm and the dust component retains a spiral-like structure towards the nucleus. This Liner galaxy has a de Vaucouleurs classification of SAB(rs)ab and a measured $Q_{g(3.6)}$ of 0.24+/-0.01. The optical classification fits well to the quantitative torque measurement in this case, whereas the 8.0µm $Q_{g(8.0ns)}$ falls off to 0.00+/-0.08 with the tail end of the stellar black body spectrum subtracted out. Elmegreen & Elmegreen (1987) give this galaxy an arm class of 8 signifying 'tightly wrapped ringlike arms'. A very faint single outer arm which contains numerous small HII regions is also evident. It emerges from the disk at the left hand side of the IRAC images and winds counterclockwise for at least half a revolution. This galaxy provides a good example for the case where strong dust lanes are prevalent at 8.0µm.

Dust lanes have been modeled in a series of theoretical studies regarding the hydrodynamic response of gas and dust in disks, in close proximity to rotating bars. Prendergast (1962) pioneered hydrodynamic models including the phenomena of gas shocks in the neighbourhood of a bar. Early velocity field predictions are detailed in Huntley et al. (1978), which have subsequently been summarized by Prendergast (1983) for SBb and SBc galaxies as follows:

i. Weak bars give open spiral patterns which extend throughout the gas; stronger bars give spirals which emerge at sharp angles to the bar, as in NGC1300 and NGC1365.
ii. The gas response leads the bar, by an angle which is greater the weaker the bar.
iii. Strong bars favour the appearance of strong shocks within the bar.

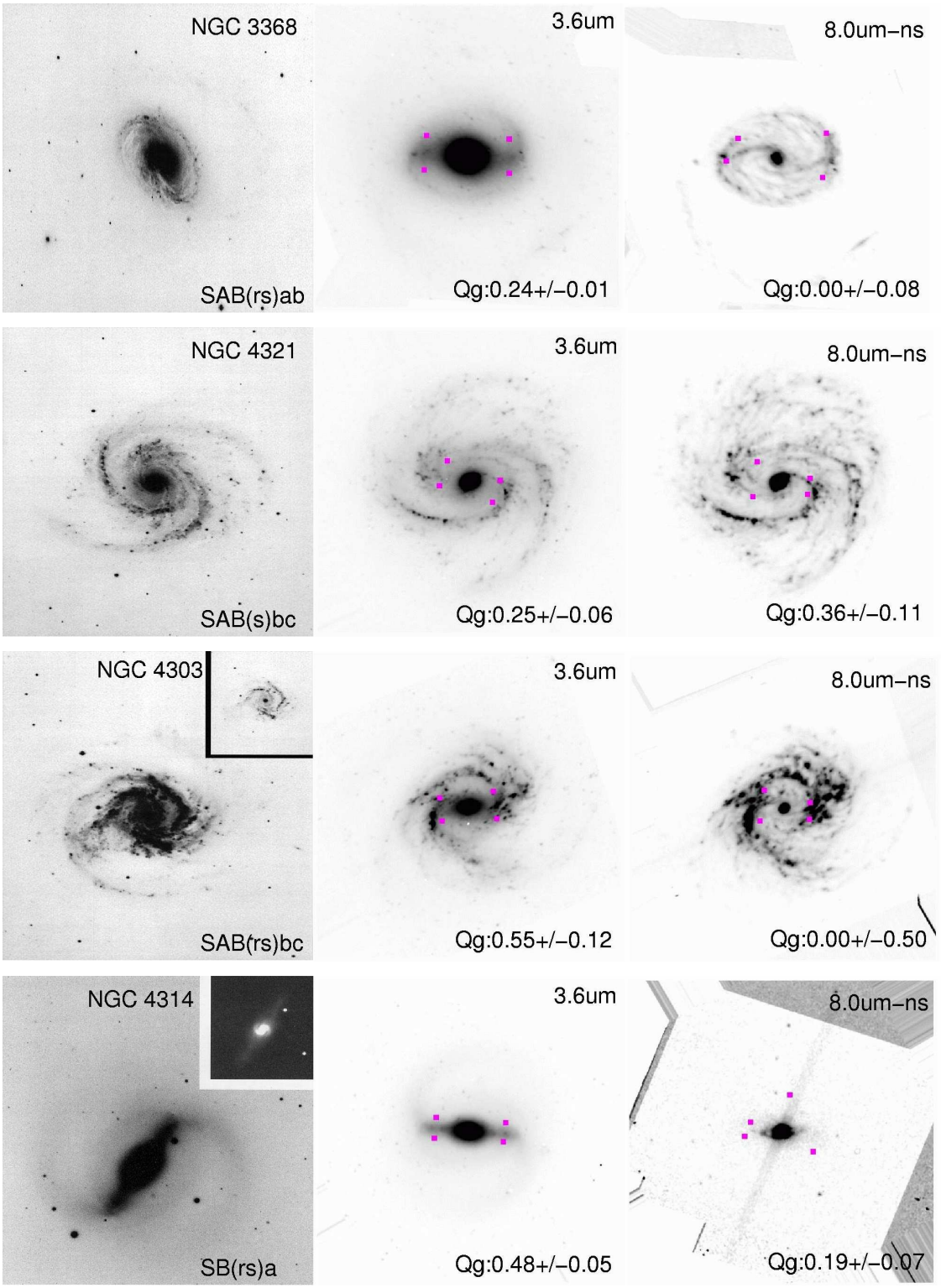

Figure 5.4: *Type Θ_2 Barred Spirals – Dust filaments are observed to connect the spiral arms with the nuclear region of these galaxies which have a very definite stellar bar at 3.6μm. The dust morphologies are induced by the gas only and there is no evidence of a bar at 8.0μm.*

The well known galaxy NGC4321=M100 (**Sc(s)I**) is one of the largest spirals in the Virgo Cluster with an angular size of 6.9' as listed in the RC2, measured to an isophote of 25 mag arcsec^{-2}. Photographs of many Virgo Cluster spirals are given in Sandage, Binggeli and Tammann (1985a), which when printed to a common angular size, show the true spatial extent of NGC4321. This SAB(s)bc Liner galaxy presents very similar gravitational torques across the near-infrared spectrum with $Q_{g(3.6)}$ = 0.25+/-0.06 and $Q_{g(8.0ns)}$ = 0.36+/-0.11. The two grand design arms in NGC4321 begin near the bulge as dust lanes and one side of a dust lane terminates smoothly at the beginning of the first luminous arm. Elmegreen & Elmegreen (1987) classify this prototypically grand design spiral as a category 12 in arms strength due to its 'two long symmetric arms dominating the optical disk'. The dominant contribution of the torque derives from the very strong spiral arms prominent in this galaxy with its numerous HII regions, and the individual brightest stars are difficult to separate from HII regions in optical images. Most of the knots in spiral galaxies are HII regions as inferred by Hubble (1936) which he used with his calibrations of brightest stars (Humason, Mayall and Sandage 1956).

NGC4303 (**Sc(s)I.2**) is also a very large spiral in the Virgo Cluster region. Two thin dust lanes terminate near the bulge, and spiral outward towards the two prominent spiral arms. The grand design arms contain multiple HII regions and one of the arms has a "kink". NGC4303 shows a significant bar torque at 3.6µm with $Q_{g(3.6)}$ = 0.55+/-0.12. It is the only galaxy in this sample of type SAB's that exceeds a $Q_{g(3.6)}$ of ~0.33 at 3.6µm. At 8.0µm the "torque" value of the bar region drops to $Q_{g(8.0ns)}$ = 0.00+/-0.50. De Vaucouleurs classifies NGC4303 as SAB(rs)bc, and Elmegreen & Elmegreen (1987) place NGC4303 in their category 9, representing 'two symmetric inner arms' and 'multiple long and continuous outer arms'.

NGC4314 is another dramatic example of a strongly barred galaxy at both optical and stellar emission near-infrared wavelengths, with a calculated torque of $Q_{g(3.6)}$ = 0.48+/-0.05. The 8.0µm dust response however reduces to $Q_{g(8.0ns)}$ = 0.19+/-0.07, with only the central region near the bulge providing the remaining "torque" component. While this

galaxy is optically reminiscent of NGC7552 for example, the dust response in the bar region is significantly weaker as is evident in the 8.0μm non-stellar image which has already been contrast-stretched to include as much of the fainter detail as possible.

GALAXY	3.6μm	+/-	8.0μm	+/-	8.0μm n-stell.	+/-	De Vauc.	E&E
NGC0514	0.15	0.03	0.00	0.20	0.00	0.05	SAB(rs)c	9
NGC2500	0.20	0.03	0.07	0.14	0.00	0.24	SB(rs)d	1
NGC3351	0.27	0.01	0.08	0.03	0.11	0.04	SB(r)b	6
NGC3368	0.24	0.01	0.11	0.17	0.00	0.08	SAB(rs)ab	8
NGC3486	0.06	0.02	0.05	0.25	0.06	0.27	SA(r)c	9
NGC3627	0.29	0.03	0.00	0.20	0.00	0.20	SAB(s)b	7
NGC4136	0.16	0.11	0.00	0.26	0.00	0.26	SAB(r)c	9
NGC4303	0.55	0.12	0.00	0.60	0.00	0.50	SAB(rs)bc	9
NGC4314	0.48	0.05	0.15	0.08	0.19	0.07	SB(rs)a	12
NGC4321	0.25	0.06	0.30	0.11	0.36	0.13	SAB(s)bc	12
NGC4450	0.19	0.02	0.23	0.07	0.29	0.20	SA(s)ab	12
NGC4579	0.22	0.01	0.20	0.14	0.20	0.14	SAB(rs)b	9
NGC4725	0.22	0.03	0.24	0.09	0.24	0.09	SAB(r)ab	6
NGC5371	0.33	0.13	0.00	0.70	0.00	0.70	SAB(rs)bc	9
NGC5377	0.13	0.03	0.10	0.06	0.06	0.14	(R)SB(s)a	6

Table 5.2: Type Θ_2 Barred spiral galaxies

5.4.2 Characteristics of Bars and the Hydrodynamics of Shock Loci

Like a spectacular waterfall, shock fronts reveal vast streams of galactic dust cascading down a potential well towards the centres of galaxies. Sellwood & Wilkinson (1993) have shown that the stellar component of bars comprise periodic orbits which are denoted X_1 and span the major axis of the bar. In the presence of inner Lindblad resonances (ILRs) (see §2.4.2), there are also two perpendicular families, denoted X_2 and X_3. The 4:1 periodic orbits, which have rectangular shapes, are prevalent further out from the nuclear region. These orbital families, along with harmonics, serve to trap other regular orbits. Athanassoula (2000) notes that chaotic orbits may also be present and their influence depends on the properties of the bar's gravitational potential. In the greater part of the bar region the gas has a very low density. However, most of the gas is concentrated in two narrow strips along the leading edges of the bar. Towards the centre of the bar, these overdensities arc into a nuclear spiral or ring-like structure. Such a flow is a direct result of the bar's main periodic orbits and structure.

Athanassoula (1992b) and Athanassoula (2000) show that the density maxima are the loci of shocks. This is treated comprehensively in Athanassoula (1992b) where the shape of the shock loci has been found to coincide with different optical bars strengths. Shock loci in strong bars are often more straight, while ovals and weak bars have "loci which are curved with their concave part towards the bar major axis." Indeed, Athanassoula show that in order for the shock loci to have the shape of the observed dust lanes, the corotation radius, R_{CR}, must be equal to $R_{CR} = (1.2\pm0.2)a$, where a is the length of the bar semi-major axis.

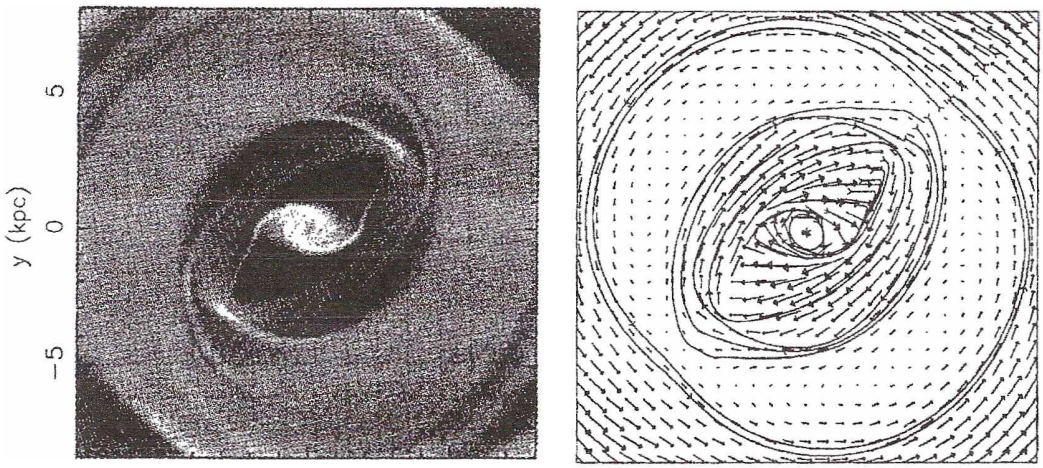

Figure 5.5: *A model of the gas response in the presence of a bar (Athanassoula, 2000, Figure 1). At left, gas density is presented in grey-scale with dark areas representing regions of lower densities. The right panel depicts gas flow lines and the velocity vectors. The bar is at rest in this frame of reference.*

In cases where no shocks are evident, there is no net inflow as indicated by the concentric ellipse-like flow lines in Figure 5.5. However, in cases with shocks, the gas flow is considerably more complicated. The trailing sides of the bar exhibits gas outflow where the gas density is very low. This outflow continues until it reaches the shock front, where it abruptly turns inward.

Gas velocities for both in- and out- flows are typically of the order of 100 km/sec or more. The outward flow is not as spectacularly evident as it extends over an area which is large with a corresponding low gas density. The in-flow by comparison, is concentrated

in a small area with a high gas density. The density-averaged radial velocity is typically less than one km s^{-1}, depending on various models. Models with thin, slowly rotating massive bars with centrally concentrated axisymmetric components are found to yield a maximum net inflow (Athanassoula 1992b; Piner, Stone & Teuben 1995). These correspondingly also exhibit the strongest shocks. Observational biases need to be considered when comparing observations since the low density regions are inherently more prone to observational limitations, and correspondingly, there is a tendency to overestimate the inflow.

Galaxies with ILRs contain gas which is brought from regions that correspond to roughly a radius equal to the bar's semi-major axis with reference to the circumnuclear ring. Similarly, for galaxies with no ILR, the inflow may well reach very near to the nucleus. Athanassoula (1994) finds that most barred galaxies have one or two ILRs, so that in general the bar will not push the gas sufficiently inwards to reach the nucleus and ultimately feed an AGN. Gas can however still reach the bulge region in some cases with ILR's, if for instance, a smaller secondary bar is found nested inside the primary dominant one. There are yet other mechanisms for breaking the ILR barrier, which rely on the self-gravity of the gas accumulating in the central area. Such mechanisms are described in Elmegreen (1994), and Heller & Shlosman (1994).

The shock loci are by definition regions of high density maxima. This leads to the question of whether this should lead to an increase in the local star formation rate. The reason star formation is not prevalent at all is attributed to the high shear encountered in straight shock loci. Molecular clouds will thus tend to shear out before they have time to collapse, preventing any star formation in that region. Shocks whose loci are curved however may well harbour more benign environments for incipient star formation. Examples of these two scenarios can be seen when comparing the dust lanes in the bar of NGC1300 with the corresponding ones in NGC1566. The ends of the bar are also regions where star formation could occur, since despite their higher density, there is not much shear. This also often betrays strong gas concentrations.

5.5 Type Θ_3 Stellar Bars – Bars devoid of Dust

5.5.1 Strongly Decoupled 3.6µm and 8.0µm bar morphologies

There is a family of stellar bars as seen in 3.6µm images which do not reveal themselves in the dust-emission dominated 8.0µm regime. In examples such NGC5371 (**Sb(rs)I/SBb(rs)I**), a weak bar evident in optical images which reveals a gravitational torque of $Q_{g(3.6)}$ = 0.33+/-0.13 at 3.6µm. There is no indication of the presence of this feature at all in the Spitzer 8.0µm image which yields a "torque" measurement of $Q_{g(8.0ns)}$ = 0.00+/-0.70. Optically, NGC5371 has type SAB(rs)bc and is given an Elmegreen & Elmegreen (1987) classification of 9 with its 'two symmetric inner arms; multiple long and continuous outer arms'. The thin, well formed spiral arms contain numerous HII regions.

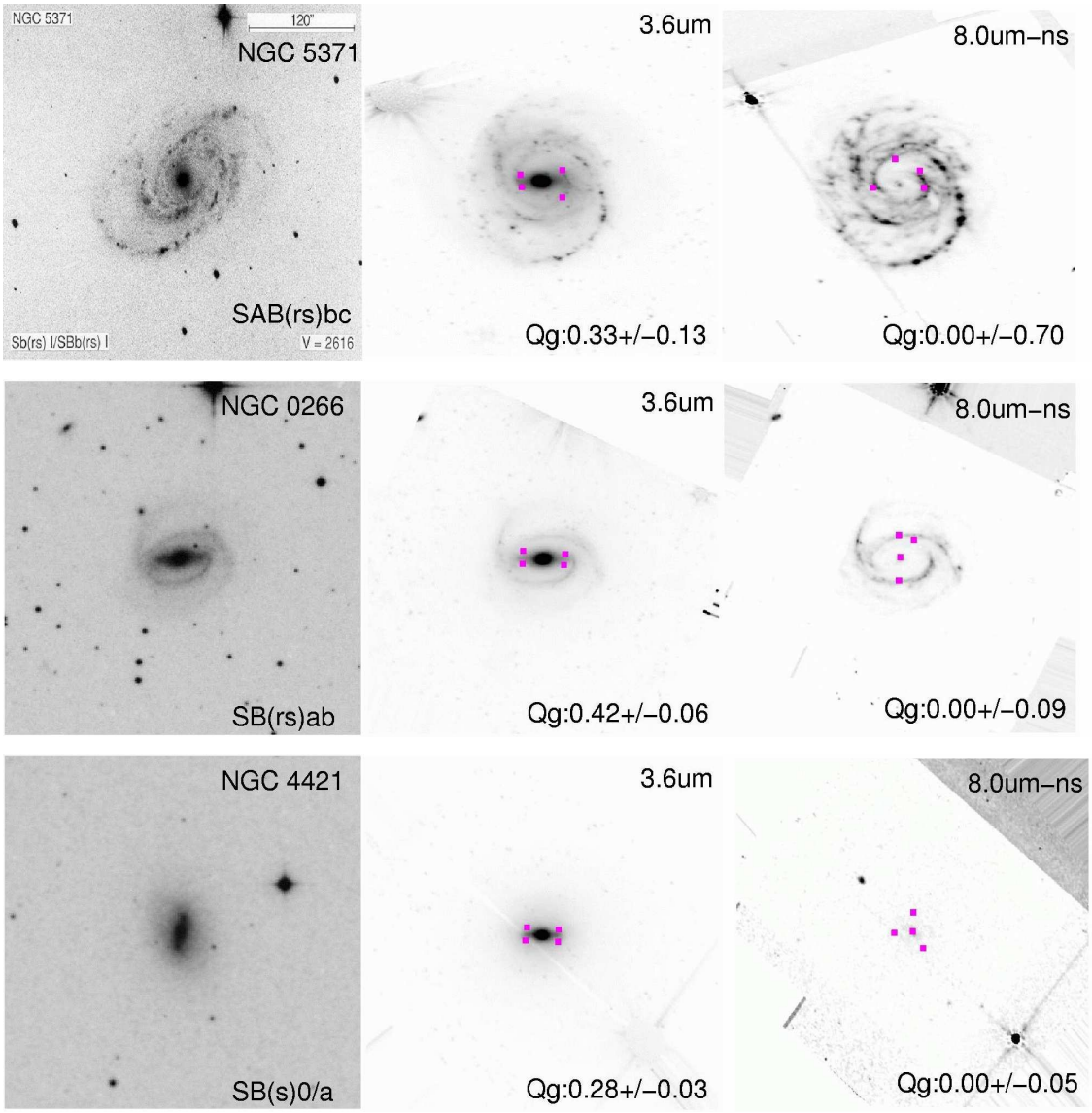

Figure 5.6: *Type Θ_3 Barred Spirals – Stellar bars devoid of gas and dust bars. These prototypically barred galaxies have very pronounced bars at 3.6μm, with no associated gas or dust at 8.0μm.*

NGC0266 presents the strongest near-infrared bar at 3.6μm in this sample with a relative gravitational torque calculated to be $Q_{g(3.6)}$ = 0.42+/-0.02. This calculated bar strength corroborates well with its attributed SB(rs)ab de Vaucouleurs designation, thereby resulting in a Q_g classification that is described as being a class 4 bar. No evidence of this very prominent bar is found in the 8.0μm image with the corresponding "torque" measured as $Q_{g(8.0ns)}$ = 0.00+/-0.09 with stellar component subtraction. However, the underlying dust arms do wrap around to form an almost-complete ring. The torque

maxima (small squares on the image) try unsuccessfully to hunt for definitive maxima positions. Elmegreen & Elmegreen (1987) classify this galaxy as a grand design archetype with an arm class of 12.

NGC 4421 is one of the most dramatic examples of Θ_3 type galaxies, optically classified as SB(s)0/a, with a bar torque measured at 3.6µm to be $Q_{g(3.6)}$ = 0.28+/-0.03 which places it in a bar class of 3. There is very little signal from this galaxy in 8.0µm images, even when contrast-stretched to the amount seen in the figure above. (Note the saturation of the region outside the frame boundary.) At this wavelength the $Q_{g(8.0ns)}$ = 0.00+/-0.05. This predominantly stellar early type galaxy has no spiral dust arms either, unlike many of the galaxies in this sample. It is very surprising to find a galaxy which appears to harbour a significant older stellar population, without traces of warm dust even in exaggerated image scalings. This implies the prominent bar in both the optical and 3.6µm images is almost exclusively stellar with very little dust concentration at all. There is no reference to NGC4421 in Elmegreen & Elmegreen (1987).

GALAXY	3.6µm	+/-	8.0µm	+/-	8.0µm n-stell.	+/-	De Vauc.	E&E
NGC0266	0.42	0.06	0.00	0.14	0.00	0.09	SB(rs)ab	12
NGC3344	0.05	0.05	0.00	0.13	0.00	0.20	(R)SAB(r)bc	9
NGC4421	0.28	0.03	0.14	0.03	0.14	0.05	SB(s)0/a	–

Table 5.3: Type Θ_3 Barred spiral galaxies

5.6 Conclusion

We know that the optical component of disk galaxies represents an extremely poor tracer of the underlying stellar backbone. We have now found that there is also a decoupling in the distribution of warm dust grains in the bars of a significant number of galaxies. The degree of decoupling is proportional to the uncertainty that arises in predicting the morphology of the underlying stellar component. For example, NGC0266 shows grand design structure at optical wavelengths, with a definitive bar in the optical (SB(rs)ab) and a substantial torque (Q_b = 0.42) at 3.6μm, but no bar is evident at all at 8.0μm.

It would seem that the dynamical mass distribution of a galaxy cannot, *a priori*, be predicted or inferred from its transient Population I morphology (Hubble Type). Moreover, the morphology of dust emission in a barred spiral galaxy cannot be definitively predicted from optical photographs or even images at 3.6μm.

– CHAPTER 6 –

CONCLUSION

"We shall not cease from exploration. And the end of all our exploring, will be to arrive where we started, and know the place for the first time", *– T.S. Elliot*

"In classification we find a "point of contact" between learning and science. It has two aspects: considered as a conception to be verified in nature, a classification belongs to science; considered as a help to memory, classification belongs to learning."

"… a true system of classification, such as shall be found verified in nature, reduces the mass of facts from a confusion which none can follow to an order which none can mistake."

From a book found in the Collingwood library of Sir John Herschel, entitled "The Three Essays" (author unknown, 1863)

6.1 Classification for the starry vault of the "nebulae"

Before the true nature of the "nebulae" had been revealed, attempts were already underway to devise classification schemes which would seek to bring some semblance of order in an otherwise cacophony of faint smudges of light. Classification was much on the mind of Sir John Herschel, who classified multitudes of "nebulae" in his sweeps of the southern skies from the Cape, during the period 1834-1838.

Sir John Herschel expressed himself thus, "Classification in such as case, is only another word for the announcement of general laws, the result of inductive observation – results,

that is to say, of a more elevated order than those which depend on a mere remarking of a general resemblance, or even on the specifications of particular arbitrarily selected points on which logical proof of such resemblances can be rested."

Other pioneers followed, such as Wolf, Lundmark, Curtis, Reynolds, Hubble and de Vaucouleurs, who set out to find a richer understanding of the "nebulae" by each proposing their own classification schemes.

Of all these schemes, the Hubble Classification Scheme is the one most used to classify galaxies in our Local Universe. A close friend of Hubble, the famed British theoretician Sir James Jeans, wrote in 1954:

"Thus our string or sequence of nebulae starts with something that looks like a fluffy, featureless ball of gas, and ends up as a city of stars."

The Hubble scheme brought with it a connectedness of one spiral galaxy when compared to another. A connectedness epitomized by the musically inclined James Jeans (1929) with his "Y" shaped diagram, suggestive of a tuning fork. And in Hubble's famous "The Realm of the Nebulae" (1936) the confluence of these two ideas is revealed, in what is known today as the Hubble Tuning Fork.

In the words of Sir James Jeans (1954), "We cannot ourselves go and find out what the sun, moon or stars consist of, but our huge telescopes will, in a sense, bring them near to us, which comes to much the same thing. The whole of space lies open for our exploration, at any rate until we are confronted by opaque substances which no telescope can penetrate." Jeans was of-course, for the most part, correct.

Sir John Herschel had gazed upon the Coalsack and wondered – could it be opaque or is it transparent? In the era of Hubble, cosmic dust was never an issue – not one astronomer then would believe that an entirely new world of galaxy classification would see the dawn of day wherein infrared telescopes would reveal a New Universe – a Universe

which was, to quote David Block, “dust penetrated”. Not even a master as great as Sir James Jeans himself, could have envisioned telescopes which could penetrate those “opaque substances”. Infrared camera arrays were beyond the reality of both mind and technology in the 1920s and 1930s.

A “Dust Penetrated” Universe demands New Classification schemes for the stellar backbones of extragalactic spiral disks. A New Era has emerged. It is the era for which this thesis has awaited.

6.2 Lessons from the Local Group of Galaxies

6.2.1 M33 – A Rosetta Stone for the building of galactic disks

NASA’s Spitzer Space Telescope trails the earth in heliocentric orbit. At cryogenic temperatures, instruments such as the Infrared Array Camera (IRAC) capture pristine infrared photons from the distant reaches of the realm of the “nebulae”. Photons all but invisible to the early pioneers are now the starry messengers critical to bringing this thesis to fruition. Spitzer and other infrared telescopes today provide windows on the universe unimaginable even just a few decades ago.

We have discovered that the “Triangulum Nebula”, Messier 33, stands as a pristine example of spiral galaxies being *dynamically open* systems. We have glimpsed the presence of vast populations of intermediate age (0.6 to 2.0 Gyrs) carbon stars located precisely at the gargantuan HI warp in M33. A coherent picture emerges: it is the signature of ongoing gaseous accretion from vast reservoirs in the tenuous outer regions of M33. In a very real sense, M33 represents a Rosetta stone of how the disks of spiral galaxies are formed and grow. We have learned that the implications are compatible with a “bottom up” disk formation scenario. Our technique of identifying carbon stars in M33 on the basis of their rest-frame ($J - K_s$) colours can be exploited as a means of probing the formation of disks in the higher-z Universe where individual stars cannot be resolved. Such surveys will be ideally suited to the next era of space-borne infrared telescopes, such as JWST.

6.2.2 Glowing Rings of Fire – Galaxy Morphology induced only millions of years ago

Traditionally, it was customary to believe that the morphologies of spiral galaxies were induced billions of years ago. In this thesis, the concept is overturned.

Through the infrared eyes of IRAC onboard Spitzer, we have discovered two off-centred "rings of fire" in the Andromeda Spiral – cosmic dust grains glowing in emission at 8.0μm. While dinosaurs roamed the Earth, a near-head-on collision of the Andromeda Spiral with one of her larger satellites (most likely M32) occurred.

Galactic collisions were once thought to be only important in the early universe. We now know this not to be the case – the rings of fire attest to "smoking gun" evidence for an almost head-on collision a mere 210 Myrs ago. N-body simulations performed by Bournaud & Combes, accurately recreate the present detailed morphology of the double dust ring, and other peculiarities (such as a "hole" in the outer ring, see Figure 3.3), when simulating the passage of a $1/10^{th}$ mass impacting galaxy passing within 1.5kpc of the centre of Andromeda. The bulge of this Hubble type Sb galaxy contains myriads of stars which *completely obscure* the inner dust ring. The bright bulge noted by Messier, Hubble and many others, has successfully cloaked all the forensic evidence of a major collision throughout the entire epoch of observational astronomy. It was not until the eyes of IRAC were able to penetrate the bulge of stars, that the true history of "The Empress" in the constellation of Andromeda was revealed.

6.3 Dust penetrated IRAC Morphology

6.3.1 Separating bars from their parent disks of stars

Bars in disk galaxies have been discovered to be a ubiquitous phenomenon. So ubiquitous, that least 80% of disk galaxies in our Local Universe betray bars at near infrared wavelengths.

By utilizing a technique pioneered by Combes & Sanders (1981) together with the advent of near-infrared detectors, we can probe the distribution of gravitational torques of spiral galaxies. Surveys such as the Ohio State University Sample of Bright Galaxies

(OSUSBG), images from INGRID on the 4.2m William Herschel Telescope (WHT), and the Two Micron All Sky Survey (2MASS) paved the way forward in demonstrating what has now become known as the Gravitational Torque Method (GTM) as a quantitative means of measuring the torques of bars in the near-infrared.

Refinements to this procedure have followed; refinements which allow for the separation of bars from spiral arms in barred galaxies. In this thesis, we separate the bars themselves from their parent disks to study the comparative torques in both bars and in spiral arms. A sample of 40 nearby barred spiral galaxies were thus numerically "interrogated". Approximately one-half of the sample comprises spirals imaged with IRAC onboard Spitzer, while the other half of the sample was provided by Johan Knapen who used the IRIS2 detector on the 3.9m AAT. The gravitational torques of the actual bars themselves are compared to the torques of the respective spiral arm components. This plot (see Figure 4.6) reveals a relatively large spread in the correlation between bar torque and spiral arm torque. It has been suggested by Combes, Sellwood and others that bars do not sustain themselves over a period comparable with a Hubble time, but rather may form, dissipate and reform again several times during the age of the Universe. We believe that the question as to whether stronger bars drive stronger spirals may be masked by cases where the bars of some spiral galaxies may have partially dissolved with time – yet maintain a relatively high spiral arm torque. On the other hand, there are very strongly barred galaxies with very weak spiral arms, as seen in NGC5101 and NGC3368. No clear-cut solution is at hand, but the dream of separating a bar from its parent spiral arms is now a reality. With the advent of future near and mid infrared space telescopes, the GTM can easily be extended to a quantitative method of classifying galaxies at earlier epochs.

6.3.2 Dust Grains in Emission – The Morphology of Spiral Galaxies at 8.0μm

One of the most surprising insights into the dynamics of nearby spiral galaxies has been gleaned from IRAC. We have discovered three distinct classes or "form families" of spiral galaxies which have definitive bars at 3.6μm:

(1) galaxies where the 8.0μm warm dust morphology tightly traces the older stellar (3.6μm) population – which are denoted Θ_1 type galaxies.

(2) S-shaped dust spirals within the stellar bar region, but with no obvious bar at 8.0μm – we term these the Θ_2 type galaxies.

And most surprising of all…

(3) bars which are completely devoid of dust – denoted by the Θ_3 form family. e.g.: NGC4421; the emission at 8.0μm barely delineates the galaxy at all.

Strongly barred SB-type galaxies often do show a very pronounced dust morphology which traces the stellar backbone. In cases such as these, applying the GTM to 8.0μm Spitzer images reveal surprisingly similar values for their "torques". While these cannot be interpreted as a gravitational torques *per se*, the numerical correlation between 3.6μm and 8.0μm "Q_g" values signifies the degree to which the gas and dust morphology trace – and are thus coupled/partially coupled/or fully decoupled to – the underlying old population of stars. At 3.6μm the old stellar population I in the disk is observed almost entirely free of the obscuring effects of foreground dust grains – and therein lies the true golden window for rest-frame near-infrared galaxy morphology.

6.4 The exploration of space

And so, in our conclusion, it is particularly poignant to reflect on Hubble's epic words (1936): "Thus the explorations of space end on a note of uncertainty. And necessarily so. We are, by definition, in the very centre of the observable region. We know our immediate neighbourhood rather intimately. With increasing distance, our knowledge fades, and fades rapidly. Eventually, we reach the dim boundary – the utmost limits of our telescopes. There, we measure shadows, and we search among ghostly errors of measurement for landmarks that are scarcely more substantial. The search will continue. Not until the empirical resources are exhausted, need we pass on to the dreamy realms of speculation."

HYMN TO THE NIGHT

I heard the trailing garments of the Night
Sweep through her marble halls!
I saw her sable skirts all fringed with light
From celestial walls!

I felt her presence, by it's spell of might
Stop over me from above:
The calm, majestic presence of the Night,
As of the one I love.

– Henry Wadsworth Longfellow

– REFERENCES –

Abraham, R., Tanvir, N.R., Santiago, B.X., Ellis, R.S., Glazebrook, K., van den Bergh, S. 1996a, MNRAS, 279, L47

Abraham, R., van den Bergh, S., Glazebrook, K., Ellis, R.S., Santiago, B.X., Surma, P., Griffiths, R.E. 1996b, ApJS, 107, 1

Abraham, R. and Merrifield, M.R. 2000, AJ, 120, 2835

Allen, R.J. Eyes to the Future. In 'New extragalactic Perspectives in the New South Africa', eds. Block, D.L. & Greenberg, J.M. Kluwer, Dordrecht. 585-610 (1996).

Appleton P.N., Struck-Marcell C. 1996, Collisional Ring Galaxies, Fundamentals of Cosmic Physics, Vol 16, 111-220

Athanassoula, E. 1992a, MNRAS, 259, 328

Athanassoula, E. 1992b, MNRAS, 259, 345

Athanassoula, E. 1994, in 'Mass-Transfer Induced Activity in Galaxies', Ed.: I. Shlosman (Cambridge University Press), 143

Athanassoula, E. 2000, in 'Stars, gas and dust in galaxies: Exploring the Links', Eds.: D. Alloin, K. Olsen, G. Galaz (ASP Conf. Ser.), 221, 243

Athanassoula, E. & Beaton, R.L. 2006, MNRAS, 370, 1499-1512

Baade, W. & Payne-Gaposchkin, C.H. 1963, in 'Evolution of stars and galaxies.' Cambridge, Harvard University Press

Barmby, P., Ashby, M.L.N., Bianchi, L., Engelbracht, C.W., Gehrz, R.D., Gordon, K.D., Hinz, J.L., Huchra, J.P., Humphreys, R.M., Pahre, M.A., Pérez-González, P.G., Polomski, E.F., Rieke, G.H., Thilker, D.A., Willner, S.P., Woodward, C.E. 2006, ApJL, 650, 45

Beaulieu, J-P., Buchler, J., Marquette, J-B. Hartman, J.D., Swarzenberg-Czerny, A. 2006, ApJ, 653, L101

Beck R., Berkhuijsen, E. M., Hoernes, P. 1998, A&AS 129, 329-336

Bekki K., Couch, W.J., Drinkwater, M.J., Gregg, M.D. 2001, ApJ, 557, L39

Bell, E.F. & de Jong, R.S. 2000, MNRAS, 312, 497

Benjamin, R.A.; GLIMPSE Team 2005, AAS, 207, 6307

Bertin, G., Lin, C.C., Lowe, S.A., Thurstans, R.P., 1989a, ApJ, 338, 78

Bertin, G., Lin, C.C., Lowe, S.A., Thurstans, R.P., 1989b, ApJ, 338, 104

Bertin, G. 1996, in 'New Extragalactic Perspectives in the New South Africa', Eds.: D.L. Block & J.M. Greenberg (Kluwer, Dortrecht), 227

Bessell, M.S. & Brett, J.M. 1988, PASP, 100, 1134

Binney, J. & Tremaine, S. 1987, Galactic Dynamics, (Princeton: Princeton Univ. Press)

Binney, J. 1992, ARA&A, 30, 51

Block, D.L. & Wainscoat, R.J. 1991, NATURE, 353, 48-50

Block, D.L. 1996, in 'New Extragalactic Perspectives in the New South Africa', Eds.: D.L. Block & J.M. Greenberg (Kluwer, Dortrecht), 1

Block, D.L. & Puerari, I. 1999, A&A, 342, 627

Block, D.L., Stockton, A., Elmegreen, B.G., Willis, J. 1999, ApJ, 522, L25

Block, D.L., Puerari, I., Knapen, J.H., Elmegreen, B.G., Buta, R., Stedman, S., Elmegreen, D.M. 2001, A&A, 375, 761-769

Block, D.L., Bournaud, F., Combes, F., Puerari, I. & Buta, R. 2002, A&A, 394, L35-L38

Block, D.L., Freeman, K.C., Jarrett, T.H., Puerari, I., Worthey, G., Combes, F., Groess, R. 2004a, A&A, 425, 37

Block, D.L., Freeman, K.C., Puerari, I., Combes, F., Buta, R., Jarrett, T., Worthey, G. 2004b, in 'Penetrating Bars through Masks of Cosmic Dust: The Hubble Tuning Fork Strikes a New Note', Eds.: D.L. Block, I. Puerari, K.C. Freeman, R. Groess, E.K. Block (Springer, New York), 15

Block, D.L., Bournaud, F., Combes, F., Groess, R., Barmby, P., Ashby, M.L.N., Fazio, G.G., Pahre, M.A., Willner, S.W. 2006, NATURE, 443, 832-834

Block, D.L., Puerari, I., Stockton, A., Canalizo, G., Freeman, K.C., Jarrett, T.H., Combes, F., Groess, R., Worthey, G., Gehrz, R.D., Woodward, C.E., Polomski, E.F., Fazio, G.G. 2007, IAUS, 235, 8

Borne, K.D., Lucas, R., Appleton, P., Struck, C., Schultz, A., Spight, L. 1994, Bulletin of the American Astronomical Society, 26, 1422

Bournaud, F. & Combes, F. 2002, A&A, 392, 83-102

Bournaud, F. & Combes, F. 2003, A&A, 401, 817-833

Bouwens, R., Broadhurst, T. & Silk, J. 1998, ApJ, 506, 557

Bouwens, R.J., Illingworth, G.D., Rosati, P., Lidman, C., Broadhurst, T., Franx, M., Ford, H.C., Magee, D., Benítez, N., Blakeslee, J.P., Meurer, G.R., Clampin, M., Hartig, G.F., Ardila, D.R., Bartko, F., Brown, R.A., Burrows, C.J., Cheng, E.S., Cross, N.J.G., Feldman, P.D., Golimowski, D.A., Gronwall, C., Infante, L., Kimble, R.A., Krist, J.E., Lesser, M.P., Martel, A.R., Menanteau, F., Miley, G.K., Postman, M., Sirianni, M., Sparks, W.B., Tran, H.D., Tsvetanov, Z.I., White, R.L., Zheng, W. 2003, ApJ, 595, 589

Braun R. 1991, ApJ, 372, 54-66

Brinks E., Shane W.W. 1984, A&AS, 55, 179-251

Bruzual, A.G. Charlot, S. 1993, ApJ, 405, 538-553

Buchanan, C.L., Kastner, J.H., Forresst, W.J., Hrivnak, B.J., Sahai, R., Egan, M., Frank, A., Barnbaum, C. 2006, AJ, 132, 1890

Burstein, D. & Rubin, V.C. 1985, ApJ, 297, 423

Burton, W.B. & Gordon, M.A. 1976, ApJ, 207, L189

Buta, R. 1986, ApJS, 61, 631

Buta, R. & Block, D.L. 2001, ApJ, 550, 243

Buta, R., Block, D.L., Knapen, J.H. 2003, AJ, 126, 1148

Byrd, G.G. 1978, ApJ, 226, 70

Byrd, G.G. 1983, ApJ, 264, 464-469.

Casoli F., Combes F., Stark A.A. 1987, A&A, 173, 43-48

Charlot, S. 1996, in 'The Universe at High-z, Large-Scale Structure and the Cosmic Microwave Background', Ed.: E. Martinez-Gonzalez & J.L. Sanz (Springer Lecture notes in Physics), 470, 53

Ciardullo, R. Rubin, V.C., Ford, W.K., Jacoby, G.H., Ford, H.C. 1998, ApJ, 95, 438-444

Clerke, A. 1903, in 'Problems in Astrophysics', London, A. & C. Black, 567

Combes, F. and Sanders, R.H. 1981, A&A, 96, 164

Considère, S. & Athanassoula, E. 1988, A&AS, 76, 365-404

Cook, K.H., Aaronson, M., Norris, J. 1986, ApJ 305, 634

Corbelli, E. & Schneider, S.E. 1997, ApJ, 479, 244-257

Curtis, H.D. 1918a, Descriptions of 762 nebulae and clusters photographed with the Crossley reflector. Publications of the Lick Observatory, XIII, 11-42

Curtis, H.D. 1918b, A Study of Occulting Matter in the Spiral Nebulae. Publications of the Lick Observatory, XIII, 45-54

Dame, T.M., Koper, E., Israel, F.P., Thaddeus, P. 1993, ApJ 418, 730-742

Danielson, R.E., Woolf, N.J., Gaustad, J.E. 1965, ApJ, 141, 116

de Grijs, R. 1998, MNRAS, 299, 595

Demers, S., Battinelli, P. 2005, A&A 436, 91

Depoy, D.L., Quillen, A.C., Berlind, A., Ramirez, S.V. 1996, in 'New Extragalactic Perspectives in the New South Africa', Eds.: D.L. Block & J.M. Greenberg (Kluwer, Dortrecht), 109

Deul, E.R. & van der Hulst, J.M. 1987, A&AS, 67, 509-539

de Vaucouleurs, G. 1956, Mem. Commonw. Obs. (Mount Stromlo), 3, No. 13.

de Vaucouleurs, G. 1959, ApJ, 130, 728-738

de Vaucouleurs, G., de Vaucouleurs, A., Corwin, H.G., Buta, R.J., Paturel, G., Fouque, P. 1991, in 'Third Reference Catalogue of Bright Galaxies', Volume 1-3, XII (Springer-Verlag Berlin Heidelberg New York)

Devereux, N.A., Price, R. Wells., L.A., Duric, N. 1994, AJ, 108, 1667

Disney, M.J., Davies, J., Phillips, S. 1989, MNRAS, 239, 939

Draine, B.T. & Li, A. 2007, ApJ, 657, 810

Dreyer, J.L.E. 1888, in 'A New General Catalogue of Nebulae and Clusters of Stars', Mem. Royal Astronomical Society, 49, Part I.

Driver, S.P., Fernández-Soto, A., Couch, W.J., Odewahn, S.C., Windhorst, R.A., Phillipps, S., Lanzetta, K., Yahil, A. 1998, ApJ, 496, L93

Elmegreen, D.M. 1981, ApJS, 47, 229.

Elmegreen, D.M. & Elmegreen, B.G. 1982, MNRAS, 201, 1021.

Elmegreen, B.G. & Elmegreen, D.M. 1985, ApJ, 288, 438

Elmegreen, D.M. & Elmegreen, B.G. 1987, ApJ, 314, 3-9

Elmegreen, B.G. 1994, ApJ, 425, L73

Elmegreen, B.G. & Block, D.L. 1999, MNRAS, 303, 133

Eskridge, P.B., Frogel, J.A. 1999, Astrophysics & Space Science, 269, 427

Fazio, G.G., Pahre, M.A, Willner, S.P., Ashby, M.L.N. 2004a, in 'Penetrating Bars through Masks of Cosmic Dust: The Hubble Tuning Fork Strikes a New Note',

Eds.: D.L. Block, I. Puerari, K.C. Freeman, R. Groess, E.K. Block (Springer, New York), 389

Fazio, G.G., Hora, J.L., Allen, L.E., Ashby, M.L.N., Barmby, P., Deutsch, L.K., Huang, J.-S.m Kleiner, S., Marengo, M., Megeath, S.T., Melnick, G.J., Pahre, M.A., Patten, B.M., Polizotti, J., Smith, H.A., Taylor, R.S., Wang, Z., Willner, S.P., Hoffmann, W.F., Pipher, J.L., Forrest, W.J., McMurty, C.W., McCreight, C.R., McKelvey, M.E., McMurray, R.E., Koch, D.G., Moseley, S.H., Arendt, R.G., Mentzell, J.E., Marx, C.T., Losch, P., Mayman, P., Eichhorn, W., Krebs, D., Jhabvala, M., Gezari, D.Y., Fixsen, D.J., Flores, J., Shakoorzadeh, K., Jungo, R., Hakun, C., Workman, L., Karpati, G., Kichak, R., Whitley, R., Mann, S., Tollestrup, E.V., Eisenhardt, P., Stern, D., Gorjian, V., Bhattacharya, B., Carey, S., Nelson, B.O., Glaccum, W.J., Lacy, M., Lowrance, P.J., Laine, S., Reach, W.T., Stauffer, J.A., Surace, J.A., Wilson, G., Wright, E.L., Hoffman, A., Domingo, G., Cohen, M. 2004b, ApJS, 154, 10-17

Ferguson, A.M.N., Irwin, M.J., Ibata, R.A, Lewis, G.F., Tanvir, N.R. 2002, AJ, 124, 1452

Ferguson, A.M.N., Irwin, M.J., Chapman, S., Ibata, R.A., Lewis, G.F., Tanvir, N.R. 2006, in 'Island Universes - Structure and Evolution of Disk Galaxies', Ed.: R.S. de Jong (Springer: Dordrecht)

Freedman, W.L. Wilson, C.D. & Madore, B.F. 1991, ApJ, 372, 455-470

Freeman, K.C. 1970, ApJ, 160, 811

Freeman, K.C. 1992, in 'Physics of Nearby Galaxies: Nature or Nurture?', Eds.: Thuan, T.X., Balkowski, C., Tran Thanh, J., (Gif-sur-Yvette, Editions Frontiere), 201

Frogel, J.A. & Whitford, A.E. 1987, ApJ, 320, 199.

Frogel, J.A., Quillen, A.C., Pogge, R.W. 1996, in New Extragalactic Perspectives in the New South Africa, ed. D.L. Block & J.M. Greenberg (Kluwer Dordrecht), 65

Gehrz, R.D., Roellig, T.L., Werner, M.W., Fazio, G.G., Houck, J.R., Low, F.J., Rieke, G.H., Soifer, B.T., Levine, D.A., Romana, E.A. 2007, Rev. Sci. Instrum. 78, 011302

Giavalisco, M., Livio, M., Bohlin, R.C., Macchetto, F.D. & Stecher, T.P. 1996, AJ, 112, 369

Gilmore, G. & Reid, N. 1983, MNRAS, 202, 1025.

Glazebrook, K., Peacock, J.A., Miller, L., Collins, C.A. 1995, MNRAS, 275, 169

Gordon, K.D., Bailin, J., Engelbracht, C.W., Rieke, G.H., Misselt, K.A., Latter, W.B., Young, E.T., Ashby, M.L.N., Barmby, P., Gibson, B.K., Hines, D.C., Hinz, J., Krause, O., Levine, D.A., Marleau, F.R., Noriega-Crespo, A., Stolovy, S., Thilker, D.A., Werner, M.W. 2006, ApJL, 638, L87

Greenberg, J.M. 1970, in 'Interstellar grains and spiral structure in Interstellar Gas Dynamics', Ed. H.J. Habing (Reidel, Dortrecht)

Greenberg, J.M., Yencha, A.J., Corbett, J.W., Frisch, H.L. 1972, 'Ultraviolet effects on the chemical composition and optical properties of interstellar grains', Mém. Soc. Roy. Sci. Liège, 6e série, tome III, 425-436

Greenberg, J.M. & Li, A. 1996, in 'New Extragalactic Perspectives in the New South Africa', Eds.: D.L. Block & J.M. Greenberg (Kluwer, Dortrecht), 118

Greenberg, J.M. & Shen, C. 1999, Ap&SS, 269, 33

Groess, R., Block, D.L., Puerari, I. 2004, in 'Penetrating Bars through Masks of Cosmic Dust: The Hubble Tuning Fork Strikes a New Note', Eds.: D.L. Block, I. Puerari, K.C. Freeman, R. Groess, E.K. Block (Springer, New York), 777

Grosbøl, P.J. 1985, A&AS, 60, 261

Haas M., Lemke, D., Stickel, M., Hippelein, H., Kunkel, M., Herbstmeier, U., Mattila, K. 1998, A&A, 338, L33-36

Heller, C.H. & Shlosman, I. 1994, ApJ, 424, 84

Helou, G., Roussel, H., Appleton, P., Frayer, D., Stolovy, S., Storrie-Lombardi, L., Hurt, R., Lowrance, P., Makovoz, D., Masci, F., Surace, J., Gordon, K.D., Alonso-Herrero, A., Engelbracht, C.W., Misselt, K., Rieke, G., Rieke, M., Willner, S.P., Pahre, M., Ashby, M.L.N., Fazio, G.G., Smith, H.A. 2004, ApJS, 154, 253

Henderson A.P. 1979, A&A 75, 311-315

Herschel, J.F.W. 1864, Philos. Trans. R. Soc. London, 154, 1-137

Higdon, J.L. 1996, ApJ, 467, 241

Hodge, P.W. Skelton, B.P. & Ashizawa, J. An Atlas of Local Group Galaxies. Kluwer, Dordrecht (2002)

Holmberg, H. 1958, Lund Medd. Astron. Obs. Ser., II, 136

Horellou C., Combes F. 2001, Ap&SS 276, 1141

Hubble, E. 1917, Ph.D. Thesis, 'Photographic Investigations of Faint Nebulae', (University of Chicago)

Hubble, E. 1926, ApJ, 64, 321

Hubble, E. 1936, in 'The Realm of the Nebulae', (Dover Publications Inc., New York)

Humason, M.L., Mayall, N.U., Sandage, A. 1956, AJ, 61, 97

Humphreys, R.M. & Sandage, A. 1980, ApJS, 44, 319-381

Huntley, J.M. 1978, ApJ, 225, 101

Ibata, R., Irwin, M., Lewis, G., Ferguson, A.M.N., Tanvir, N. 2001, NATURE, 412, 49-51

Ibata, R., Chapman, S., Ferguson, A.M.N., Lewis, G., Irwin, M., Tanvir, N. 2005, ApJ, 634, 287

Jacoby G. H., Ford, H., Ciardullo, R. 1985, ApJ, 290, 136-139

Jarrett, T.J., Chester, T., Cutri, R., Schneider, S.E., Huchra, J.P. 2003, AJ, 125, 525-554

Jeans, J.H. 1919, in 'Problems of Cosmogony and Stellar Dynamics', Cambridge Univ. Press

Jeans, J.H. 1929, in 'Astronomy and Cosmogony', Cambridge Univ. Press

Jeans, J.H. 1954, in 'The Stars in their Courses', Cambridge Univ. Press

Johnson, H.M. & Hanna, M.M. 1972, ApJ, 174, L71

Kapteyn, J.C. 1904, AJ, 24, 115

Kauffmann, G. & Charlot, S. 1998, MNRAS, 297, L23

Keeler, J.E. 1908, Photographs of nebulae and clusters made with the Crossley reflector, Publ. Lick Obs., 8, 1

Kereš, D., Katz, N., Weinberg, D.H., Davé, R. 2005, MNRAS, 363, 2

King, I.R., 1992, in 'Morphological and Physical Classification of Galaxies' Eds.: Longo, G., Capaccioli, M. Busarello, G. (Kluwer, Dordrecht), 371

Knapen, J.H., Shlosman, I, Peletier, R.F. 2000, ApJ, 529, 93

Knox-Shaw, H. 1915, Helwan Obs. Bull., 15, 129

Kormendy, J. 1988, ApJ, 325, 128

Kormendy, J. & Kennicutt, R.C. 2004, Annual Review of Astronomy & Astrophysics, 42, 603

Kregel, M., van der Kruit, P.C., de Grijs, R. 2002, MNRAS, 334, 646

Lauer, T.R., Faber, S.M., Groth, E.J., Shaya, E.J., Campbell, B., Code, A., Currie, D.G., Baum, W.A., Ewald, S.P., Hester, J.J., Holtzman, J.A., Kristian, J., Light, R.M., Ligynds, C.R., O'Neil, E.J., Jr., Westphal, J.A. 1993, AJ, 106, 1436

Laurikainen, E., Salo, H., Rautiainen, P. 2001, ASPC, 249, 183

Laurikainen, E. & Salo, H. 2002, MNRAS, 337, 1118

Le Bertre, T., Tanaka, M., Yamamura, I., Murakami, H. 2003 A&A 403, 943

Leitherer, C., Alloin, D., Fritze-v. Alvensleben, U., Gallagher, J.S., Huchra, J.P., Matteucci, F., O'Connell, R.W., Beckman, J.E., Bertelli, G., Bica, E., Boisson, C., Bonatto, C., Bothun, G.D., Bressan, A., Brodie, J.P., Bruzual, G., Burstein, D., Buser, R., Caldwell, N., Casuso, E., Cerviño, M., Charlot, S., Chavez, M., Chiosi, C., Christian, C.A., Cuisinier, F., Dallier, R., de Koter, A., Delisle, S., Diaz, A.I., Dopita, M.A., Dorman, B., Fagotto, F., Fanelli, M.N., Fioc, M., Garcia-Vargas, M., Girardi, L., Goldader, J.D., Hardy, E., Heckman, T.M., Iglesias, J., Jablonka, P., Joly, M., Jones, L., Kurth, O., Lançon, A., Lejeune, T., Loxen, J., Maeder, A., Malagnini, M., Marigo, P., Mas-Hesse, J.M., Meynet, G., Moller, C.S., Molla, M.L., Morossi, C., Nasi, E., Nichols, J.S., Odegaard, K.J.R., Parker, J.Wm., Pastoriza, M.G., Peletier, R., Robert, C., Rocca-Volmerange, B., Schaerer, D., Schmidt, A., Schmitt, H.R., Schommer, R.A., Schmutz, W., Roos, M.S., Silva, L., Stasinska, G., Sutherland, R.S., Tantalo, R., Traat, P., Vallenari, A., Vazdekis, A., Walborn, N.R., Worthey, G., Wu, C. 1996, PASP, 108, 996-1017

Li, A. & Draine, B.T. 2001, ApJ, 554, 778

Lindblad, B. On a Barred Spiral Structure in the Andromeda Nebula, Stockholms Observatoriums Annaler, Band 19, No. 2, p. 2-12, 1956.

Lundmark, K. 1926, Ark. Math. Astron. Phys. Ser. B, 19, No. 8

Lundmark, K. 1927, Medd. Astron. Obs. Uppsala, No. 30.

Lynds, R., Toomre, A. 1976, ApJ, 209, 382-388

Magrini, L., Corbelli, E., Galli, D. 2007, A&A, 470, 843-855

Maraston, C. 1998, MNRAS, 300, 872

Maraston, C. 2005, in 'Multiwavelength mapping of galaxy formation and evolution', Eds.: A. Renzizi, R. Bender (Springer, Berlin), 290

Marigo, P. Girardi, L. Chiosi, C. 1996, A&A, 316, L1-L4

Marigo, P. Girardi, L. Chiosi, C. 2003, A&A, 403, 225-237

Martin, P.G. and Whittet, D.C.B. 1990, ApJ, 357, 113

Martin, P. 1995, AJ, 109, 2428

Massey, P., Strobel, K., Barnes, J.V., Anderson, E. 1988, ApJ 328, 315

Mateo M.L. 1998, ARA&A, 36, 435-506

Mathews, W.G. & Baker, J.C. 1971, ApJ, 170, 241

Mathewson, D.S., Ford, V.L., Buchhorn, M, 1992, ApJS, 81, 413

Mouhcine, M. & Lançon, A. 2003, A&A, 402, 425

Nieten, Ch., Neininger, N., Guélin, M., Ungerechts, H., Lucas, R., Berkhuijsen, E.M., Beck, R., Wielebinski, R. 2005, A&A, 453, 459

Ohta, K., Hamabe, M., Wakamatsu, K. 1990, ApJ, 357, 71

Oke, J.B., Cohen, J.G., Carr, M., Cromer, J., Dingizian, A., Harris, F.H., Labrecque, S., Lucinio, R., Schaal, W., Epps, H., Miller, J. 1995, PASP, 107, 375

Pagel, B.E.J. & Edmunds, M.G. 1981, ARA&A, 19, 77

Peletier, R.F., Valentijn, E.A., Moorwood, A.F.M., Freudling, W. 1994, A&AS, 108, 621

Pellet, A., Astier, N., Viale, A., Courtes, G., Maucherat, A., Monnet, G., Simien, F. 1978, A&AS 31, 439

Persson, S.E. Aaronson, M. Cohen, J.G. Frogel, J.A., Matthews, K. 1983, ApJ, 266, 105-129

Pfenniger, D., Combes, F., Martinet, L. 1994, A&A, 285, 79

Pfenniger, D., Combes, F., Martinet, L. 1996, in 'New Extragalactic Perspectives in the New South Africa', Eds.: D.L. Block & J.M. Greenberg (Kluwer, Dortrecht), 291

Piner, B.G., Stone, J.M., Teuben, P.J. 1995, ApJ, 449, 508

Prendergast, K.H. 1962, IAUS, 15, 126

Prendergast, K.H. 1983, IAUS, 100, 215

Puerari, I. & Dottori, H.A. 1992, A&AS, 93, 469-493

Quillen, A.C., Frogel, J.A., Gonzalez, R. 1994, ApJ, 437, 162

Quillen, A.C. 1996, in 'ASP Conf. Ser. 91, Barred Galaxies', Eds.: Buta, R., Crocker, D.A., Elmegreen, B.G. (San Francisco:ASP), 390

Regan, M.W. & Vogel, S.N. 1994, ApJ, 434, 536-545

Reynolds, J.H. 1920, MNRAS, 80, 746.

Reynolds, J.H. 1927, The Observatory, 50, 185

Rhoads, J.E. 1998, AJ, 115, 472

Rieke, G.H. & Lebofsky, M.J. 1985, ApJ, 288, 618-621

Rix, H.W. & Rieke, M.J. 1993, ApJ, 418, 123

Rix, H.W. & Zaritsky, D. 1995, ApJ, 447, 82

Rogstad, D.H., Wright, M.C.H., Lockhart, I.A. 1976, ApJ, 204, 703

Rowe, J.F., Richer, H.B., Brewer, J.P., Crabtree, D.R. 2005, AJ, 129, 729

Rozas, M. Knapen, J.H., Beckman, J.E. 1998, MNRAS, 301, 631

Rubin, V.C. and Ford, W.K. 1971, ApJ, 170, 25

Sancisi, R. 1983, in 'Internal Kinematics and Dynamics of Galaxies', IAUS, 100, 55

Sandage, A. 1961, Hubble Atlas of Galaxies, Carnegie Institution of Washington

Sandage, A. & Humphreys, R.M. 1980, ApJ, 236, L1-L5

Sandage, A. & Tammann, G.A. 1981, A Revised Shapley-Ames Catalogue of Bright Galaxies, Carnegie Institution of Washington

Sandage, A., Binggeli, B., Tammann, G.A. 1985, AJ, 90, 1759

Sandage, A. & Bedke, J. 1994, The Carnegie Atlas of Galaxies, Carnegie Institute of Washington publication, No. 638

Sandage, A. 2004, in 'Penetrating Bars through Masks of Cosmic Dust: The Hubble Tuning Fork Strikes a New Note', Eds.: D.L. Block, I. Puerari, K.C. Freeman, R. Groess, E.K. Block (Springer, New York), 39

Sandage, A. 2005, ARA&A, 43, 581-624

Sanders, R.H., Tubbs, A.D. 1980, ApJ, 235, 803

Sato, N.R. & Sawa, T. 1986, PASJ, 38, 63

Schalén, C. 1929, Astron. Nachr., 236, 249

Schweizer, F. 1976, ApJS, 31, 313

Searle, L. 1971, ApJ, 168, 327

Seigar, M.S. & James, P.A. 1998, MNRAS, 299, 672

Sellwood, J.A. and Wilkinson, A. 1993, Rep. Prog. Phys., 56, 173

Shapley, H. & Curtis, H.D. 1921, Bull. Nat. Res. Council 2, 217

Sheinis, A.I., Bolte, M., Epps, H.W., Kibrick, R.I., Miller, J.S., Radovan, M.V., Bigelow, B.C., Sutin, B.M. 2002, PASP 114, 851

Shu, F.H., Milione, V., Roberts, W.W. 1973, ApJ, 183, 819

Simien, F., Pellet, A., Monnet, G., Athanassoula, E., Maucherat, A., Courtes, G. 1978, A&A 67, 73-79

Slipher, V.M. 1913, Lowell Obs. Bull. No.58, II, 8

Slipher, V.M. 1914, Lowell Obs. Bull. No.62, II, 12

Slipher, V.M. 1917, Proceedings of the American Philosophical Society, 56, 403-409

Stanek, K.Z. & Garnavich, P.M. 1998, ApJ, 503, L131

Stark, A.A. & Binney, J. 1994, ApJ, 426, L31-L33

Strom, S.E., Strom, K.M., Jensen, E.B. 1976, ApJ, 206, 11

Struck-Marcell, C. & Higdon, J.L. 1993, ApJ, 411, 108-124

Terndrup, D.M., Davies, R.L., Frogel, J.A., DePoy, D.L., Wells, L.A. 1994, ApJ, 432, 518

Thronson, Jr., H.A., Hereld, M., Majewski, S., Greenhouse, M., Johnson, P., Spillar, E., Woodward, C.E., Harper, D.A., Rauscher, B.J. 1989, ApJ, 343, 158

Toth, G. & Ostriker, J.P. 1992, ApJ, 389, 5

Trumpler, R.J. 1930, Preliminary results on the distances, dimensions and space distribution of open star clyusters, Lick Obs. Bull. XIV, 154

Tsalmantza, P., Kontizas, E., Cambrésy, L., Genova, F., Dapergolas, A., Kontizas, M. 2006, A&A 447, 89

Tsujimoto, T., Yoshii, Y., Nomoto, K., Shigeyama, T. 1995, A&A 302, 704

Tully, R.B. & Fisher, J.R. 1987, in 'Atlas of Nearby Galaxies', Cambridge University Press

Unwin, S.C. 1983, MNRAS, 205, 773

Valentijn, E.A. 1990, Nature, 346, 153

van den Bergh, S. 1960a, ApJ, 131, 215

van den Bergh, S. 1960b, ApJ, 131, 558

van den Bergh, S., Abraham, R.G., Ellis, R.S., Tanvir, N.R., Santiago, B.X., Glazebrook, K.G. 1996, AJ, 112, 359

van den Bergh, S. 1998, Galaxy Morphology and Classification, (Cambridge University Press), 87

van de Hulst, H.C. 1949, The solid particles in interstellar space, Rech. Astron. Obs. Utrecht 11, pt. 2

Vazdekis, A. 2001, Ap&SS, 276, 921-929

Wainscoat, R.J., Hyland, A.R., Freeman, K.C. 1990, ApJ, 348, 85

Weil, M.L., Eke, V.R., Efstathiou, G. 1998, MNRAS, 300, 773

Weiner, B.J. 1998, Ph.D. Thesis, Rutgers University.

Werner, M.W., Roellig, T.L., Low, F.J., Rieke, G.H., Rieke, M., Hoffmann, W.F., Young, E., Houck, J.R., Brandl, B., Fazio, G.G., Hora, J.L., Gehrz, R.D., Helou, G., Soifer, B.T., Stauffer, J., Keene, J., Eisenhardt, P., Gallagher, D., Gautier, T.N., Irace, W., Lawrence, C.R., Simmons, L., Van Cleve, J.E., Jura, M., Wright, E.L., Cruikshank, D.P. 2004, ApJS, 154, 1-9

Whitford, A.E. 1948, ApJ, 107, 102

Wilson, J.C., Eikenberry, S.S., Henderson, C.P., Hayward, T.L., Carson, J.C., Pirger, B., Barry, D.J., Brandl, B.R., Houck, J.R., Fitzgerald, G.J., Stolberg, T.M. 2003, Proceedings of the SPIE 4841, 451

Witt, A.N., Thronson, H.A., Jr., Capuano, J.M., Jr. 1992, ApJ, 393, 611

Wolf, M. 1908, Publikationen des Astrophysikalischen Instituts Koenigstuhl-Heidelberg, 3, 109-112

Worthey, G. 1994, ApJS, 95, 107-149

Zwicky, F. 1955, PASP, 67, 232

Zwicky, F. 1957, 'Morphological Astronomy', Springer-Verlag, Berlin